UNIVERSIDAD DE GUANAJUATO

Centro de Investigaciones en Óptica, A.C.

DEVELOPMENT OF THE PARTICLE IMAGE VELOCIMETRY (PIV) TECHNIQUE FOR THREE DIMENSIONS: TUNNELING VELOCIMETRY

A dissertation submitted by

Ing. J. Ascención Guerrero Viramontes

In partial fulfillment of the requirements for the degree of

Doctor in Science (Optics)

León, Gto. February 2002

DEVELOPMENT OF THE PARTICLE IMAGE VELOCIMETRY (PIV) TECHNIQUE FOR THREE DIMENSIONS: TUNNELING VELOCIMETRY.

A dissertation submitted
by

Ing. J. Ascención Guerrero Viramontes

In partial fulfillment of the requirements for the degree of
Doctor in Science (Optics)

Centro de Investigaciones en Óptica A. C.

February 2002

Supervisors: Dr. Fernando Mendoza Santoyo
Dr. Marcelo Funes-Gallanzi (INAOE)

Special Thanks to:

God. Thanks to let me know my position into Your Creation.

My best friend and beautiful wife Claudia Rubí. Thanks for loving me.

My Dad José and Mom Reyes, thanks for your testimony and your love.

My brother and sisters, Memo, Toña, Lety, Mella, Chabe and Ceci, my teachers.

My second family: Luis, Juanita, Cheli, Sagra, Marlene and Dany. Thanks to let me feel at home.

Marcelo and Claudia and their beautiful daughters Gaby, Sofy and Ale, Fernando and Lucy. Thanks for your friendship, support, love and much more…

All my family: Ramón, Cuco, Lola, Concha, Chema, Chole, lupe, Orlando, Paola, Nadia, Lulú, Euridice, Lalo, Quique y Kikin, Paquito,Mario y Mary, Rei, Karina, Ariel y Tere, Andrea, Arielito, Alfredo "Pez" y Lilian "La Diva", Lilieired, Periquin, Hugo, Memo y Paty, Gisela, Memo, Diana, Rubichunda, Chuy y Gaby, Zaira, Valeria, Jaime and Alicia, Lichita, Alejandra, Maritza, Rodolfo and Tere, Kuku, Renato and Aldo. Thanks to all for your trust.

Psalms 139:6-10. This knowledge is beyond me, Its lofty, I can't attain it. Where could I go from your Spirit? Or where could I flee from your presence?. If I ascend up into heaven You are there!. If I make my bed in Shed, behold You are there!. If I take the wings of the dawn and settle in the uttermost parts of the sea, even there Your hand will lead me and Your right hand will hold me.

Más maravillosa es la ciencia que mi capacidad; alta es, no puedo entenderla. ¿Adónde me iré de tu Espíritu? ¿Y a dónde huiré de tu presencia?. Si subiere a los cielos, allí estas Tú y si en el abismo hiciere mi estrado, he aquí allí Tu estás. SI tomare las alas del alba y habitare en el extremo de la mar, aún allí me guiará Tu mano y me asirá Tu diestra.

ACKNOWLEDGEMENTS

Main acknowledgement is credited to Dr. Fernando Mendoza Santoyo from Centro de Investigaciones en Óptica A.C. (CIO) and Dr. Marcelo Funes-Gallanzi from the Instituto Nacional de Astrofísica Óptica y Electrónica (INAOE) for their tireless efforts and guidance associated with this research. The author gratefully acknowledges the scholarship granted by Consejo Nacional de Ciencia y Tecnología (CONACYT) under projects 32709-A and 35062-E. I would also like to thank ASCI SA de CV, Alstom Power Plc., and Centro de Investigaciones en Óptica, A.C. for their installation facilities. Thanks also to my teachers: Memo, Samuel, Nachito, Miramontes, Dr. Ramón Rodríguez, Dr. Cristina Solano, Dr. Daniel Malacara, Dr. Zacarias Malacara, Dr. Bernardo Mendoza, Dr. Sergio Calixto and Dr. Oracio Barbosa. To my revisers: Dr. Bernardino Barrientos and Dr. Jorge Rojas. My honest thanks go to all my friendly pals from CIO: Eli, Carlos P.L., Laura, Pepillo, David “Don Moletrompero”, Marcial, Charo, Claudia, Manuel, Apolinar, Alejandro, Gaby, Luis, “La guera”, Guille, Miguel, Ili, Juanjo, Juan Carlos, Alma and Juan Manuel, Javier, Chemo, Chuy Lee, Marco, Luis, Ese, The Santos Team, Reyna, Noe, Los Tolucos, Saul, Chuy Cervantes, Angeles, Marite, Luli, Rodolfo, Pepe Puga, Paty Padilla, Doña Liz, Carmelita, Raymundo, Carlos P.S, Lic. Martínez, Erika. And my outsiders pals: Felipe and Angelica del Castillo, Bibiano and Nohemí Medina, José Luis and Perla Ortega, Joel and Luli Vázquez, Miguel and Adi, Orlando and Ceci, Adan and Vero Segura, Joseph and Azucena, Laura, Victor and Bertha H. Anteles, Gabriel, Memo and Sofy Caballero, Marisol, Alejandro, Los Bombones, Humberto and Rober. Paty, Irma and Moises Olvera, Nila, Petre, Daci and Aleks. I am sorry if I forgot someone.

ABSTRACT

Conventional velocimetry has an intrinsic limitation because it yields 2D data, neglecting the third velocity component. For this reason, 3D-PIV has recently evolved as an area of research with success at the cost of increasing complexity in its methodology. The increased complexity and the limited optical access found in most industrial applications, meant that many of the 3D-PIV techniques, although of academic interest, cannot be used in practical industrial applications.

For practical applications restricted viewing eliminates stereoscopic approaches. Lack of robustness and ease to perform an experiment make of conventional holography an unattractive option due to the fact that it involves a wet developing process, hence is very slow to yield results. However, its large depth of field and storing capacity makes it a technique that should, under the correct environment, be used. Scanning light-sheets are difficult to obtain for restricted optical access and high speeds, so they have not been tried in industrial conditions.

The required capabilities for 3D real-time measurement include the following three aspects: illumination of a volume rather than a plane, particle positioning in 3D from 2D camera information, and positioning calculation at low-magnification. Three-dimensional position and velocity information can be extracted by directly analyzing the diffraction patterns of seeding particles in imaging velocimetry using real-time CCD cameras. The Generalised Lorenz-Mie theory is shown to yield quantitative accurate models of particle position, such that it can be deduced with good accuracy from typical experimental particle images.

Tunneling Velocimetry, the proposed technique to perform 3D velocity measurements, is able to provide the means to obtain particle images in a volume of interest rather than on a light sheet. Moreover, with this technique pressure and temperature measurements are feasible from the system background surface. The research reported here is concentrated in the experimental characterization of Tunneling Velocimetry and the problems involved with it. A discussion of the preliminary results is presented.

DEVELOPMENT OF THE PARTICLE IMAGE VELOCIMETRY (PIV) TECHNIQUE FOR THREE DIMENSIONS: TUNNELING VELOCIMETRY.

By J. Ascención Guerrero Viramontes.

CONTENTS

LIST OF FIGURES

LIST OF PUBLICATIONS AND CONFERENCES DERIVED OF THIS RESEARCH

I. REFEREED PUBLICATIONS

1. J. A. Guerrero, F. Mendoza Santoyo, D. Moreno, M. Funes-Gallanzi and S. Fernandez Orozco, “Particle positioning from CCD images: experiments and comparison with the generalized Lorenz-Mie theory”, Measurements Science and Technology, **11**, pp 568-575 (2000).
2. J. A. Guerrero, F. Mendoza Santoyo, D. Moreno, and M. Funes-Gallanzi, “The case of a spherical wave-front in the Generalized Lorenz-Mie Theory including a comparison to experimental data”, Accepted Optics Communications, January 2002.
3. D. Moreno, F. Mendoza Santoyo, J. Ascención Guerrero and M. Funes-Gallanzi, "Particle positioning from CCD images using the Generalized Lorenz-Mie Theory and comparison to experiment", Applied Optics, **39** (28), pp. 5117-5124 (2000).
4. P. Padilla Sosa, D. Moreno, J. A. Guerrero, M. Funes-Gallanzi,“Low- Magnification Particle Positioning for 3D Velocimetry Applications”, Accepted Optics and laser Technology, 2001.
5. J. A. Guerrero, F. Mendoza Santoyo, M. Funes-Gallanzi, D. Moreno and P. Padilla Sosa, “Tunneling Velocimetry: A technique combining 3D velocimetry with Parameter Sensitive Paint”, sent to Review of Scientific Instruments 2001.

II. NATIONAL CONFERENCES

1. J.A.Guerrero, F. Mendoza Santoyo y M.Funes-Gallanzi, “SISTEMA DE ADQUISICIÓN DE IMÁGENES POR MEDIO DE LA TÉCNICA DE PIV”, XLI Congreso Nacional de Física, San Luis Potosi, Octubre 1998.
2. J.A.Guerrero, F.Mendoza-Santoyo, D.Moreno y M.Funes-Gallanzi, “ANALISIS EXPERIMENTAL DE IMÁGENES DE PIV PARA DETERMINAR LA VELOCIDAD FUERA DE PLANO DE UN FLUIDO”, XLII Congreso Nacional de Física, Villahermosa, Tabasco, Noviembre de 1999.

3. D. Moreno, F. Mendoza Santoyo, J. Ascención Guerrero, y M. Funes-Gallanzi, “MODELO TEÓRICO DE LA IMAGEN DE UNA PARTÍCULA ESFÉRICA ILUMINADA CON UNA HOJA DE LUZ, PARA APLICARSE A PIV: TEORÍA Y COMPARACIÓN CON EL EXPERIMENTO”, XLII Congreso Nacional de Física, Villahermosa, Tabasco, Noviembre de 1999.
4. J. A. Guerrero, F. Mendoza Santoyo, D. Moreno, M. Funes-Gallanzi, “VELOCIMETRÍA VOLUMÉTRICA: OBTENCIÓN DE LAS TRES COMPONENTES DE VELOCIDAD DE UN FLUIDO EN FORMA INSTANTANEA”, VI congreso nacional de la división de dinámica de fluidos de la sociedad mexicana de física, Puebla, Puebla, Octubre 2000.
5. J. Ascención Guerrero Viramontes, Fernando Mendoza Santoyo, Marcelo Funes-Gallanzi y David Moreno.”TUNNELING VELOCIMETRY : UNA NOVEDOSA EXTENSIÓN DE PIV PARA TRES DIMENSIONES CON UN SOLO ACCESO Y SU APLICACIÓN PRACTICA”. Taller de Velocimetría por Imágenes de Partículas (PIV), 6 y 7 de septiembre de 2001, UAM-I, México DF,CIE UNAM, Temixco, Morelos, México.
6. Funes-Gallanzi, M. & Guerrero, J.A. “The applicability of tunnelling velocimetry to the measurement of secondary flow in a two-stage air turbine rig”, Septima Conferencia de Ingenieria Electrica CIE-2001, Septiembre 3-7, 2001,CINVESTAV-IPN, México DF.

III. INTERNATIONAL CONFERENCES

1. J. A. Guerrero, M. Funes-Gallanzi, D. Moreno and F. Mendoza Santoyo, “TUNNELLING VELOCIMETRY: VOLUMETRIC VELOCIMETRY”, Simposio XX aniversario CIO, León, Gto, junio de 2000.
2. D. Moreno, F. Mendoza Santoyo, J. Ascencion Guerrero and M. Funes-Gallanzi, “Exact model for the image of a spherical particle using Generalized Lorenz-Mie Theory (GLMT) for application in three-dimensional Particle Image Velocimetry (3D PIV)” ,Simposio XX aniversario CIO, León, Gto, junio de 2000.
3. J. A. García Aragón,P. Morales, P. Padilla, J.E. Valdez, J.A.Guerrero, D. Moreno, M. Funes-Gallanzi, ”Non-spherical particle positioning from CCD images for velocimetry applied to two-phase flows”, Third International Symposium on Environmental Hydraulics, Tempe, Arizona, December 5-7, 2001.

INTRODUCTION

The aerospace and power generation industries are constantly seeking improvements in efficiency, performance and reliability, while meeting increasingly tight regulations for engine noise and pollution parameters. For instance, a prediction of the heat transfer to blade and endwalls is particularly important for an accurate assessment of turbomachinery component life. On the endwalls, there are complex 3D secondary flows present that make predictions of heat transfer difficult. In order to increase thrust-to-weight ratios and achieve maximum cycle efficiencies with gas turbine engines it is necessary to raise the cycle temperatures to the maximum, within constraints of structural integrity. Thus, the need to understand in detail and predict accurately the heat transfer distributions for high-pressure turbines becomes an important factor. The presence of complex three-dimensional secondary flows within the turbine passage makes the turbine designer's task very difficult and requires accompanying detailed aerodynamic information. Moreover, in turbulent flow conditions, where free-stream turbulence is high, heat flux on the blades is largely controlled by both free stream eddies of large size and energy reaching deep into the blade's boundary layer [1]. Furthermore, aeroelastic interaction between fluid and machine blades that induce blade vibrations, known as flutter, is the subject of much research. These vibrations can cause blade failure, and hence endanger turbomachines.

Aerodynamic structures, such as aircraft and aircraft components, are commonly tested in a wind tunnel in order to gather data to be used in the verification of their characteristics and in design improvements. Various quantities are measured in wind tunnel testing including, for example, the pressure distribution at the surface of the structure under study. The pressure information is used to calculate air flows and pressure distributions. Thus, the aerodynamic structure can be effectively “instrumented” for wind tunnel testing by painting it with a Pressure/Temperature Sensitive Paint (PSP/TSP), illuminating it with the required wavelength, and measuring the luminescence and light output intensities over its surface using an optical imaging system. These measurements are often made over the entire structure, but if corresponding local aerodynamic information is required – such as in wakes, shock/vortex interactions, stagnation regions, transition, etc. - simultaneous data

acquisition between the parameter sensitive paint and aerodynamic information is difficult to achieve.

A variety of techniques have evolved to achieve fluid-variable measurements. Some techniques are able to measure intrusively by point measurements, some are basically two-dimensional, while others being three-dimensional and non-intrusive integrate in one of the three dimensions. In recent years a lot of successful development effort has been oriented towards measuring the fourth variable: velocity.

Existing methods for measuring flow velocity in wind tunnels are mainly based on single point Laser Doppler Velocimetry (LDV) and Laser-2-Focus (L2F) velocimeters. These techniques, and their sundry variants, require scanning over the region of interest to obtain whole-field velocity measurements and are therefore time-consuming. They are primarily effective for steady flows, though there has been a shift towards developing the ability of LDV to deal with unsteady flows. For unsteady turbulent flows several methods of multi-point or whole-field measurement have been proposed, such as Doppler Global velocimetry [2,3], Laser Induced Fluorescence [4], and Particle Image Velocimetry (PIV) [5]. The last technique has been shown to work even in hostile industrial environments [6].

The conventional way to achieve three-component fluid velocity measurements has been to use holography [7] or a stereoscopic camera arrangement. An image-shifted version of stereoscopic viewing has been reported [8], as well as a version using two parallel light sheets [9]. Brücker [10], describes a scanning light sheet approach. Grant [11], used a beam-splitter and two cameras focussed on two different planes to achieve 3D measurements. However, these methods mainly look at a light sheet perpendicularly and consist of essentially two modules: the light delivery module, and a stereo camera arrangement which have to be correctly placed and calibrated in relation to each other.

A method using a dual-reference-beam to record PIV images holographically is described by Cha [12]. It uses an off-axis holographic set-up and correlation between "slices" of the recorded volume to calculate the out-of-plane displacement. This method, although volumetric, does not use the particle-scattered field to achieve three-dimensional positioning and it is not integrated in a single instrument. A single-port access implementation of PIV using holographic recording of the particle back-scattered light has been reported in the literature [13], where off-axis recording was employed. However, the arrangement was not aimed at creating a single measurement instrument,

it used wet processing so it was intrinsically not for real-time applications, and it used a conventional beam splitter rather than exploiting polarization to maximize the sensed light reflected from the particles that fall on the detector. A cumbersome stereo multiplexed holographic particle velocimeter has also been described by Adrian [14] to estimate 3D fluid velocity fields. In this case, the system comprises a number of sub-assemblies, with separate light-delivery and recording optics, and the physical access required around the working volume is so large that it rules out almost all industrial applications. There has even been an attempt at combining holography, laser sheet illumination and stereoscopic analysis to achieve 3D measurements [15].

Another development is Forward Scattering PIV [16]. It is a microscopic technique, which uses forward-scattering information to yield 3D information, though this is a development of a 30-year old pioneering method [17]. However, it presents field-of-view, alignment and optical access problems due to the magnification employed. The system has the light source and imaging module on either side of the measured volume, rather than having a single module to do the light delivery and sensing.

A more recent development is that of Three-State-Anemometry (3SA) [18], a spin-off from PIV, which uses a combination of three mono-disperse sizes of seeding particles to yield velocity, viscosity and density, by the differential paths of each particle seeding population. From the viscosity information, temperature can be derived, and by using the perfect-gas thermodynamic law pressure can also be inferred. There, for the first time, a technique was proposed which aims at having a non-intrusive, instantaneous and simultaneous measurement of all four variables in a fluid flow. However, this technique also suffers from the same experimental deficiencies as PIV.

There was a need therefore, to provide a system for measuring and visualizing an arbitrary velocity field. A system that: minimized alignment/experimental errors, for instance by integration of all components into a single instrument; required low power so high repetition lasers can be used; could be operated in real-time; was intrinsically volumetric in order to measure flows more reliably; and had single optical-access requirements.

It was also desirable to have a system capable of measuring temperature/pressure of near-surfaces, using a single apparatus able to derive fluid flow and surface data. The

aim of such a system was to provide a technique to solve the disadvantages of holography, conventional PIV, and 3SA, complementing it with parameter-sensitive coating information.
Thus, this thesis layout is such that the reader can understand the proposed technique and the development of the experimental work. A background introduction is given to understand the relevance of this research.

Chapter I describes the more used techniques to measure fluid flow velocity. It gives their characteristics and limitations like a reference to the proposed technique.

Chapter II gives a description of temperature and pressure fluid flow techniques, their advantages and disadvantages and the limitations to their application.

Chapter III shows the application of diffraction theory to the measurement of fluid flow three dimensional (3D) velocity from the diffraction pattern of a particle image.

Chapter IV describes the proposed technique, Tunneling Velocimetry (TV), that measures 3D fluid flow velocity from a single CCD image, and the surface temperature/pressure of the background from a single access. It is ideal to measure velocity and temperature/pressure in structures with complex access.

REFERENCES

1. D. G. Holmberg and D. J. Pestian, "Wall-Jet Turbulent boundary layer heat flux, velocity, and temperature spectra and time scales", ASME 96-GT-529, June 10-13, 1996.
2. H. Komine, U.S. Pat. No. 4,919,536, 1990.
3. K. Bütefisch, U.S. Pat. No. 5,684,572, 1997.
4. J. C. McDaniel, "Investigation of Laser-Induced Iodine Fluorescence for the measurement of density in compressible Flows", Stanford University, SUDAAR No. 532, 1982.
5. R. J. Adrian, "Particle-Tracking Techniques for Experimental Fluid Mechanics", Annu. Rev. Fluid Mech., 23, 261-304, 1991.

6. M. Funes-Gallanzi, P. J. Bryanston-Cross and K. S. Chana, "Wake Region Measurement of a highly three- dimensional nozzle guide vane tested at DRA Pyestock using Particle Image Velocimetry", ASME, 94-GT-349, The Hague, June 13-16, 1994.
7. J. M. Coupland and N. A. Halliwell, "Holographic Particle Image Velocimetry: three-dimensional Fluid Velocity Measurements Using holographic recording and Optical Correlation", Applied Optics, Vol. 31, 1005-1007, 1992.
8. M. Raffel, J. Kompenhans and H. Hofer, U.S. Pat. No. 5,440,144, 1995.
9. M. Raffel, J. Kompenhans and H. Hofer, U.S. Pat. No. 5,610,703, 1997.
10. Ch. Brücker, "Whole-volume PIV by the concept of a scanning light sheet: technique and application to 3D unsteady bluff body wakes", ASME FED-229, Laser Anemometry, 115-121, 1995.
11. I. Grant, X. Pan, F. Romano and X. Wang, "Neural- network method applied to the stereo image correspondence problem in three-component particle image velocimetry", Applied Optics, Vol. 37, No. 17, 3656-3663, June 1998.
12. S. S. Cha, U.S. Pat. No. 5,532,814, July 1996.
13. S. D. Woodruff, D. J. Cha and G. A. Richards, "Single Port Access Holographic Particle Image Velocimetry", ASME FED, Vol. 229, Laser Anemometry, 65-70, 1995.
14. R. J. Adrian, D. H. Barnhart and G. A. Papen, U.S. Pat. No. 5,548,419, August 1996.
15. E. P. Fabry, “3D holographic PIV with forward-scattering laser sheet and stereoscopic analysis”, Exp. In Fluids, Vol. 24, pp. 39-46, 1998.
16. B. Ovryn, T. Wright and J. D. Khaydarov, "Measurement of three-dimensional velocity profiles using forward scattering particle image velocimetry (FSPIV) and neural net pattern recognition", SPIE Vol. 2546, pp. 112-123, 1995.
17. R. Menzel and F. M. Shofner, “An investigation of Fraunhofer Holography for Velocimetry Applications”, App. Optics, Vol. 9, pp. 2073-2079, 1970.
18. M. Funes-Gallanzi, "A Numerical Investigation of Flow Past a Bluff Body Using Three-State- Anemometry (3SA)", Int. J. for Numer. Meth. in Fluids, Vol. 26, pp. 1023-1038, 1998.

CHAPTER I

VELOCITY MEASUREMENT TECHNIQUES

1.0 INTRODUCTION

In modern fluid mechanics, considerable attention has been paid to the study of turbulent and highly unsteady flows. The importance of these phenomena is apparent when considering technical processes as fuel-air mixture in combustion chambers, the study of separated flows in high angle of attack aerodynamics or the wake generated by rotors and wind turbines.

Aerodynamic structures such as aircraft and aircraft components are commonly tested in a wind tunnel to gather data for use in verification of their characteristics and in design improvements. Various quantities are measured in wind tunnel testing including, for example, the pressure distribution at the surface of the structure. The pressure information is used to calculate air flows and force/pressure distributions over the structure.

A quantitative analysis of these types of flows is needed to complement the qualitative insight provided by flow visualisation. Also, accurate data about the velocity and vorticity fields are required in Computational Fluid Dynamics (CFD) to validate the numerical simulations of turbulent and unsteady flows.

A variety of techniques have evolved to achieve fluid-variable measurements. Some are able to measure intrusively point wise like hot wire anemometry and pitot tube anemometry and non intrusively like Laser Doppler Velocimetry; some are basically two-dimensional and non-intrusive like Particle Image Velocimetry and Global Doppler Velocimetry, while others are three-dimensional integrating in one of the three dimensions. In the last few years, a lot of successful development effort has been oriented towards measuring velocity.

1.1 FLUID VELOCITY INTRUSIVE MEASUREMENT TECHNIQUES

1.1.0 THERMAL ANEMOMETRY (HOT-WIRES AND HOT-FILMS)

Thermal hot-wire or hot-film anemometry, is a technique in which fluid properties are measured via a very small heated wire or thin film [1]. The thermal balance between the small heated element and the fluid stream is the fundamental concept at the heart of thermal anemometry. The fluid mass flux, or Reynolds number, can be determined via a heat transfer law (calibration curve) by equating the power across the element to the heat transfer between the element and the fluid. Constant temperature and constant current anemometry are the two common modes of operation. The constant temperature method monitors the voltage required to maintain the element at a constant temperature (or resistance), while the constant current technique fixes the current across the element. Hot-wire or hot-film anemometry is a popular instrument for measuring turbulence [2].

There are two primary considerations to evaluate thermal anemometer systems: present requirements and possible future requirements. Some requirements are: velocity range (and, therefore, frequency response), number of sensors operating simultaneously, number of velocity components to measure (one, two, or three), temperature fluctuations in the flow that need to be measured, the need to use an automated traversing system to position the thermal anemometry probe during measurements, and an adequate computer system for data processing.

A hot-wire sensor is a small-diameter, solid metallic cylinder, usually made of tungsten, platinum, or platinum-iridium. The typical diameter is approximately 4 microns (0.00015 inch) with a length of 1 to 2 mm. The ends of the wire are copper plated to isolate the sensing portion from the support needles. This defines the sensing area better and reduces flow interference from the needles. Plating reduces the heat conducted from the sensor to the support needles and results in a more uniform temperature distribution along the sensor length.

1.1.1 PITOT-STATIC PROBES

A pitot-static probe [3] is perhaps the simplest device for measuring flow-velocity at a point. A pitot probe measures stagnation pressure (the pressure produced to bring the flow to a stop). It consists of a tube connected at one end to a pressure-sensing

device (such as a manometer or pressure transducer) and open at the other. Stagnation pressure is measured by pointing the open end of the tube towards the oncoming flow.

A static probe measures static pressure (the actual pressure in the flow). It consists of an opening (or 'pressure tap') parallel to the local flow direction. The pressure tap may be located in a tube (as shown in the figure 1.1), or in the surface of a structure.

A pitot-static probe is a combination of a pitot tube and a static tube. Given the flow density a pitot static probe can thus be used to measure velocity. The main sources of error in velocity measurements made with a pitot-static probe are misalignment and turbulence.

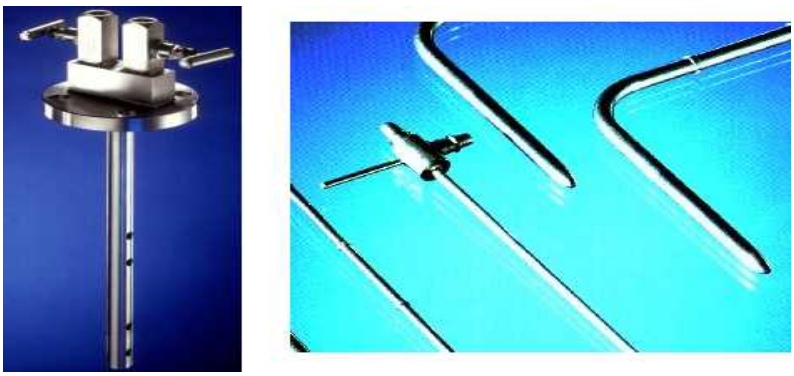

Figure 1.1. Example of pitot tubes.

Since the local direction of the flow around a structure is not known in advance, it is usual to make measurements with the pitot-static probe pointing in the direction of the oncoming free stream. Some misalignment of the pitot-static probe may therefore occur. Errors in velocity measurements as a function of angle misalignment become substantial for angles greater than 30º.

A pitot-static probe is designed only to measure velocities in a steady flow. In a turbulent flow, where the magnitude and direction of the velocity fluctuates with time, the pitot-static probe measures, approximately, the time-averaged flow velocity. The errors in this measurement depend on the scale of the turbulent eddies encountered by the probe. If the open end of the probe is large in comparison to the turbulent eddies then eddies stagnate at the end of the probe, artificially increasing the pressure difference it senses. If it is small then turbulent fluctuations in the flow direction produced by eddies passing the probe, appear as misalignment and artificially decrease the measured pressure difference.

1.2 FLUID VELOCITY IN-PLANE MEASUREMENT TECHNIQUES

1.2.0 LASER TWO FOCUS (L2F) VELOCIMETRY

The conventional Laser-Two-Focus (L2F) method also known as Laser Transit Anemometry (LTA) measures two components of the flow vector in the plane normal to the optical axis by measuring the time of flight of particles crossing two laser beams in the probe volume [1].

L2F is a non-intrusive technique for the measurement of flow velocities in gases and liquids. Here the velocity of extremely small particles, which are usually present in all technical flows or may be added if required, is recorded. The light scattered by the particles is used in this measurement. The required particles are in the size range of the light wavelength (<1μm), and follow the flow even at high acceleration so that correlation between particles and flow velocity is assured.

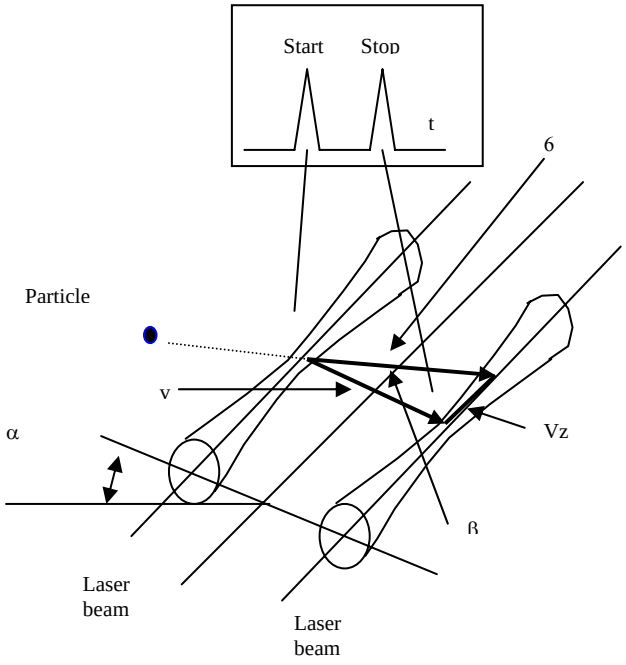

Figure 1.2. L2F system

In the measuring volume of the L2F device [4] (see figure 1.2), two highly focussed parallel beams are projected and employed as a time-of-flight gate. Particles which traverse the two beams in this volume, emit two scattering light pulses which are detected by two photodetectors, each one assigned to a beam in the measuring volume.

The two scattering signals have a time interval that provides a value for the velocity component in the plane perpendicular to the beam axis. Two associated double signals are obtained when the plane through which the two beams are spread out is nearly parallel to the flow direction. The beam plane is routable and its angular position is determined by the angle α. In turbulent flows the magnitude and direction of the momentary velocity vector changes constantly. The flow values are therefore usually given as mean values, measuring fluctuation. For this reason the beam plane for L2F measurements is adjusted in various positions (angle α) in the range of the mean flow direction and some thousands of time-of-flight measurements are carried out for each position. The measured data may be represented graphically as a two-dimensional frequency distribution. Incorrect measurements are then separated from correct measurements by means of a statistical method. Incorrect measurements, which arise when two different particles trigger the start and stop signals of the time measurement process, appear in the statistical representation as a constant background and can thus be recognized and subtracted. Further evaluation of the data results in the 2-dimensional components of the flow vector: magnitude and direction as well as the degree of turbulence, shearing stress and other high order moments of the fluctuation velocities.

1.2.1 PARTICLE IMAGE VELOCIMETRY (PIV)

A comprehensive introduction to PIV is contained in Adrian [5]. Adrian describes particle Image Velocimetry (PIV) as a method of measuring fluid velocity almost instantaneously, over extended regions of a flow domain. This approach combines the accuracy of single-point methods such as Laser Doppler Velocimetry with the multi-point nature of flow visualisation techniques. Numerous research groups have undertaken efforts along these lines during the past decade. PIV is one of several approaches that has been aimed at measuring accurately whole-field velocity information in two or three dimensions.

Typically, a double exposure of the light scattered by particles in the flow, when lit by a pulsed light source, is recorded during a sampling period gathering images of particle pairs, where the displacement between the particle pair images relates to their velocity (see figure 1.3). The seeding marker used to visualise the high-speed flows using PIV is a small particle, such as Styrene, or liquid droplet (such as water) in gaseous flows. An analysis system is then employed which measures velocity from individual particle pairs

in the spatial approach, or interrogation regions if correlation is employed; which requires high seeding densities.

Seeding-particle concentrations in high-speed flows are low and so do not justify the use of correlation-based techniques. The spatial pairing strategy allows the original image and the resulting vector to be overlaid, which aids the interpretation of the flow structure. When the flow field is unsteady, multi-point measurement techniques are capable of creating instantaneous pictures of the flow field that are unavailable from single-point measurements. Such information is needed in the study of unsteady turbulent flow, where it is now widely recognised that the instantaneous coherent realisations of the flow may bear little resemblance to the average structure [6].

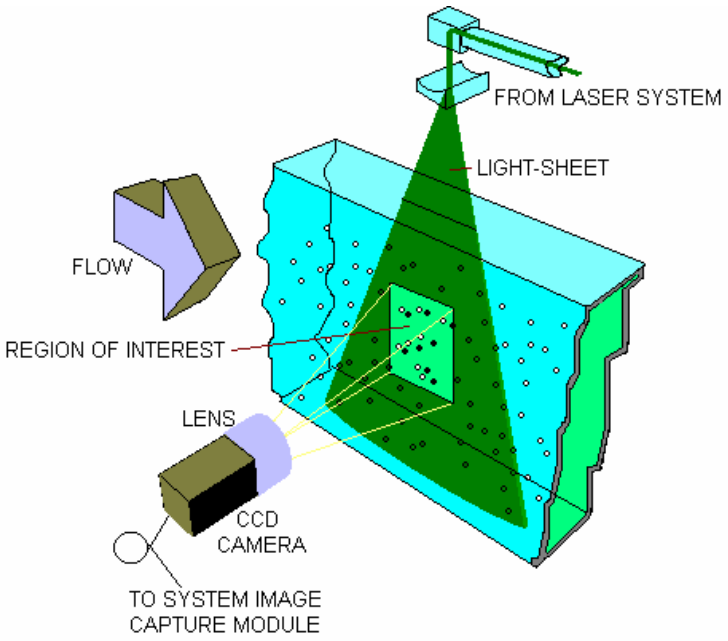

Figure 1.3. Basic PIV system configuration

A characteristic of turbulent flows is that they contain a range of motions at a variety of scales. Experimental techniques must therefore be able to be adapted and to capture a wide range of coherent structures, given the spatial resolution limitations, down to small scale features.

There are a variety of ways of encoding velocity in the images. In fact two pulses are normally used so that the resultant images contain "particle pairs" as previously described. Some other possible coding schemes are shown in [5].

Double-pulsed Pockels or Kerr switched lasers such as Nd/YAG produce high energies in pulses of very short duration, of the order of 10 to 25ns. Because the particles being imaged are so small the power supplied by such lasers is a must. This is related to the light scattering properties of small particles (the Mie light scattering theory is described in detail in [7]). The particles have to be small to faithfully follow the flow. Bryanston-Cross & Epstein [8] have explored the subject of visualising such small particles in PIV.

The Mie theory shows that the size of a sub-micron particle is related logarithmically to its ability to scatter light. Thus, halving the particle size from 500nm to 250nm theoretically decreases an order of magnitude the scattered light which can be collected in the side-scatter mode.

There is a limiting balance between the amount of light scattered from a particle and the speed and resolution of the film required to image it. It is also known that this is of particular importance when sub-micron particles are considered [9].

Grant and Smith [10] give a summary of the development of PIV. The history below is based upon this reference. PIV was first described in papers by Grousson and Mallick [11], Barker and Fourney [12] and Dudderar and Simpkins [13]. Grousson and Mallick [11] employed polystyrene spheres of 0.5 μm diameter as a seeding material in their fluid, and an electro-optic modulator in the path of their 0.8 Watt continuous wave laser to generate light pulses. A cylindrical lens was used to create the light sheet. The image of the fluid consisted of a speckle structure. Illumination of the fluid by two pulses left two mutually displaced speckle patterns upon the film. The displacement is different for different areas of the flow. The analysis technique employed was based upon Fourier plane methods. The application of PIV in these first reports was to liquid flows. Experimental difficulties limited the speed of flows that could be investigated to the order of millimetres per second and over regions of the order of square centimetres.

Adrian and Yao [14] detailed the differences between the particle image and the speckle regimes, and discussed the effects of particle scattering characteristics. They also point out the difference between the techniques to record multiple exposures of the speckle pattern translation during surface motion and applications involving fluids.

The light scattering characteristics of fluids containing small particles can be quite different from those of solid surfaces. For example, a pulsed sheet of laser whose thickness is of the order of 1mm is used to illuminate fluids. Hence scattering occurs from a volume distribution of particle scattering sites rather than a surface distribution.

The particles are typically small (0.1-10 micrometers), and they act as discrete point sources of scattered light. The density of particles per unit volume and their size can vary over a very wide range of values, depending upon the fluid and its treatment. For speckle patterns to exist, the number of scattering sites per unit volume must be so high that many images overlap creating random phase in the image plane. Since the density of scatterers in fluids can be quite low, it is possible that speckle is not present in many fluid applications, and those discrete images of particles are photographed instead. This then changes the mode of operation from laser speckle velocimetry to particle image velocimetry. Finally they conclude that the source densities encountered in many air and water flows of interest in research and practical applications are often not high enough to produce speckle, and that seeding in large scale flows or high speed flow becomes increasingly difficult and expensive as the concentration increases.

The intuitively simplest processing method, for resolved particles, is direct analysis of the PIV negative to determine the distance and direction through which the particles have translated between exposures. The problem then is to identify a particle and its partner. In densely seeded flows the probability of mis-matching particle images is high. One method that helps to resolve this problem is to pulse the laser several times, to create multiple images of each particle, which provides additional criteria for allocating particles to unique groups. Alternatively, two pulses of different wavelength can be used in order to distinguish the first and second partner in the pair, thereby accounting for any directional uncertainty.

An alternative processing method demonstrated by Meynart [15] uses whole field analysis of the image by optical Fourier transformation and filtering. This provides a pattern of fringes that represent iso-velocity contours.

The most appropriate method of analysis depends on the particle density within the image. In the application of high speed PIV it is difficult and expensive to introduce the seeding material, which makes images produced from high speed PIV sparse. Due to the sparse nature of the data, methods which rely upon local statistical averaging of many particle pairs are not appropriate.

Thus, the two general and powerful analysis methods although of great theoretical interest, namely a) full two-dimensional correlation in the case of the image plane, and b) full two-dimensional spectrum analysis of the Young's fringe pattern in the case of analysis in the Fourier transform plane, are not applicable to high speed flows due to the sparse nature of the particle distribution.

So, in summary Particle Image Velocimetry was developed from Laser Speckle Velocimetry in the early 1980s, and has now reached an advanced state. The technology required to implement PIV is well documented in the literature e.g., Adrian [5]. The process of velocity measurement with PIV can be divided into the following stages:

1. Seeding of the flow with small, passive tracer particles which follow the motion of the fluid.
2. Illumination of the measurement area with a two-dimensional pulsed light sheet.
3. Image capture, using either a photographic camera, a video camera or a CCD camera, with a resolution which allows individual particles to be distinguished.
4. Analysis of the image by dividing it up into a number of small ``interrogation areas'', and calculating the velocity vector for each interrogation area.
5. Post-processing of the resulting vector map to remove systematic errors, noise and erroneous vectors.

1.2.2 LASER SPECKLE VELOCIMETRY (LSV)

The system and procedures just described for PIV are similar for Laser Speckle Velocimetry (LSV). The differences between PIV and LSV rest on the effects of the mean concentration of scattering particles per unit volume upon the image field and in relation to the scales of the fluid flow field [5].

In LSV the concentration of scattering particles in the fluid is so large that the images of the particles overlap on the image plane. The random phase differences between the images of individual randomly located particles create the random interference patterns commonly known as laser speckle. The local speckle pattern is the superposition of images from a local group of scattering particles. Hence, velocity can be measured by measuring speckle displacement.

LSV has its roots in non-specular objects, where coherent light scattered from the opaque surfaces forms speckle patterns [16]. Simple manual analysis of a double exposed specklegram is not feasible, because the human eye cannot untangle the superposed speckle fields. Analysis of such fields became possible with the development of the Young's fringe method of interrogation, in which an interrogation spot on a double-exposed specklegram is illuminated with a laser beam. The speckle field from the first exposure diffracts the light wave from the coherent interrogation beam, which interferes with another wave created from the second speckle field exposure to form a Young's fringe pattern. The orientation of the fringes is

perpendicular to the direction of the displacement, and the spacing is inversely proportional to the magnitude of the displacement. Some practical applications of such technique to measure fluid velocities are given by Barker and Fourney [12], Dudderar and Simpkins [13, 17], Grousson and Mallick [11] and Meynart [15,18,19].

1.2.3 LASER DOPPLER VELOCIMETRY (LDV)

Laser Doppler velocimetry is a well-proven technique that measures fluid velocity accurately and non-invasively [20-24]. LDV makes velocity measurements by identifying the Doppler frequency shift of scattered laser light from sub-micron sized particles present and moving within a flow . The exact frequency of the scattered light is

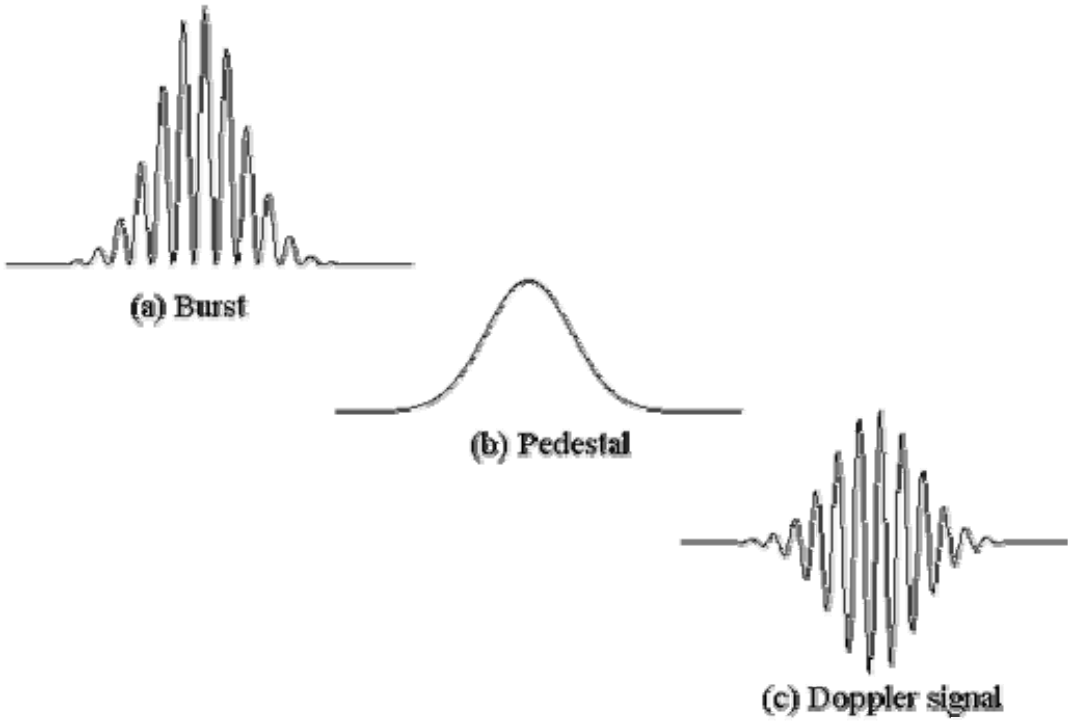

Figure 1.4 . Anatomy of a typical LDA signal burst generated when a particle passes through the measurement volume

determined through the Doppler Effect (figure 1.4). A laser beam illuminates the flow, and light scattered from particles in the flow is collected and processed. In practice, a single laser beam is split into two equal-intensity beams, which are focused at a common point in the flow field. An interference pattern is formed at the point where the beams intersect, defining the measuring volume (figure 1.5).

Particles moving through the measuring volume scatter light of varying intensity, some of which is collected by a photodetector. The resulting frequency shift of the photodetector output is related directly to particle velocity. If additional laser beam pairs with different wavelengths (colors) are directed at the same measuring volume two and even three velocity components can be determined simultaneously.

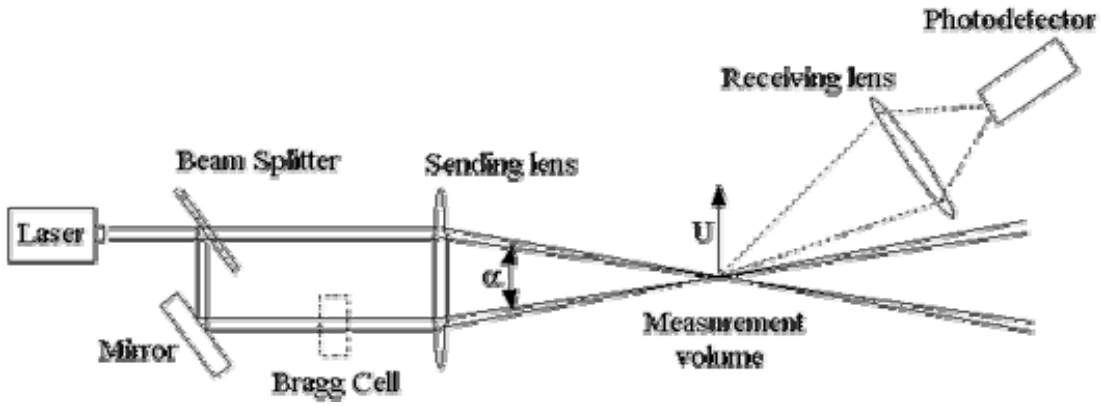

Figure 1.5 . A single-component dual-beam LDV system in forward scatter mode

Typically, the blue and green or blue, green, and violet lines of an argon-ion laser are used for multi-component measurements. If one of the beams in each beam pair is frequency shifted, the LDV system can also measure flow reversals.

LDV provides velocity data at a single point. Using a traverse system to move the laser source (the measuring volume) point-by-point makes it possible to perform an area analysis. The technique is non-invasive since laser light is the measuring tool. With proper experimental design, LDV can reach difficult measurement locations without disturbing the flow, for instance in moving propeller blades and inside engine cylinders.

LDV works in air or water. It measures over a wide velocity range, micrometers per second to Mach 8. And it works in many environments, from high temperature to highly corrosive. LDV has been used successfully in areas as diverse as transonic and supersonic flows, boundary layers, and flames. It has played a significant role in designing modern aircraft and ship propellers, ship hulls, aircraft flight structures, turbomachinery, automobile shapes, hydrofoils, and other products.

1.2.4 DOPPLER GLOBAL VELOCIMETRY (DGV)

Doppler Global Velocimetry makes velocity measurements by identifying the Doppler frequency shift of scattered laser light from sub-micron sized particles present and moving within a flow. The exact frequency shift of the scattered light is determined through the Doppler Effect .

Since a global measurement is desired, a sheet of laser light is used to illuminate the flow field. Frequency discrimination to measure flow velocity values rely on identifying the scattered light frequency shift. DGV accomplishes this task by using a unique and key component known as an Absorption Line Filter or ALF. An ALF is essentially an optical filter assembly. The amount of light passing through the filter will depend on the frequency of the input light. The DGV illumination laser is carefully tuned to a frequency which intersects the ALF transfer function at approximately the 50 percent transmission or absorption location. The flow field of interest is then directly viewed through the ALF. The unique Doppler interaction of the moving particles, illuminating laser and viewing vectors determine the scattered light frequency. Scattered light from the illuminated flow field will pass through an ALF with an output intensity level proportional to the frequency, or most importantly to the particle velocity. The ALF thus performs a linear frequency - to - intensity conversion over approximately 500 MHz. A normally difficult Doppler frequency measurement has been reduced to a relatively simple intensity measurement task, as a result of using an ALF.

Wide area, or global, intensity measurements are typically performed using Charge Coupled Device (CCD) based video cameras. The recorded intensity data, for a large flow field region viewed through the ALF, can be related to the flow velocity once the ALF transfer function has been identified through calibration.

DGV, much like other laser based methods, requires the presence of particles within the flow to make measurements. Direct injection of particles, known as seeds, into the flow is often necessary since a sufficient number and size of particles may not naturally exist. The seed size, number, and distribution must be carefully considered in order to assure good DGV measurements. Particle size and mass will affect both the scattered light intensity and the ability of the seeds to follow the flow accurately. Particle number and distribution throughout the flow will affect the data acquisition rate and the completeness of the global measurements. In general, seeding guidelines utilised for LDA flow measurements apply.

Unfortunately, practical factors prevent perfectly uniform flow field illumination and seeding. These nonuniformities produce varying scattered light intensities. DGV measurement errors would result if these intensity variations, as measured by a CCD camera, were assumed to represent velocity information. To avoid potential problems of this nature, a second camera is used to measure the simple intensity variations in the flow field. These recorded intensities are then used to normalize the output from the other CCD camera and ALF. The normalized ratio of camera outputs thus contains only velocity information. This technique has been widely used and tested in practical applications [25-30].

1.2.5 DIGITAL PARTICLE IMAGE VELOCIMETRY (D-PIV)

Digital Particle Image Velocimetry (D-PIV) [31] is the digital counterpart of conventional Laser Speckle Velocimetry (LSV) and Particle Image Velocimetry (PIV) techniques. In this novel two-dimensional non-intrusive technique, digitally recorded video images are analysed computationally, removing slow and opto-mechanical processing steps. Depending on the procedures adopted to analyse the PIV images the performance of the technique can vary dramatically [32]. The accessibility in terms of cost to more powerful computers makes it possible to develop very accurate processing techniques that are leading the technique to the top of the advanced experimental, non-intrusive, tools for quantitative multidimensional measurements [33-35]. It is worthwhile to remember that the more accurate the results of a measurement are the better the basic fluid dynamics phenomena like instability, turbulence and combustion can be understood. Nowadays, the D-PIV technique is known like conventional PIV.

1.2.6 THREE STATE ANEMOMETRY (3SA)

Three-State anemometry (3SA) is a derivative of PIV [36], which uses a combination of three monodisperse sizes of styrene seeding particles. A marker seeding is chosen to follow the flow as closely as possible, while intermediate and large seeding populations provide two supplementary velocity fields, which are also dependent on fluid density and viscosity.

The compromise required regarding the size of the intermediate and large particle sub-groups require extensive research to determine the optimum sizes and proportion in the seeding mixture. The larger particles would provide more sensitivity to

viscosity and ease the particle population discrimination requirement, to be able to separate the three velocities fields. On the other hand, the smaller the particles the more closely they will follow the flow and therefore will provide more detailed coverage of the field for all three state variables.

The nature of the particle trajectory, in a free-vortex swirling flow, is to a large degree governed by the Stokes number: $St=(w/v)^2 dp$, where w is the angular frequency of the turbulent motion, v is the viscosity and dp is the particle diameter. When this parameter is less than 0.1, the particle will closely follow the circular fluid streamlines. When Stokes is larger than 1.0 the particle will be ultimately centrifuged out across the fluid streamlines in swirling flows. For particle Stokes values higher than 0.1 in high Reynolds number flows, two extra parameters are required to describe the nature of the particle trajectory; one essentially dependent on viscosity and the other on density. Thus, the ideal composition of the seeding mixture depends on the expected radius of curvature the particles take before being centrifuged out. The Stokes number considerations determines the upper particle size limit, while discrimination between particle velocity fields determines the lower limits.

An aspect of the technique, which is of particular importance, is that since three convolved randomly distributed particle populations are being sampled, the three measurements will not refer to the same position in space. Therefore, interpolation is necessary to be able to provide three estimates of the seeding velocities at the same position. Therefore, a large number of velocity samples are required to provide well-conditioned velocity field matrices.

A limitation of the 3SA technique is that the larger particle subgroups do not follow the flow as closely as the flow marker particles by definition, and therefore some regions of the flow would not be suitably covered by all three seeding populations. In regions of high turning or back flow, it is very difficult to inject seeding at all, and if velocity is very low the dynamic range constrains would have to be altered together with the seeding rate.

1.3 FLUID VELOCITY VOLUMETRIC MEASUREMENT TECHNIQUES

1.3.0 STEREOSCOPIC PARTICLE IMAGE VELOCIMETRY (STEREOPIV)

Stereo PIV is the natural advancement of PIV [37-41]. Stereo PIV is the determination of the flow velocity in all 3 dimensions rather than two, as was the case in traditional PIV. To obtain the 3rd component of velocity, it is necessary to use two cameras or use cunning optical effects.

The PIV data to date has, as yet, inherently been of a two-dimensional nature. In order to extract the out-of-plane component various authors have concentrated on the use of geometry in a stereo set-up [42,43]. However, if only triangulation is used, the relative error in the out-of-plane direction is of the order of three times larger than in the x-y direction. This effectively makes the whole technique rather unreliable [44,45]. Furthermore, both the relative and absolute co-ordinate systems remain basically unrelated as the measurements obtained by triangulation are relative between pairs of particles and have no relation to an absolute frame of reference.

Once initial results were obtained it became clear that, given the large errors in the out-of-plane direction, the stereoscopic approach to PIV would remain impractical unless a way was found to increase the accuracy in the z-direction.

One way to increase the accuracy in general, is of course, to increase the angle subtended by the two cameras. However, this is often not possible in real applications, as facilities have to be adapted to, and often were not particularly designed for visualisation purposes. The depth of field required increases as the angle increases (leading to less photons falling on the imaging sensor), and is further restricted by the need for simplicity and economy. Furthermore, as the angle increases the absolute spatial errors also increase; thus denying some of the increase in accuracy.

As mentioned earlier, the spatial approach to PIV has as one of its advantages the ability to apply fairly intensive processing to the PIV pairs found; thanks to the large data reduction involved. Now, a digital image is a spatial, intensity and temporal quantized representation of a real-world scene. The precise representation of position is critical to the successful extraction of velocity data from a PIV image. For a reliable PIV to approach the precision of a photographic image, accurate sub-pixel position

estimates are necessary. Otherwise, the large number of required digital images represent un-surmountable problems of registration, data volume and throughput.

Note that in order to simplify the discussion, the centre of the Nd/YAG sheet and the centre of focus are made co-incident, and the depth of view is made somewhat larger than the width of the light sheet. Thus, the amplitude can be seen to depend on the z-position of the particle, and varies according to the change in intensity of the laser over the depth of the region of interest. On the other hand, the amplitude varies approximately linearly with respect to the z-position in relation to the position of focus. It has been found that the behaviour is not strictly linear but that a linear approximation is sufficient for the accuracies quoted. This focal length can be accurately calculated for a given objective in the case of the K2 diffraction limited optics.

This technique has two major advantages. Firstly, it provides three measures for the z-component. Two from the depth ratio from each image in a stereo case, and the third from triangulation. Just as importantly though, it provides a way in which these relative velocity measurements can be related to an absolute frame of reference. The depth ratio will exhibit a maximum where the particle is in line with the focal length of the lens, and will then tail off as a particle moves in front or behind this position. Thus, the system has symmetry about this focal length leading to an ambiguity in the measurement of the depth ratio. In order to account for it, triangulation needs to be used as well. Thus if a particle pair lies in a equidistant position from this axis, the ratio will be equal but triangulation will show one to lie ahead of the other, thus enabling the data to be unscrambled.

Stereo PIV appears to be a robust and well researched method. However various problems and sources of inaccuracies must be looked into. These problems, which are outlined in greater detail in Adrian [5], include:

1.The particle accurately following the fluid flow.

2.The particle reflecting enough light for it to be observed.

3.Aberrations caused by the optics within the stereo PIV system.

4.The sub-pixel accuracy of the system. There are various techniques such as; Gaussian fitting, and centre of mass estimations, to increase the accuracy in the measurement of the distance that the particle has travelled [46].

1.3.1 HOLOGRAPHIC PARTICLE IMAGE VELOCIMETRY (HOLOGRAPHIC PIV)

Holography is best known for its ability to reproduce three-dimensional images. However, it has many other applications. Holographic non-destructive testing is the largest commercial application of holography. Holography can also be used to make precise interferometric measurements, pattern recognition, image processing, holographic optical elements (eg. complex spatial filters), and storage of data and images.

Any propagating wave phenomenon, such as microwaves or acoustic waves, is a candidate for application of the principles of holography. Most interest in this field has centred on waves in the visible portion of the spectrum, and to use it in the area of flow visualisation with PIV.

There are several well-known difficulties in forming and analysing holographic particle data in the sub-micron range. It is suggested that these problems can be overcome by using a combination of research techniques. First, it has been found that it is possible to record images of sub-particles using conventional photographic materials. Essentially, a diffraction limited optical component has been used to provide aberration free particle images. Second, the sensitivity of the holographic material has been increased with the use of specialised holographic processing chemicals. Third, it has been found that it is possible to encode holographically double, slightly displaced, particle images using a pulsed laser. Thus Young's fringes can be obtained directly from the stored holographic data and the particle velocity can be measured directly from the hologram. Fourth, the holographic particle data can be automatically analysed using a software program. Finally, since the data is stored holographically, it is possible to obtain instantaneous 3-D particle velocity. Developments and applications can be found in references [47-52].

1.4 CONCLUSIONS

Different methods and techniques to measure fluid flow velocities are described in this chapter. However, each one is used for different applications and conditions. No one can measure the 3D instantaneous velocity vector in an industrial application. Some of them are point wise techniques while others measure with in-plane sensitivity. The volumetric techniques showed to distinctive restrictions. Holography is practical in

laboratory controlled environments, but not in hostile conditions. Stereo PIV requires multiple optical access, so it is impractical for industrial applications.

1.5 REFERENCES

1. Oldfield M.L.G, “Experimental Techniques in Unsteady Flows”, Lecture Notes for the VKI lectures on Unsteady Aerodynamics, April 18-22, 1988.
2. Hince, J. O., Turbulence, 2n ed., McGraw-Hill, New York, 1975.
3. Dare, J. A., Notes for experiments, Department Of Aerospace And Ocean Engineering, Virginia Tech., 1996.
4. Föster W., Karpinsky G., Krain H., Röhle I., and Schodl R., “3-Component-Doppler-Laser-Two-Focus Velocimetry Applied to a Transonic Centrifugal Compressor”, Tenth International Symposium on Applications of Laser Techniques to Fluid Mechanics, Instituto Superior Tecnico, LADOAN, Lisbon, July 10-13, 2000.
5. Adrian, R. J., "Particle-Imaging Techniques For Experimental Fluid Mechanics", Annual Review of Fluids Mechanics, Vol. 23, pp. 261-304, 1991.
6. Nixon(ed.) D., "Unsteady Transonic Aerodynamics", Vol. 120, AIAA, 1989.
7. Mie, G., "Beiträge zur Optik trüber Medien, speziell kolloidaler Metallösungen", Ann. Phys. 25, 377-445, 1908.
8. Bryanston-Cross P.J. and Epstein, A., "The application of sub- particle visualisation for PIV (Particle Image Velocimetry) at transonic and supersonic speeds", Prog in Aerospace Sci. 27, pp. 237-340, 1990.
9. Bryanston-Cross, P.J., Harasgama, S. P., Towers, C. E., Towers, D. P., Judge, T. R., and Hopwood, S. T. “The Application of Particle Image Velocimetry (PIV) in a Short Duration Transonic Annular Turbine Cascade”, Journal of Turbomachinery, Vol.114, No.3, pp504-510, July 1991.
10. Grant I. and Smith G. H., “Modern Developments in Particle Image Velocimetry”, Optics and Lasers in Engineering, Vol. 9, pp. 245-264, 1988.
11. Grousson R. and Mallick S., “Study of Flow Patterns in a Fluid by Scattered Laser Light”, Applied Optics, Vol. 16, pp. 2334, 1977.
12. Barker D. B., and Fourney M. E., “Measuring Fluid Velocities with Speckle Patterns”, Optics Letters, Vol. 1, pp. 135, 1977.

13. Dudderar T. D., and Simpkins P. G., “Laser Speckle Photography in a Fluid Medium”, Nature, Vol. 270, pp. 45, 1977.
14. Adrian R.J. and Yao C.S., “Pulsed Laser Technique Application to Liquid and Gaseous Flows and the Scattering Power of Seed Materials”, Applied Optics, Vol. 24, pp. 44-52, 1985.
15. Meynart R., “Equal Velocity Fringes in a Raleigh-Bernard Flow by a Speckle method”, Appl. Opt., 19, pp.1385-1386, 1980.
16. Archbold E. and Ennos A.E., “Displacement measurement from double-exposure laser photographs”, Optica Acta, Vol. 19(4), pp. 253-271, 1972.
17. Dudderar T. D., and Simpkins P. G., ”Laser Speckle measurements of transcient Bénard convection”, Journal of Fluid Mechanics, Vol. 89(4), pp.665-671, 1978.
18. Meynart R., “Instantaneous Velocity Field Measurement in Unsteady Gas Flow by Speckle Velocimetry”, Applied Optics, Vol 22(4), pp. 535-540, 1983.
19. Meynart R., “Speckle Velocimetry Study of Vortex pairing in a Low-Re unexcited jet”, Physcics of Fluids, Vol. 26(8), pp. 2074-2079, 1983.
20. Gartrell Luther R., Tabibi Bagher M., Hunter William W. Jr., Lee Ja H. and Fletcher Mark T. , Application of Laser Doppler Velocimeter to Chemical Vapor Laser System , NASA TM-4409, January 1993.
21. Sellers William L. III, Meyers James F. and Hepner Timothy E., “LDV Surveys Over a Fighter Model at Moderate to High Angles of Attack”, SAE Aerospace Technology Conference and Exposition, Anaheim, California, SAE Paper No. 881448, October 3-6, 1988.
22. Podboy Gary G., Bridges James E., Saiyed Naseem H., and Krupar Martin J. “Laser Doppler Velocimeter System for Subsonic Jet Mixer Nozzle Testing at the NASA”, Lewis Aeroacoustic Propulsion Lab. Prepared for the 31st Joint Propulsion Conference and Exhibit cosponsored by AIAA, ASME, SAE, and ASEE, July 10-12, 1995, San Diego, California.
23. Gartrell Luther R., Tabibi Bagher M., Hunter William W., Jr., Lee Ja H., and Fletcher Mark T., “Application of Laser Doppler Velocimeter to Chemical Vapor Laser System”, NASA Technical Memorandum 4409 JANUARY 1993.
24. Neuhart Dan H., Wing David J. and Henderson Uleses C. Jr., “Simultaneous Three-Dimensional Velocity and Mixing Measurements by Use of Laser Doppler Velocimetry and Fluorescence Probes in a Water Tunnel”, NASA TP-3454 , September 1994.

25. Meyers James F., “Technology and Spin-Offs From Doppler Global Velocimetry”, 12th International Symposium on the Unification of Analytical Computational and Experimental Solution Methodologies, Worcester, Massachusetts, July 6-8, 1995.
26. Meyers James F., “Development of Doppler Global Velocimetry for Wind Tunnel Testing”, AIAA 18th Aerospace Ground Testing Conference, Colorado Springs, Colorado, AIAA-94-2582, June 20-23, 1994.
27. Meyers James F., Lee W., Fletcher Mark T. and South Bruce W., “Hardening Doppler Global Velocimetry Systems for Large Wind Tunnel Applications”, 20th AIAA Advanced Measurement and Ground Testing Technology Conference, Albuquerque, New Mexico, AIAA 98-2606, June 15-18, 1998.
28. Meyers James F. and Komine Hiroshi, “Doppler Global Velocimetry---A New Way to Look at Velocity”, 4th International Conference on Laser Anemometry---Advances and Applications, Cleveland, Ohio, August 5-9, 1991.
29. Gorton S. A., Meyers J. F. and Berry J. D., “Laser Velocimetry and Doppler Global Velocimetry Measurements of Velocity Near the Empennage of a Small-Scale Helicopter Model”, 20th Army Science Conference, Norfolk, Virginia, June 24-27, 1996.
30. James F. Meyers, “Doppler Global Velocimetry - The Next Generation?”, AIAA 17th Aerospace Ground Testing Conference, Nashville, Tennessee, AIAA 92-3897, July 6-8, 1992.
31. J. Westerweel, “Fundamentals of Digital Particle Image Velocimetry”, meas. Sci. Technol. 8, pp. 1379-1392, 1997.
32. Funes-Gallanzi, M., “High Accuracy techniques Applied to the Extraction of Absolute Position Estimation in DPIV systems”, VII International Symposyum on Applications of Laser Techniques to Fluid Mechanics, Lisbon, July, 1994.
33. Willert, C. E. and Gharib, M. ”Digital particle image velocimetry”, Experiments in Fluids, Vol. 10, no. 4, p. 181-193, 1991.
34. William M. Humphreys, Jr., Scott M. Bartram, Tony L. Parrott and Michael G. Jones, “Digital PIV Measurements of Acoustic Particle Displacements in a Normal Incidence Impedance Tube”, 20th AIAA Advanced Measurement and Ground Testing Technology Conference, Albuquerque, New Mexico, AIAA 98-2611, June 15-18, 1998.

35. Bruecker, CH. ”Digital-Particle-Image-Velocimetry (DPIV) in a scanning light-sheet: 3D starting flow around a short cylinder”, Experiments in Fluids, Vol. 19, no. 4, p. 255-263, 1995.
36. Funes-Gallanzi, M. " A novel fluids research Technique: three state anemometry", International Gas Turbine and Aeroengine Congress & Exhibition, Birmingham, UK, June 10-13, 1999.
37. Funes-Gallanzi M. and Bryanston-Cross P.J., “Solid State Visualization of a highly three dimensional flow using stereoscopic Particle Image Velocimetry (3DPIV)”, SPIE Vol. 2005, pp.360-369, 1995.
38. Westerweel J. and Nievwstadt F.T.M., “Performance test on 3-Dimensional Velocity Measurements with a two Camera digital particle-image velocimeter”, Laser Anemometry Vol. 1 ASME, pp.349-355, 1991.
39. Arroyo M.P. and Greated C.A., “Stereoscopic Particle Image Velocimetry”, Meas. Sci. Technol. 2, pp. 1181-1186, 1991.
40. Prasd A.K. and Adrian R.J., “Stereoscopic Particle Image Velocimetry Applied to Liquid Flows”, Experiments in Fluids, Vol. 15, pp.49-60, 1993.
41. Hinsch K.D., “ Three Dimensional Particle Velocimetry”, Meas. Sci. Technol. Vol. 6, pp. 742-753, 1995.
42. Willert C., “Stereoscopic Digital Particle Image Velocimetry for Application in Wind Tunnel Flows”, Meas. Sci. Technol. Vol 8, pp. 1465-1479.
43. Lecert A., Renou B., Allano D., Boukhalfa A. and Trinité M., “Stereoscopic PIV: Validation and Application to an Isotropic Turbulent Flow”, Experiments in Fluids, pp. 107-115, 1999.
44. Lawson N.J. and Wu J., “ Three Dimensional Particle Image Velocimetry: Experimental Error Analysis of a Digital Angular Stereoscopic System”, Measc. Sci. Tech. Vol. 8, pp.1455-1464, 1997.
45. Blostein S.D. and Huang T.S., “ Error Analysis in Stereo Determination of 3D Point Positions”, IEEE Transactions on Pattern Analysis and Machine Intelligence, Vol.PAMI-9, No. 6, 1987.
46. Burnett, M., ‘Methods of Quantitative Flow Visualisation,’ MRes paper, University of Warwick, 1996.
47. Bryanston-Cross P.J., Funes-Gallanzi M., Quan C. and Judge T.R., “ Holographic Particle Image Velocimetry (HPIV)”, Optics and Laser Technology, Vol. 24(5), pp.251-256, 1992.

48. Malyak P.H. and Thompson B.J., “Particle Displacement and Velocity Measurement Using Holography”, Optical Engineering, vol 23(5), pp.567-576,1984.
49. Judge T.R., Quan C. and Bryanston-Cross P.J., “Holographic Deformation Measurements by Fourier Transform Technique with Automatic Phase Unwrapping”, Optical Engineering, Vol. 31(3), pp.533-543, 1992.
50. Trolinger J.D., “ Diagnostics of Turbulence by Holography”, Advances in Laser Technology for Atmospheric Sciences, SPIE, vol 125, pp. 105-113, 1997.
51. Fabry E.P., “ 3D Holographic PIV with Forward-Scattering Laser Sheet and Stereoscopic Analysis”, Experiments in Fluids, vol 24, pp. 39-46, 1998.
52. Royer H., “ Holography and Particle Image Velocimetry”, Meas. Sci. Technol., Vol. 8, pp. 1562-1572, 1997.

CHAPTER II

PRESSURE AND TEMPERATURE MEASUREMENTS

2.0 INTRODUCTION

Because temperature affects material properties, there are numerous methods for measuring temperature [1]. The simplest methods employ thermal expansion. The most common electrical-based sensors are thermocouples and resistance elements. Optical methods such as liquid crystals, infrared detectors and thermographic phosphors have the advantage of non-contact measurement. They can provide a two-dimensional temperature field over a surface. However it is more difficult to obtain absolute temperatures and they require more sophisticated data acquisition equipment.

Pressure is defined as the normal force per unit area acting upon some real or imaginary boundary. The static pressure, p, in a fluid stream is the normal force per unit area on a boundary moving with the flow. Assuming local thermodynamic equilibrium, this definition is consistent whit the thermodynamic definition of pressure.

Many convenient and useful temperature sensing devices, based on the phenomenon of thermal expansion of the materials, may be found for a specific temperature range. Most common ones are the liquid-in-glass thermometers, particularly the mercury-in-glass thermometer, which has an operating temperature range from the freezing point to the boiling point. The latter can be increased by pressurising the inert gas in the capillary space above the liquid.

Pressure thermometers, which are widely used in industrial applications, consist of three basic elements: a sensitive bulb containing a liquid, gas or vapour, an interconnecting capillary tube, and a pressure-sensing devise such as a Bourdon tube. Temperature variations in the bulb results in a volume change of the fluid, causing a pressure change which can be calibrated to record the temperature variation.

The phenomenon of thermal expansion in metals is employed in bimetallic thermometers. When two strips of metals with different thermal expansion coefficients are bonded together, a change in temperature will result in a deflection of the strip due to differential expansion. This kind of thermometers have an operating temperature range of about 200-810 K.

The most important of all temperature sensors is the thermoelastic sensor, commonly known as the thermocouple. The operating principle is as follows: when two wires of dissimilar metals, A and B, are joined to form a circuit with the two junctions maintained at two different temperatures T1 y T2, an electromotive force E is obtained, wich can be measured by a voltmeter or potentiometer.

The electrical resistance of most materials changes with temperature. Due to the fact that electrical circuits for measuring resistance are common, this is an easy method for measuring temperature. The resulting sensors have a variety of names. RTD's generally refer to metal wires wrapped around an insulator to minimise the effects of strain. An RTS usually refers to a metal thin film deposited in an insulator to give fast time response. The resistance measurement is usually performed by passing a small known current through the resistor and monitoring the corresponding voltage drop.

All these techniques are point wise and do not provide an area temperature map.

In compressible flows the density changes with velocity to give measurable results in the variation of the refractive index so the temperature can be inferred from it. For compressible flows, such as free convection where the velocity is relatively low, the density, and hence the refractive index is directly related to temperature. Methods for observing this density variation include Schlieren, shadowgraph and some interferometric techniques. In these methods, light and dark patterns are formed by the bending of light as it passes through a region of varying density.

A Schlieren arrangement is illustrated in figure 2.1. A light source such as an arc lamp is focused onto one point at the same distance from the two lenses, and through the gas or flame. A camera behind a knife-edge is focused onto the test object and can record the deviation of the light due to changes in the refractive index [2,3]. Tomographic or temperature mapping utilising Schlieren methods have been reported by Schwarz [4].

In the shadowgraph method, the linear displacement of a perturbed light beam is observed, rather than the angular deflection as in the Schlieren method [2].

In the Mach-Zender interferometric technique (figure 2.2) a beam of light is split in two, with one beam avoiding the test section called the reference beam, and the other beam falling through the test section, also called the object or measuring beam. The splitter plate near the screen is used to combine and convey the beams onto it for optical mixing and recording. Light and dark patterns are formed as a result of phase shifts between the reference and measuring beams.

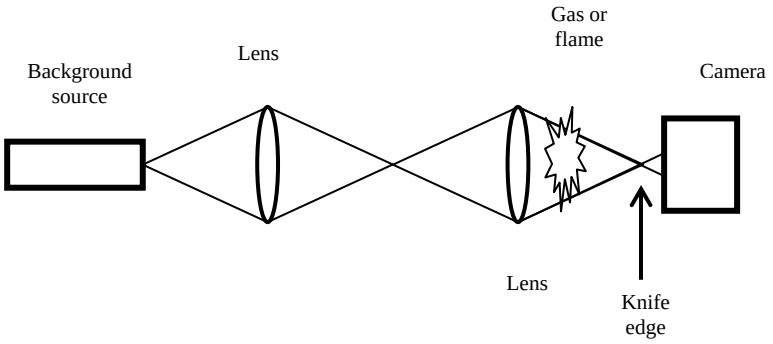

Figure 2.1 Schlieren method for determining gas temperature.

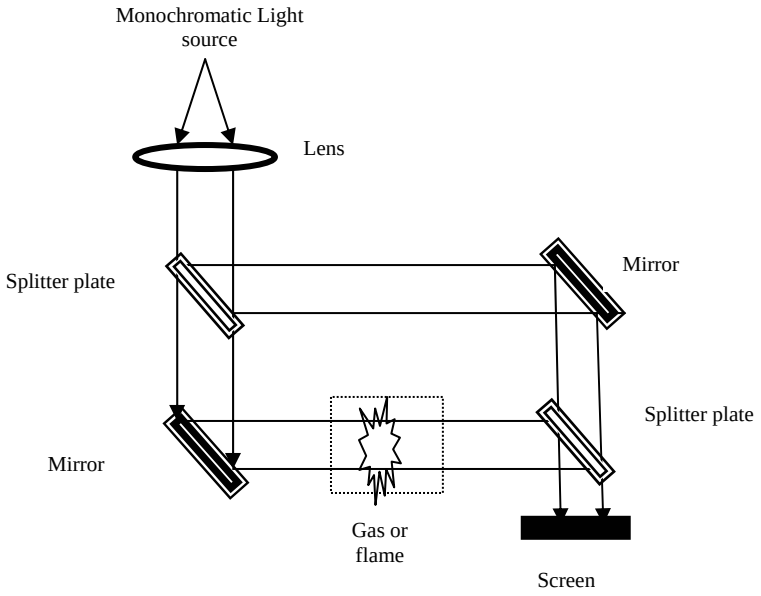

figure 2..2. Mach-Zender interferometer for gas temperature measurement, [1]

2.1 PARAMETER SENSITIVE PAINTS

Parameter sensitive paints are luminescent coatings engineered such that the luminescence is a function of pressure, temperature, strain, or some other parameter of interest. By measuring some characteristics of luminescence (intensity of lifetime) the corresponding parameter can be determined. The concept of this method was invented in the Central Aerohydrodynamic Institute (TsAGI) of Russia, with the idea to use this phenomenon for pressure measurements in experimental aerodynamics, by G. Pervushin and L. Nevsky [5].

Several types of parameter sensing paints are under development, the most mature of these are the Pressure Sensitive Paint (PSP) and the Temperature Sensitive Paint (TSP) [6,7]. Both types of paints can be used with the same set of excitation lamps, detectors, computer hardware, and software. The main difference is that PSP contains a luminescent compound that is sensitive to local pressure, and TSP contains a luminescent compound that is sensitive to local temperature.

2.2 PRESSURE SENSITIVE PAINT (PSP)

The ability to determine instantaneous two-dimensional pressure distributions on the surface of a structure in test facilities like wind tunnels or turbomachines, by applying pressure-sensitive paint (PSP), is a major advance in the field of non-contact measurement techniques in aerodynamics. This so-called PSP method allows one to obtain not only qualitative pressure images, but also quantitative absolute pressure values at the desired locations on the structure, without introducing flow-disturbing probes or affecting the surface of the structure [8]. Such a fluorescent image arising under the flow conditions in a wind tunnel can be recorded using a CCD camera (in the intensity method) or a photomultiplier with an appropriate filter for the luminescent emission (in the lifetime method). The final pressure map is obtained using complex image processing techniques.

Impurities, such as oil, solvents or large dirt particles in the test facility can adversely affect the achievable accuracy and can also damage the optical pressure sensor.

Conventional pressure measurement methods, based on pressure sensors installed at discrete points on the structure surface, may give better accuracie of measurement, but the two-dimensional PSP method has definite advantages. Firstly, in the case of these conventional techniques there are restrictions to creating holes on a thin wind tunnel structure; secondly the deformation of the structure due to several holes, and the geometry change associated with them due to the wind forces, leads to increased measurement errors.

The determination of the hole locations at the points of measurement must also be done prior to the preparation of the structure, that is, without exact knowledge of the flow pattern which will be occurring later.

Other methods of flow visualisation on the structure surface, such as the use of oil or phenol coatings, indeed give information on the wall streamline, but allow no quantitative expression of the pressure distribution. On the other hand, they facilitate the recognition of flow separation as well as the laminar–turbulent flow changeover.

2.3 TEMPERATURE SENSITIVE PAINT (TSP)

Temperature Sensitive Paint is a luminescent paint good enough to determine surface temperature distributions. TSP may be used for visualisation of heat transfer rate, boundary layer transition, flow separation and flow reattachment on the structure in transonic, supersonic and shock wind tunnels.

This technique is very similar to PSP except that the coating is temperature sensitive rather than pressure sensitive. The luminescence of TSP decreases as the temperature increases. As in PSP, a ratio of two images provides the temperature. In this case, one image is taken at a known, constant temperature, and the other is taken at the unknown conditions. The ratio of the two images is then converted to temperature using the appropriate calibration (which is too, close to PSP). As in PSP testing, during the acquisition of the images the test surface is exposed to excitation light in only a narrow frequency band. The detector is then notch filtered to pass only the luminescence band for the luminescent molecule.

Temperature sensitive paint (TSP) has recently been used to detect small temperature differences on aerodynamic structure surfaces [9]. These types of applications impose stringent performance requirements on a paint system. The TSP must operate over a broad temperature range, must be physically robust, must be polishable to at least the smoothness of the structure surface, must be easily applied over a large surface area, must be removable without damaging the structure surface finish to which it is applied, and must have sufficient sensitivity to detect small temperature differences.

2.4 TSP AND PSP PHYSICAL PRINCIPLES

The PSP measurement procedure is based on the deactivation of photochemically excited molecules, i.e. luminophores by oxygen molecules. By means of a special technique and application of suitable optical systems, static pressure values can be measured on the surface of the structure in the test facility (wind tunnel) and the flow phenomena can be assessed quantitatively. However, the precise determination of

pressure needs a measurement system with a high local resolution capability, as required in the transonic velocity range. Most PSP and TSP formulations use organic luminophores [10]. A molecule absorbs a photon [11] ultraviolet or blue (see figure 2.3 for TSP and figure 2.4 for PSP excitation and emission responses) and jumps to an excited energy level. There is a finite probability that the excited molecule will emit a photon at a longer wavelength, generally red, and collapse to the ground state.

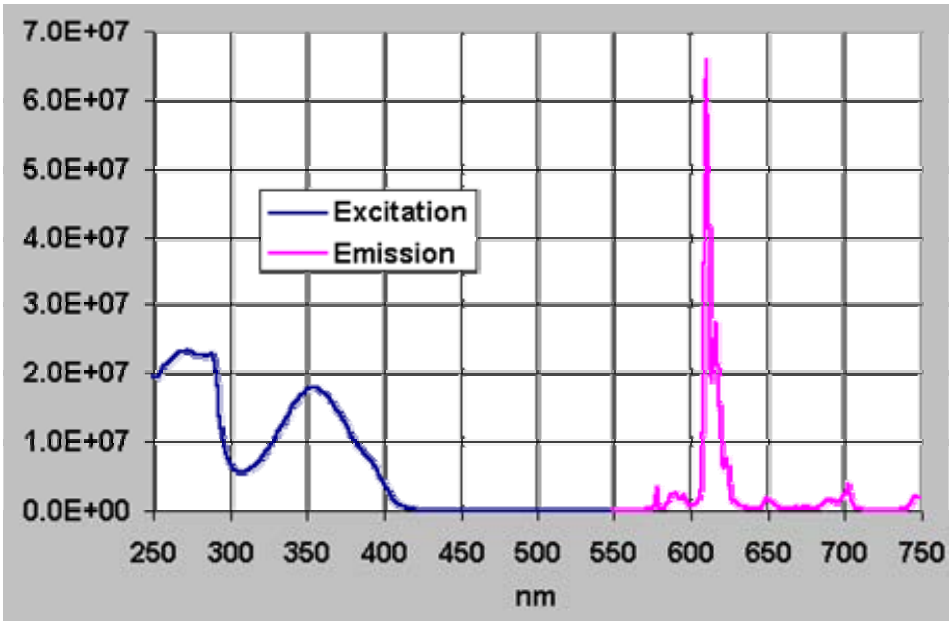

Figure 2.3. Emission and excitation spectra of Temperature Sensitive Paint TSP E40 from Optrod, Ltd.

There is also a finite probability that the excited molecule will interact with nearby molecules so that the excited molecule drops to ground state without emitting a photon. This process is commonly called "internal conversion". For some paint mixtures, the probability of internal conversion depends on temperature. As temperature increases, collision frequency increases, and the probability of internal conversion increases. Conversely, the probability of emitting a photon decreases, and the intensity of luminescent emission decreases. This phenomena is called thermal quenching and forms the basis for temperature sensitive paints. For a typical TSP, the brighter the surface, the lower the temperature.

Some paints have a small dependence on temperature. The probability of internal conversion depends strongly on the types of molecules in the paint film and the type of supporting polymer. For some luminescent molecules, if an oxygen molecule

collides with an excited probe molecule, the probability of deactivation is very large. This deactivation mechanism is commonly called oxygen quenching. The presence of oxygen reduces the probability of emission. If the paint is permeable to oxygen, then the number density of oxygen molecules inside the paint film depends directly on the partial pressure of oxygen at the paint surface. This quenching phenomenon forms the basis for a pressure sensitive paint. For a typical PSP, the brighter the surface, the lower pressure.

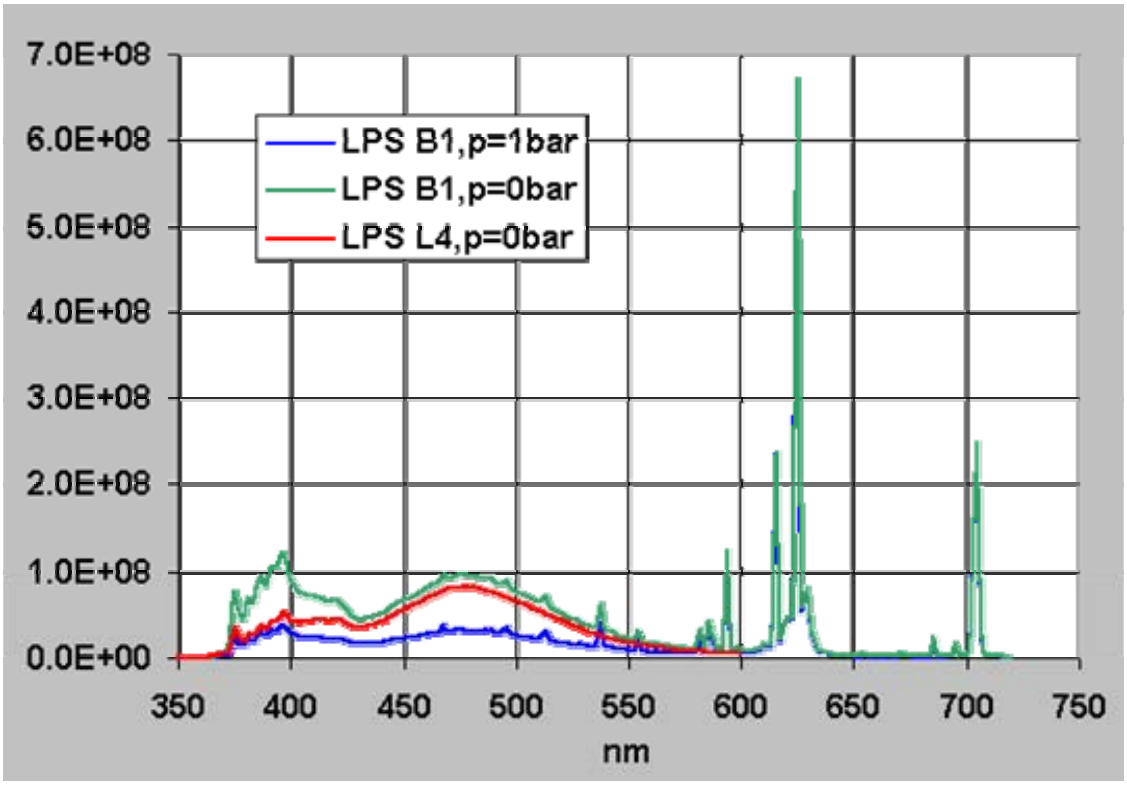

Figure 2.4. Emission spectra of different kinds of PSP also called Luminescent Pressure Sensor LPS, by Optrod Ltd.

2.5 CALIBRATION OF PRESSURE/TEMPERATURE SENSORS

Engler et al [12], showed that calibration of the optical pressure sensor is necessary for reconstructing a quantitative pressure image from the initial qualitative image of the flow phenomenon on the surface of the structure. This can be done in two different ways. In the first method, a test specimen is calibrated parallel to the structure paint and subsequently subjected to known pressures and temperatures in an external calibration chamber. In the second method, the entire structure can be calibrated in the wind tunnel itself, provided pressure changes can be statically produced at constant temperature in the test section. In the external calibration chamber the pressure and

temperature can be varied and consequently the temperature-dependent calibration constants described can be determined and related to pressure reconstruction. When large temperature distribution effects exist on the structure surface it is necessary to correct the pressure computations using thermocouples or IR cameras. The disadvantage of an external calibration procedure is that the test specimen can indeed be painted simultaneously with that of the structure, but will definitely not possess identical optical properties to the latter due to possible differences in the thicknesses of the layers.

Therefore, if possible, direct calibration of the model is always preferable, since the peculiarities of the structure geometry and the layer thickness are automatically taken into account. A special calibration cuvette must be mounted in direct contact with the model surface in which the pressure and temperature can be controlled. In addition, for every angle of attack of the structure a separate calibration data set can be calculated. Besides, there is the advantage that a separate calibration data set is available for each pixel of the recorded image of the wind tunnel model and therefore a higher pressure resolution is possible.

Oglesby, et al [13] discuss the dependence of the relative error in pressure with signal intensity, and a sensitivity analysis of the PSP technique.

2.6 CONCLUSIONS

The techniques, other than optical, just described are point wise and do not provide an area map for temperature/pressure. Optical techniques are non-contact and give two dimensional temperature/pressure measurements requiring special conditions to operate. Some fluid temperature measurement techniques that detect variations of the refractive index are inadequate for practical applications due to instability conditions.

TSP and PSP are simple and non-expensive measurement techniques that gives three-dimensional temperature and pressure data. The two techniques can be used in conjunction with velocimetry techniques.

2.7 REFERENCES

1. Childs P. R. N., Greenwood J. R. and Long A.., "Review of temperature measurement.", Review of Scientific Instruments, v 71, pp.2959-2978, 2000.

2. Goldstein R. J., "Optical Measurement of Temperature," Measurement techniques in Heat Transfer, edited by E. R. G. Eckert and R. J. Goldstein (AGARD, Slough, 1970), pp. 177-228.
3. Gaydon A.G. and Wolfhard H.G., Flames. Their Structure, Radiation and Temperature (Chapman and Hall, London, 1979).
4. Schwarz A., "Multi-tomographic Flame Analysis with a Schlieren Apparatus," Meas. Sci. Technol. Vol.7, pp. 406-413, 1996.
5. Pervushin G.E. and L. Nevsky B., " Composition for Indicating Coating.", Patent of USSR – SU 1065452 A, 1981 (In Russian).
6. McLachlan, B.G. and Bell, J.H., "Pressure-Sensitive Paint in Aerodynamic Testing." Exp. Thermal and Fluid Science, Vol. 10, pp. 470-485.1995
7. Tianshu Liu, Campbell, B.T., Burns, S.P. and Sullivan, J.P.,"Temperature- and Pressure-Sensitive Luminescent Paints in Aerodynamics.", Appl. Mech. Rev., Vol. 50, no. 4. (1997)
8. Navarra K., “Development of the pressure-sensitive paint technique for advanced turbomachinery applications”, Master of Science Thesis, Faculty of the Virginia Polytechnic Institute and State University, Blacksburg, VA,1997
9. Donald M. Oglesby, Billy T. Upchurch, Bradley S. Sealey, Bradley D. Leighty, Cecil G. Burkett, Jr. and Amir J. Jagharghi, "Development Of Temperature Sensitive Paints For The Detection Of Small Temperature Differences" , Isa 43rd International Instrumentation, Symposium, Orlando, Florida, May 4-8, 1997.
10. Lumb, M. D., "Organic Luminescence", published in Luminescence Spectroscopy, Academic Press, 1978, pp 94-146.
11. Crites R. and Morris M., "Parameter Sensing Paints-Current Capabilities and Future Potencial", McDonnell Douglas Aerospace, McDonnell Douglas Corporation. St. Louis, Missouri USA.
12. Engler R H, Klein Chr and Trinks O, "Pressure sensitive paint systems for pressure distribution measurements in wind tunnels and turbomachines",Meas. Sci. Technol. 11 (2000) 1077–1085.
13. Donald M. Oglesby, Chith K. Puram and Billy T. Upchurch, "Optimization of Measurements With Pressure Sensitive Paints", NASA Technical Memorandum 4695, Old Dominion University Norfolk, Virginia.

CHAPTER III

PATTERN DIFFRACTION ANALYSIS

3.0 INTRODUCTION

Conventional velocimetry has an intrinsic limitation because it yields 2D data, neglecting the third velocity component. For this reason, 3D-PIV has recently evolved as an area of research [1-16], with success at the cost of increasing complexity in its methodology. The increased complexity and the limited optical access found in most industrial applications, mean that many of the 3D-PIV techniques, although of academic interest, cannot be used in practical industrial applications. Some of the techniques used involve scanning light-sheets, stereoscopic views, holographic recording, parallel light-sheets, graded intensity light-sheets, or combinations thereof.

For practical applications restricted viewing eliminates stereoscopic approaches. Lack of robustness and ease to perform an experiment make of conventional holography an unattractive option due to the fact that it involves a wet developing process, thus is very slow to yield results. However, its large depth of field and storing capacity makes it a technique that should, under the correct environment, be used. When holography is used, the hologram is interrogated with the aid of cameras mounted on a high-precision 3D positioning system to resolve position based on particle image information. Scanning light-sheets are difficult to obtain for restricted optical access and high speeds, so they have not been tried in industrial conditions.

CCD cameras are nowadays being used as image recording medium, replacing conventional storage medium. Restricted optical access to flows of interest, such as those found in turbomachinery, means that only one camera is often what can be accommodated. An extension to the high-accuracy techniques for 3D, exploiting the digital representation of particle images in intensity as well as spatially, is described in previous work [17]. The analysis of digital PIV data typically involves two quantization steps: spatial and intensity quantization. It is of crucial importance to have reliable error bounds and a sufficiently accurate estimate of particle position, taking into consideration both types of quantization. The approach of using the Gaussian profile of the particle images to yield sub-pixel accurate position estimates has resulted in robust

measurements being taken to an accuracy of 1/10th pixel and 1% in velocity for the in-plane velocity, even in hostile industrial environments. The out-of-plane velocity estimate can be derived from the change in the ratio of amplitude to variance - known as the depth factor - of the Gaussian form, as a particle traverses the beam profile. However, such measurements are crucially dependent not only on an accurate position estimate but also on an equally accurate estimate of the amplitude and variance. The accuracy of the Gaussian profile fit using a Nelder-Meade optimization method was not capable of providing the required accuracies. Therefore, a development of the "locales" approach to position estimation was presented to achieve the desired objective of high accuracy PIV measurements. This approach makes use of the fact that by considering the possible digital representations of the Gaussian particle profile, regions of indistinguishable position can be derived. These positions are referred to as "locales". By considering the density, distribution, and shape of these locales, the available precision can be estimated and a high in-plane velocity accuracy can be obtained, while at the same time providing high-accuracy estimates of the depth factor. This work described the implementation of an efficient algorithm to provide velocity estimates, together with a discussion of the required constraints imposed on the imaging. The algorithm was used to map an experimental transonic flow field of the stator trailing edge region of a full-size annular cascade with an estimated error of 0.5%. The experimental results were found to be in good agreement with a previously reported steady state viscous calculation and PIV mapping. This work has been extended to a model, using simplified Fraunhoffer particle diffraction, for pattern-matching low-magnification 3D particle positioning, where particles are illuminated by monochromatic light [18]. Detailed theoretical models will then be useful for examining the effect of changing the aperture size on the observed particle images, the nature of image quality variation with the degree of particle defocus, etc. The most advanced such model is that based on the Generalised Lorenz-Mie theory which takes into account typical wave-fronts occurring in velocimetry applications, such as that of a light sheet which is elliptical, rather than the simple plane wave-front assumption of classical Lorenz-Mie theory. These models need to be validated against experimental data, so they may be used to find out what parameters are more important and therefore require further modelling, in order to achieve a quantitatively accurate representation of diffraction for a given position and particle characteristics.

The case of a spherical absorbing particle illuminated with monochromatic coherent light is considered. Three different illumination wavefront shapes and three viewing positions are used, and their relative merit is studied. The data obtained has been used to validate a model of particle scattering. An experimental 18 μm glass sample image is quantitatively compared to the calculated image for a Gaussian wavefront in forward scatter. This sample image in this viewing configuration has been chosen and described by a number of authors [19-23] and therefore was chosen as the sample case for the present research.

3.1 DIFFRACTION THEORY.

Adrian & Yao [24] first proposed using a quadrature to derive a nominal particle image diameter d_e according to:

$$d_e = \sqrt{(M^2 d_p^2 + d_s^2)} \tag{1}$$

where M is the lateral magnification of a lens, and d_p is the particle diameter.
In this equation

$$d_s = 2.44(M+1)\lambda \ f/\# \tag{2}$$

is the diameter of the point response function of a diffraction-limited lens measured at the first dark ring of the intensity distribution of the Airy disk, λ is the wavelength of the laser light used, and the focal length of the lens divided by the aperture diameter is f/#. As defined here, d_s may also be regarded as equal to the mean diameter of a laser speckle. Equation (1) shows the combined effects of magnification and image blurring and is an approximate quadrature determining the final diameter of the image. If the point response function and the geometric image were both Gaussian, equation (1) would be exact. In fact a Gaussian intensity distribution has been widely used as an adequate approximation to the Airy intensity distribution for velocimetry applications. Hence, equation (1) was used as an approximation, assuming the geometric image distribution is not too different from a Gaussian distribution function.
This approach represents a compromise between geometrical optics and a simplified approximation to the Lorentz-Mie Theory (LMT). However, the former is only valid

when the wavelength λ is much smaller than a length given by the standard deviation of surface roughness (scattering size), i.e., for optically smooth surfaces, and the latter is valid only when the particle is illuminated by a plane wave. The plane wave assumption holds when the scattering size of the particle is small compared to the characteristic dimensions of the incident beam, however in many cases this condition is not satisfied. Even if the plane wave assumption holds in a velocimetry set-up, the orientation of this wave-front relative to the viewing camera, generally changes across the field of view in such a way that major corrections are required for each particle's scattered image because particles are away from the optical axis and intensity distributions are not uniform over the whole image. This effect may not be readily apparent in applications involving thin light sheets and small particles, viewed by imaging lenses focussed on said light sheet, where the particle image approximates a Gaussian function and it is only a few pixels in diameter. However, where larger illumination depths are used the particle image diameter quickly extends substantially. Even for thin light sheets, where the CCD camera is adjusted so it saturates at the higher light intensities, diffraction rings become visible and these vary substantially with particle position within the light sheet down to a movement of as little as 20 μm.

An accurate analysis of the resulting diffraction field relies, for any position in the illuminated field, on the Generalised Lorentz-Mie Theory (GLMT). The GLMT deals with arbitrarily shaped incident beams [25,26]. It is thoroughly covered in a complementary article applied to velocimetry [27], where the full mathematical approach is described.

Simplifications in formulating the physical problem to be solved were considered, e.g., assuming a particle as a point function. However, such a treatment does not consider the particle complex refractive index, neither the incident laser power, nor the different intensity distributions exhibited by particles that are within an equal distance away from focus on opposite sides of the focal plane. The latter aspect is of crucial importance in making such an approach worthwhile, since if a particle position behind of and in front of the focal plane cannot be distinguished, the approach would be meaningless.

Initially, a theoretical model was signed which allows calculation of the image produced by a spherical absorbing particle illuminated with monochromatic light, including the amount of light energy falling onto a CCD sensor.

The imaging system under consideration has been described in detail in previous work by other authors [19,20] and can be summarised in Figure 3.1. This system was used as a starting point to validate the theoretical model and experimental results [28]. An object located on plane z_0 is illuminated with a He-Ne laser. The object image is formed by letting the scattered light go through a plano-convex lens (f = 90 mm, D = 32mm) onto a sensor (plane z_3). The image captured is then sent to a frame grabber.

Assuming that the laser/droplet interaction can be modelled as a linearly polarised plane wave incident on a spherical absorbing particle, the electromagnetic field distribution at any point can be obtained using the classic Lorenz-Mie theory [29,30]. These equations give the correct solution for the electromagnetic field at every point within the aperture located at z_1. The scalar diffraction theory outlined by Goodman [31] assumes that the x-component of the electric field will be the only significant electric field component throughout the imaging system, and makes use of the Fresnel approximation to propagate the field to the image plane.

The actual physical problem depicted in Figure 3.1 can be further simplified based on several experimental observations. Diffraction effects due to a given aperture size for the imaging system may be neglected, and if the aperture decreases the effective lens diameter the f/# is increased. As the aperture size becomes smaller, however, diffraction effects should be taken into account and the model needs to include the shape of the aperture.

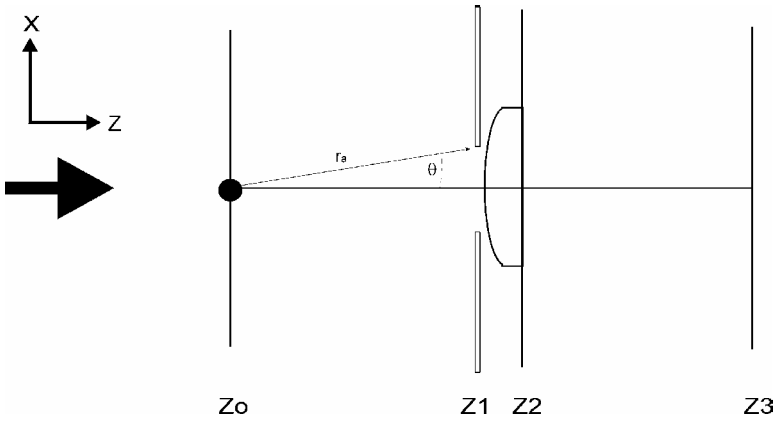

Figure 3.1. Simplified imaging layout.

3.2 THEORETICAL MODEL

The theory for a plane wave scattered by a spherical, isotropic, homogeneous, non-magnetic particle can be found in the literature [29,30]. More advanced theoretical and experimental techniques may be used, but these depend on the solution to the general problem where the scatter centre is illuminated by a laser beam, leading to the so-called Generalised Lorenz-Mie Theory (GLMT) [25,26]. The Gaussian beam case has been extensively explored and applied in the analysis and improvement of practical devices such as Phase Doppler systems. However, these techniques have not been previously applied to velocimetry. Velocimetry requires the application of GLMT techniques to the case of a beam with an elliptical cross-section, which is the case of laser sheets.

If we want a high interrogation area, it is necessary to expand the illumination source into a spherical wave. Moreover, in the case of holographic PIV the volume of interest is often illuminated by a spherical wave front, and it is therefore of interest to be able to estimate particle position from these holographic recordings. Thus, the need to develop the GLMT for the case of light scattered by spherical particles illuminated with a spherical wavefront. A spherical wave front makes particle positioning more exact because digital image representation changes makes it approximately 30 times more sensitive to a depth movement than the same particle illuminated by a plane wave front [32].

3.2.1 THE GLMT FOR A ELECTROMAGNETIC SPHERICAL WAVE

The GLMT is a generalization of Lorenz-Mie Theory for arbitrary incident shaped beams such as Gaussian, light sheet and top hat beams. GLMT describes the angular and integral properties (amplitudes, intensities, phase angle, cross section including radiation pressure cross-section) of the light scattered by an ideal sphere arbitrarily located in an arbitrary shaped beam. Formalism details can be found in reference [26].

The geometry used for the incident field and particle location is defined in Figure 3.2. Consider two Cartesian co-ordinate systems ($O_{PS}uvw$) and (O_pxyz), attached to the incident field and to the particle center respectively, with $O_{PS}u$ parallel to O_px and $O_{PS}v$ parallel to O_py. O_{PS} and O_p are the point source localization for a spherical wave and the particle center respectively. The incident field is linearly polarized, propagating

towards the positive w axis with the electric field E parallel to the u axis. The scattered light is observed at point M'(r,θ,ϕ), where r, θ, ϕ are spherical co-ordinates attached to the particle system ($O_p$xyz).

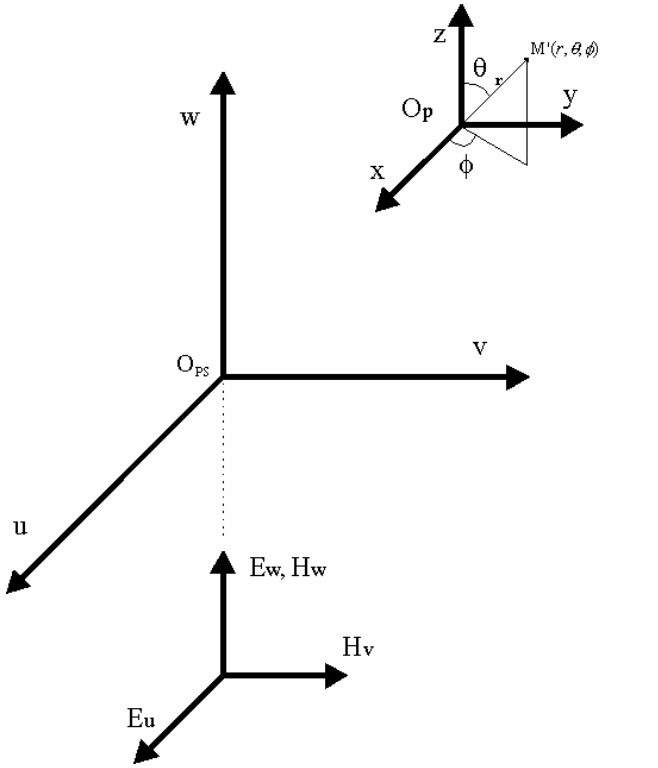

Figure 3.2. System geometry for the GLMT calculations using a spherical wavefront.

3.2.2 INCIDENT FIELD DESCRIPTION

This section derives the vectorial form of the incident field, for a vectorial spherical wave. The expressions for this wave assume its most convenient form with the Hertz vector, which represents the radiation emitted by a linearly oscillating dipole. The magnetic field lines are circles about the direction of oscillation, while the electric field lines are the meridian planes of that direction.

A physical light source contains all possible directions of oscillation. Such a source emits an average field in which no single direction is preferred. The field intensity is therefore spherically symmetric. Furthermore, a field intensity emanating from an ideal lens or a pinhole is spherically symmetric too. Thus, we may model the electromagnetic spherical wave as it emanates from a point source of unit strength.

In the *TM*-mode, the electric field *E* is polarized parallel to the *u*-axis, i.e. E_v=E_w=0 and consequently H_u=0. We consider a point source of unit strength located at the position (u_0,v$_0$,w$_0$). Thus, the field equation in the presence of a source satisfies the inhomogeneous wave equation [33].

$$\left(\frac{\partial^2}{\partial u^2}+\frac{\partial^2}{\partial v^2}+\frac{\partial^2}{\partial w^2}+k^2\right)E_u=\delta(u-u_0)\delta(v-v_0)\delta(w-w_0) \tag{3}$$

Where $k=\omega_0(\varepsilon_0\mu_0)^{1/2}=2\pi/\lambda$, λ is the point source light wavelength and ω is the angular frequency. In the *TE*-mode, the magnetic field *H* is polarized parallel to the *u*-axis, i.e. H_v=H_w = E_u= 0and H_u satisfies equation (3).

Equation (3) can be solved by using Green's functions. The Green's function that satisfies the inhomogeneous wave equation is given as:

$$G(r_1,r_2)=\frac{e^{ik|r_1-r_2|}}{4\pi|r_1-r_2|} \tag{4}$$

where r_1 and r_2 are position vectors representing the field point and source point, respectively. Thus, the electric field can be obtained from Green's function expressions given by equation (4), as:

$$E_u=\frac{e^{ik|r_1-r_2|}}{4\pi|r_1-r_2|} \tag{5}$$

Equation (5) represents the electric field of a diverging spherical wave from a point source. From equation (5), we obtain by simple projections the field components in the (r,θ,ϕ) system:

$$E_r=\cos\phi\,\sin\theta\,\frac{e^{(ik|r_1-r_2|)}}{4\pi|r_1-r_2|} \tag{6}$$

$$E_\theta=\cos\phi\cos\theta\,\frac{e^{(ik|r_1-r_2|)}}{4\pi|r_1-r_2|} \tag{7}$$

$$E_{\phi} = sin\phi \frac{e^{(ik|r_1 - r_2|)}}{4\pi|r_1 - r_2|} \tag{8}$$

In a similar way the magnetic components can be determined:

$$H_r = sin\phi sin\theta \frac{e^{(ik|r_1 - r_2|)}}{4\pi|r_1 - r_2|} \tag{9}$$

$$H_{\theta} = sin\phi \cos\theta \frac{e^{(ik|r_1 - r_2|)}}{4\pi|r_1 - r_2|} \tag{10}$$

$$H_{\phi} = -\cos\phi \frac{e^{(ik|r_1 - r_2|)}}{4\pi|r_1 - r_2|} \tag{11}$$

The radial components E_r and H_r play a special role in the theory because we need to know them to derive the Beam Shape Coefficients (BSC).

3.2.3. SCATTERED NEAR FIELD COMPONENTS

According to reference [26] the scattering field components in the near field are described as:

$$\tilde{E}_r^{(s)} = -kE_0 \sum_{n=1}^{\infty} \sum_{m=-n}^{+n} C_n^{PW} a_n g_{n,TM}^m \left[\xi_n(\alpha\tilde{r}) + \xi_n^{"}(\alpha\tilde{r})\right] P_n^{|m|}(\cos\theta) e^{(im\phi)}, \tag{12}$$

$$\tilde{E}_{\theta}^{(s)} = -\frac{E_0}{\tilde{r}} \sum_{n=1}^{\infty} \sum_{m=-n}^{+n} C_n^{PW} \begin{bmatrix} a_n g_{n,TM}^m \xi_n^{'}(\alpha\tilde{r}) \tau_n^{|m|}(\cos\theta) \\ + m b_n g_{n,TE}^m \xi_n(\alpha\tilde{r}) \Pi_n^{|m|}(\cos\theta) \end{bmatrix} e^{(im\phi)}, \tag{13}$$

$$\tilde{E}_{\phi}^{(s)} = -\frac{iE_0}{\tilde{r}} \sum_{n=1}^{\infty} \sum_{m=-n}^{+n} C_n^{PW} \begin{bmatrix} m a_n g_{n,TM}^m \xi_n^{'}(\alpha\tilde{r}) \Pi_n^{|m|}(\cos\theta) \\ + b_n g_{n,TE}^m \xi_n(\alpha\tilde{r}) \tau_n^{|m|}(\cos\theta) \end{bmatrix} e^{(im\phi)}. \tag{14}$$

$$\tilde{H}_r^{(s)} = -kH_0 \sum_{n=1}^{\infty} \sum_{m=-n}^{+n} C_n^{PW} a_n g_{n,TE}^m \left[\xi_n(\alpha\tilde{r}) + \xi_n''(\alpha\tilde{r}) \right] P_n^{|m|}(\cos\theta) e^{(im\phi)}, \tag{15}$$

$$\tilde{H}_\theta^{(s)} = \frac{H_0}{\tilde{r}} \sum_{n=1}^{\infty} \sum_{m=-n}^{+n} C_n^{PW} \begin{bmatrix} m a_n g_{n,TM}^m \xi_n(\alpha\tilde{r}) \Pi_n^{|m|}(\cos\theta) \\ - b_n g_{n,TE}^m \xi_n'(\alpha\tilde{r}) \tau_n^{|m|}(\cos\theta) \end{bmatrix} e^{(im\phi)}, \tag{16}$$

$$\tilde{H}_\phi^{(s)} = \frac{iH_0}{\tilde{r}} \sum_{n=1}^{\infty} \sum_{m=-n}^{+n} C_n^{PW} \begin{bmatrix} a_n g_{n,TM}^m \xi_n(\alpha\tilde{r}) \tau_n^{|m|}(\cos\theta) \\ - m b_n g_{n,TE}^m \xi_n'(\alpha\tilde{r}) \Pi_n^{|m|}(\cos\theta) \end{bmatrix} e^{(im\phi)}. \tag{17}$$

Where,

$$C_n^{PW} = \frac{1}{k} i^{n-1} (-1)^n \frac{2n+1}{n(n+1)} \tag{18}$$

and,

$$\alpha = ka \tag{19}$$

is the size parameter, k is the wave number of the incident beam, a is the particle radius, a_n and b_n are the partial-wave scattering amplitudes of plane-wave Mie theory, ψ_n, χ_n, and $\xi_n = \psi_n - i\chi_n$ are the Riccati-Bessel functions, which are related to the Bessel functions of half-integer order; $P_n^{|m|}(\cos\theta)$ are the associated Legendre polynomials, depending uniquely on the observation direction. $\bar{n}$ is the complex refractive index of the sphere, and $\tilde{r} = r/a$ is the normalized distance from the particle to the scattered light observation point M'. All variables having the symbol ~ are normalized with respect to the particle radius. Primed quantities denote differentiation with respect to the argument of the function. The beam shape coefficients, $g_{n,TM,TE}^m$, are specific to GLMT and involve the characterization of the incident beam. They are described by use of expansions into partial waves expressed in the spherical coordinate system (r,θ,ϕ), and can be determined from the mathematical expressions of the radial electric field E_r (for $g_{n,TM}^m$) and the radial magnetic field H_r (for $g_{n,TE}^m$), by use of the quadrature, the finite series method or localized approximations.

3.2.4 THE BSC COMPUTATIONS

Different methods have been developed to compute the BSC's. A rigorous approach is based on the surface integral [34]. The coefficients of a Gaussian beam can also be computed by finite series for on-axis particle positions [35]. The localized approximation of the beam shape coefficients leads to the fastest algorithm, as has been demonstrated by Lock [36]. In this thesis we used a combination of the localized approximation and integral quadrature given in reference [37].

To ease the procedure outlined in reference [37], the absolute value $|r_1 - r_2| = \sqrt{(x - x_0) + (y - y_0) + (z - z_0)}$ in equations (6) and (9) is approximated by taking the first two terms of the binomial expansion,

$$|r_1 - r_2| = z\left[1 + \frac{1}{2}\left(\frac{x - x_0}{2}\right)^2 + \frac{1}{2}\left(\frac{y - y_0}{2}\right)^2\right] \tag{20}$$

which can be transformed into spherical coordinates, as:

$$|r_1 - r_2| = \left[(r\cos\theta - z_0) + \frac{(r\sin\theta)^2 - 2r\sin\theta(x_0\cos\phi + y_0\sin\phi) + (x_0^2 + y_0^2)}{2(r\cos\theta - z_0)}\right] \tag{21}$$

Equation (21) is substituted in equations (6) and (9). For space shortness only the radial electric field is shown:

$$E_r = \frac{\cos\phi\,\sin\theta}{\left[(r\cos\theta - z_0) + \frac{(r\sin\theta)^2 - 2r\sin\theta(x_0\cos\phi + y_0\sin\phi) + (x_0^2 + y_0^2)}{2(r\cos\theta - z_0)}\right]} \times \exp\left(ik\left[(r\cos\theta - z_0) + \frac{(r\sin\theta)^2 - 2r\sin\theta(x_0\cos\phi + y_0\sin\phi) + (x_0^2 + y_0^2)}{2(r\cos\theta - z_0)}\right]\right) \tag{22}$$

Consider the simplest case where the particle is located on axis, thus the radial electric field is reduced to:

$$E_r = \frac{\cos\phi \sin\theta}{\left[(r\cos\theta - z_0) + \frac{(r\sin\theta)^2}{2(r\cos\theta - z_0)}\right]} \times \exp\left(ik\left[(r\cos\theta - z_0) + \frac{(r\sin\theta)^2}{2(r\cos\theta - z_0)}\right]\right) \tag{23}$$

The BSC's for a particle located on axis are given as, viz. [37]:

$$g_{n,TM}^{\pm 1} = \frac{1}{2\pi E_0}\int_0^{2\pi} \hat{G}\left[E_r(r,\theta,\phi)\right]\exp\left(-i(\pm 1)\phi\right)d\phi \tag{24}$$

$$g_{n,TE}^{\pm 1} = \frac{1}{2\pi H_0}\int_0^{2\pi} \hat{G}\left[H_r(r,\theta,\phi)\right]\exp\left(-i(\pm 1)\phi\right)d\phi \tag{25}$$

Applying the procedure outlined in reference [37] , we obtain the following expressions for the BSC's

$$g_{n,TM}^{1} = g_{n,TM}^{-1} = \frac{A}{2E_0} \tag{26}$$

$$g_{n,TE}^{1} = -g_{n,TE}^{-1} = -\frac{iA}{2E_0} \tag{27}$$

Where *A* is given as:

$$A = \frac{-1}{z_o + \frac{R^2}{2z_0}}\exp\left(-ikz_0\right)\exp\left(-ik\frac{R^2}{2z_0}\right) \tag{28}$$

where *R* is the rescaled coordinate expressed as:

$$R = kr = n + 1/2 \tag{29}$$

3.2.5. NUMERICAL RESULTS

The GLMT for the case of an electromagnetic spherical wave will be compared with the classical Lorenz-Mie theory that is, the plane wave case. Close to the source we have a spherical electromagnetic wave, but as the light source moves away from the particle the electromagnetic wave can be considered as plane. We will use this fact to compare our proposed model.

The technique used to compute the Ricatti-Bessel functions, and the coefficients a_n, b_n are described elsewhere [38]. Computation of the associated Legendre function is accomplished by using standard recursion formulas such as those presented by Abramowitz and Stegun [39]. All electric field quantities are normalized based on an assumed uniform incident electric field of unit amplitude.

The observation point M' receives light from the scattered and incident waves. The total field in the forward scatter case is composed by the incident plus scattered fields. The intensity value at the observation point M' is given by Poynting vector, as is the direction of propagation, and is symmetrical to the axis $O_p z$. Hence, the intensity value needs only to be calculated for one axis, like $O_p y$. Figure 3.3 shows forward scatter plots of a 220 μm glass spherical particle illuminated with a He-Ne laser, as the illumination source was moved away from the particle to 0.1, 0.5, 1.0, 3.0 and 10.0 m, considered for practical purposes as infinity. The vertical axes in these plots show the scattering calculations for the electromagnetic spherical wave case normalized to the central value of the intensity found at the start of the $O_p y$ axis, shown as the horizontal axes in the plots. The plots show that the particle scattering when using a spherical wave front approximates, in the limit of a large distance, to the plane wave scattering case.

The model is also compared to experimental Fraunhofer in-line holograms of spherical particles [32]. The experiment used coherent light from a laser passed through a condensing lens-pinhole system to produce a diverging beam, which illuminated spherical particles introduced into its path, at a distance z_o from the pinhole. Light diffracted by the particles adds coherently with light that has not been diffracted, i.e. background light. The resulting amplitude distribution forms an interference pattern whose fringes are recorded as intensities on film, at a distance z_1 from the particle. The interference pattern is symmetrical about the z axis which is the optical axis originating at the pinhole. Figure 3.4 shows the results from the theoretical model when using the same conditions than those for the experimental result (two spherical particles of

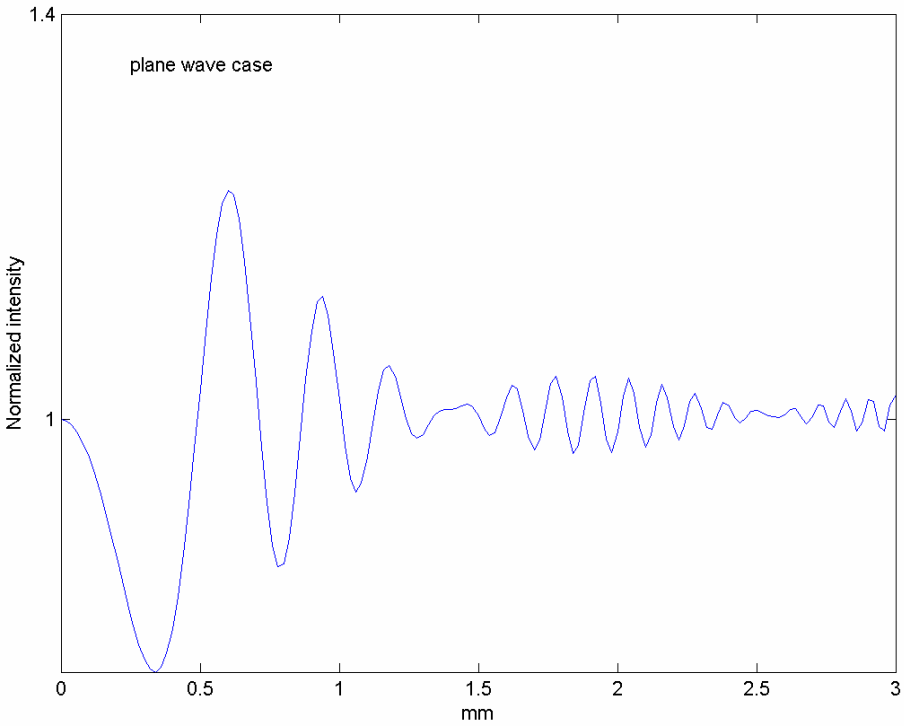
plane wave case
Normalized intensity
1.4
1
0
0.5
1
1.5
2
2.5
3
mm

a)

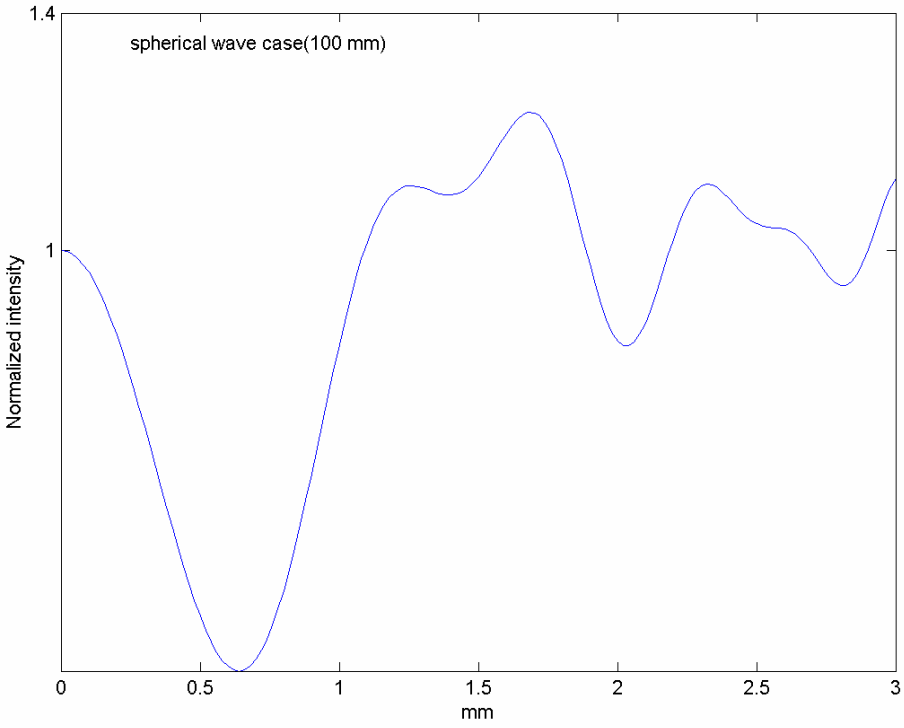
spherical wave case(100 mm)
Normalized intensity
1.4
1
0
0.5
1
1.5
2
2.5
3
mm

b)

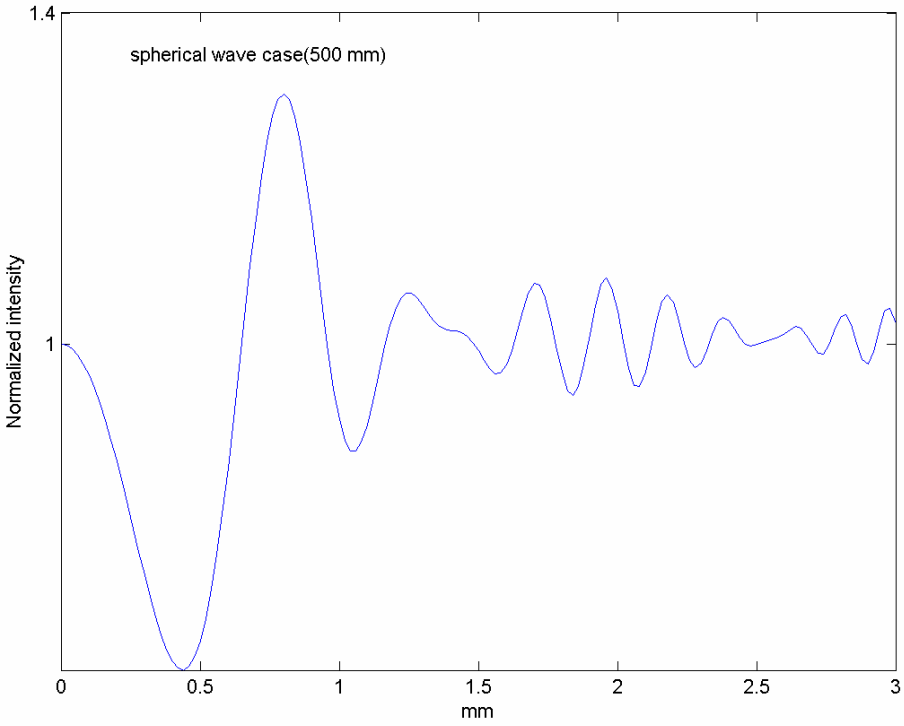
spherical wave case(500 mm)
Normalized intensity
1.4
1
0
0.5
1
1.5
2
2.5
3
mm

c)

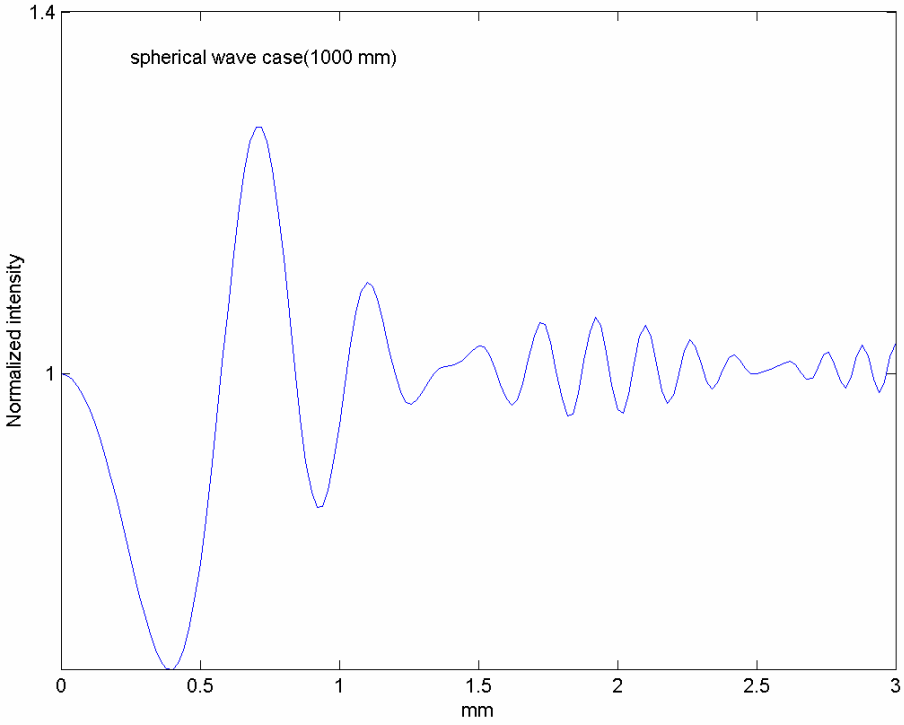
spherical wave case(1000 mm)
Normalized intensity
1.4
1
0
0.5
1
1.5
2
2.5
3
mm

d)

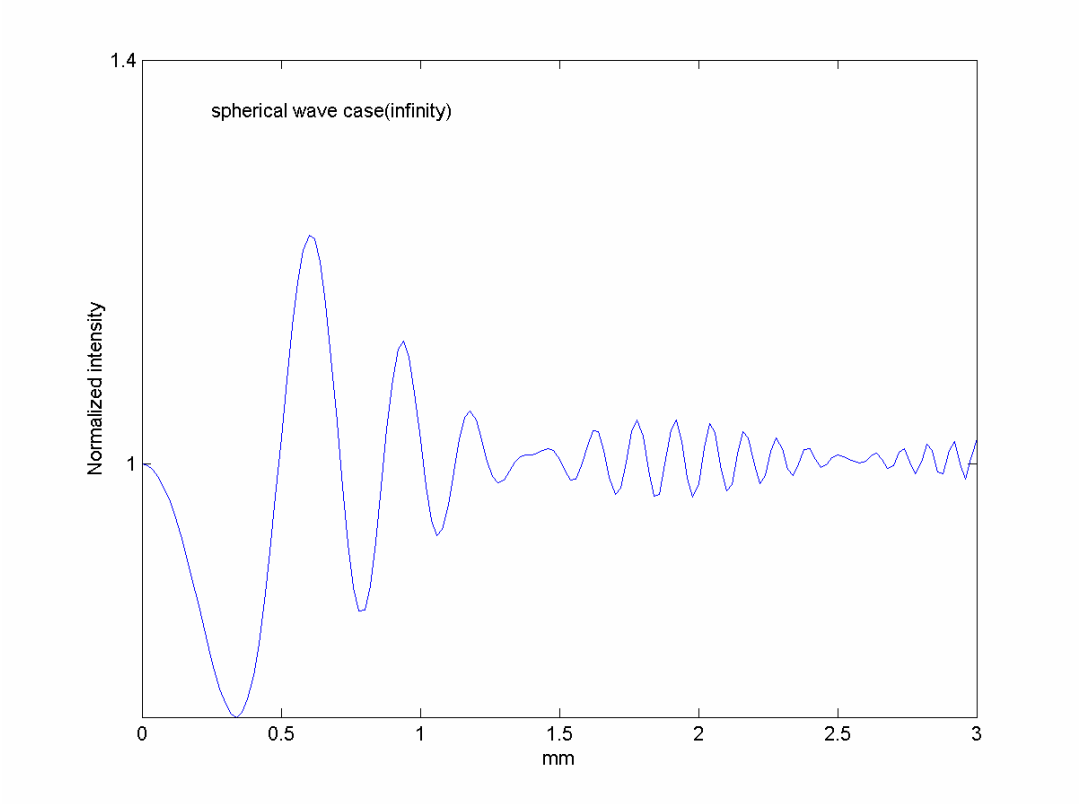

e)

Figure 3.3 Plane wave and spherical wave case comparison for a 220 μm glass spherical particle: a) plane wave, b) 0.1m, c) 0.5m, d) 1.0m and e) 10.0 m (considered for practical purposes as infinity) of distance from the particle to the illumination source. The horizontal axes represent the radial intensity, while the vertical axes represent normalized intensity values.

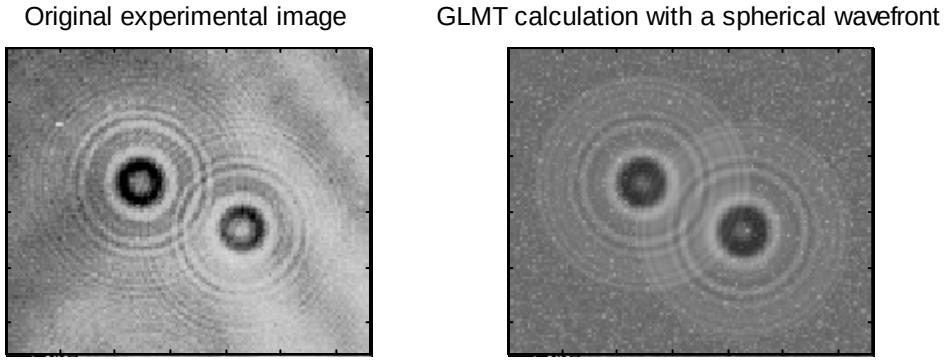

Figure 3.4. Particle image scattering computed using the GLMT with a spherical wavefront. The same conditions as those for the experimental data were used, particles separated by 1 cm.

diameter 220 μm, separated 1 cm from each other) where some background fringes are seen to dark some places on the experimental image. These fringes are due to

experimental conditions typical of a holographic experiment, and are not simulated in the theoretical model, hence the theoretical model and experimental data show good agreement. Figure 3.5 shows the convenience of using the GLMT with an electromagnetic spherical wave, depicting the difference with the plane wave case for the same experimental conditions.

Beginning with the classical treatment, the geometry for a simplified model was used. The experimental results using the classical LMT treatment however, proved insufficient to provide high accuracy 3D particle positioning and therefore the algorithm was extended to use a GLMT treatment [40] for a plane wave-front, Gaussian beam and a light sheet.

Moreover, experiments pointed towards the need to consider third-order Seidel aberrations in a typical lens used for velocimetry, such as a 90mm SIGMA Macro, in order to increase the accuracy of the model and thereby the accuracy of the particle positioning algorithm. The aberrations included in the model are sphericity and coma.
Currently, aperture shapes other than circular are being considered, for instance typical commercial lenses have 6 blades to form an aperture. It has been shown that when the aperture size is reduced the effect produced needs to be taken into consideration and at low apertures the particle image is degraded as shown in figure 3.6.
The GLMT code produced for this research work was verified in a number of different ways, namely, the Legendre polynomials were derived and compared to established algorithms [39], the numerical integration algorithm was a simple Gauss quadrature scheme, the Ricatti-Bessel coefficients were derived from the work in [38] for convenience, though faster more modern algorithms exist. For the case of a plane wave-front, the calculations were compared to the experimental results and calculations of Schaub et al [20]. Gaussian wave-fronts were also compared to experimental/computational results and found to be in good agreement. The GLMT algorithm itself was extensively compared to the results discussed by Gouesbet et al. and found to coincide well, within computational limitations [25,40,41]. No experimental data exists for comparison of the diffraction image arising out of elliptically-shaped wave-fronts. Therefore, the GLMT predictions could only be compared to the experimental images shown here.

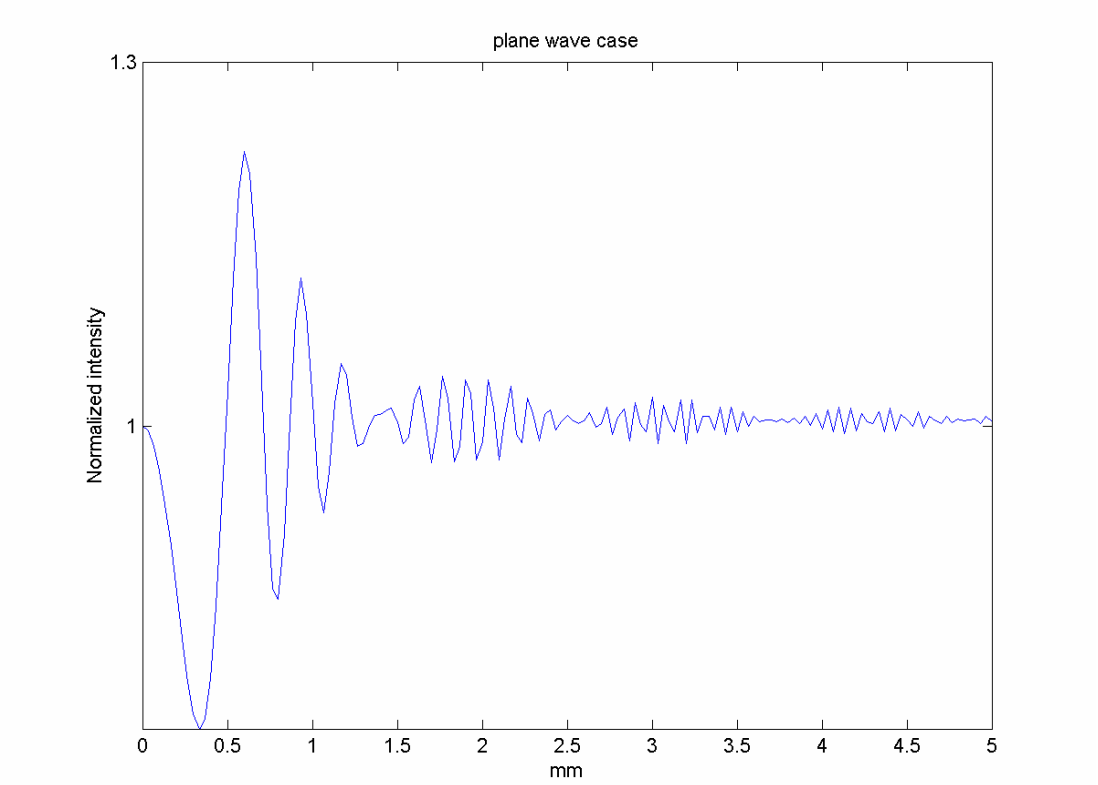

a)

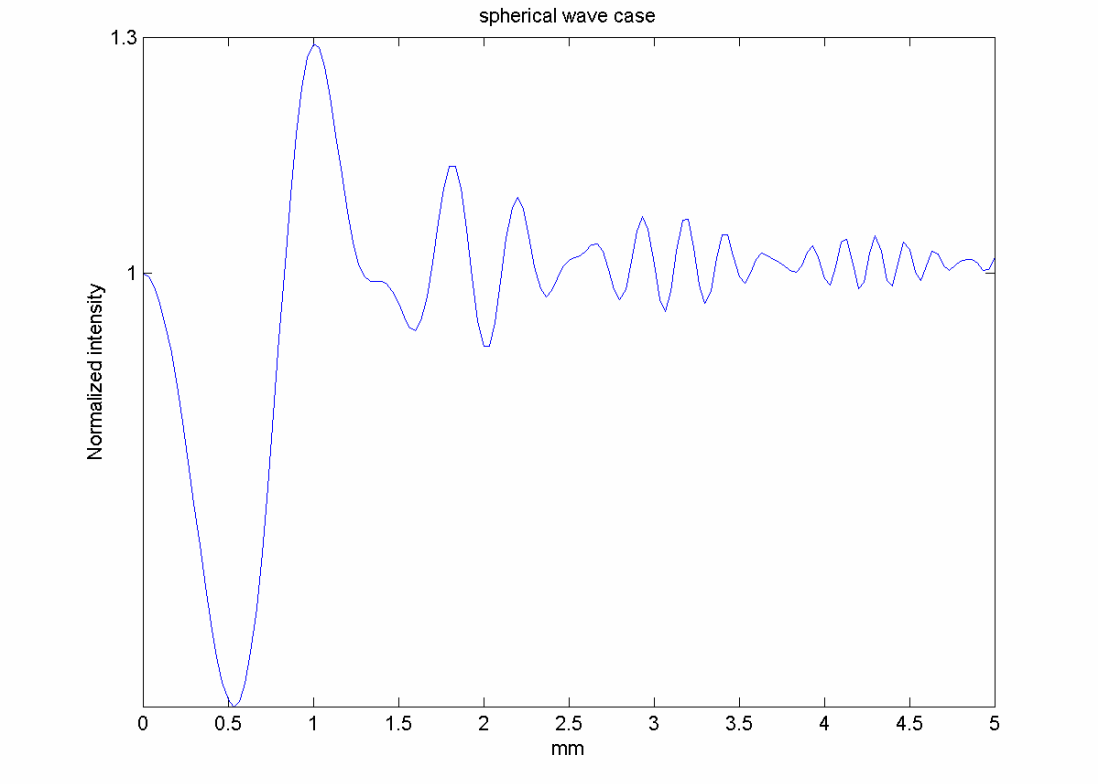

b)

Figure 3.5. Plane wave and spherical wave case comparison for the same conditions as in the experimental data. Vertical and horizontal axes as in figure 3.3.

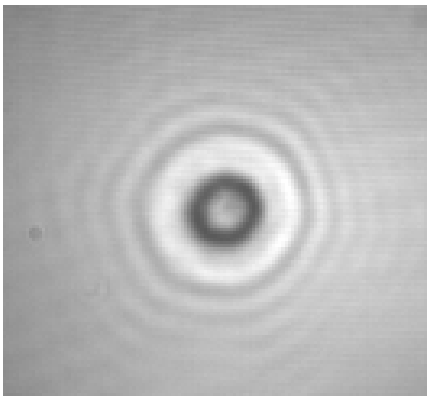

Figure 3.6. Aperture effect of the six blades commercial lens in particle scattered images. The image was taken with a SIGMA 90 lens, f# = 8, for a polystyrene particle size of 18 μm and λ = 632.8 nm. The slight asymmetry is due to camera misalignment.

To illustrate the differences between the three illumination schemes, figure 3.7 shows the intensity distribution as a function of viewing angle for a particle of 5 μm, using the Generalised Lorenz-Mie Theory. According to this figure, at 0º (forward scatter) and 180º (back scatter) the distribution is symmetrical for a given ratio in three co-ordinates, so the calculation for the particle diffraction pattern is easier to perform than that at 90º or 270º (side scatter), where the distribution shape of the diffraction pattern is not symmetrical and the calculation needs to be made at each point in the aperture, and the radial symmetry simplification does not apply. Moreover, figure 3.7 shows the vast differences in intensity between viewing positions and illumination wavefronts. Therefore, it is advantageous to carry out bespoke tuning of the CCD camera, including switching to manual gain from automatic gain, to exploit to the full the CCD dynamic range available. Finally, predictions using the GLMT confirmed the observation made by other authors [19-23] that particle images are different on either side of the focus plane.

3.3 EXPERIMENTAL ARRANGEMENT.

The experimental set-up allows recording forward scattering, as in [20], The results were compared with backward scattering, and the more conventional orthogonal viewing with a thin light-sheet used in PIV. Figure 3.8 shows this experimental set-up for the three configurations. Figure 3.8a shows a view of the particle in the conventional PIV side-scatter mode. The slide used to holds the particle was antireflection coated to optimise the signal-to-noise ratio (SNR). In order to view the same particle in back-

scatter, a polarising beam-splitter was used in conjunction with a ¼-wave retarder plate like in figure 3.8b. Figure 3.8c shows the typical forward-scatter configuration.

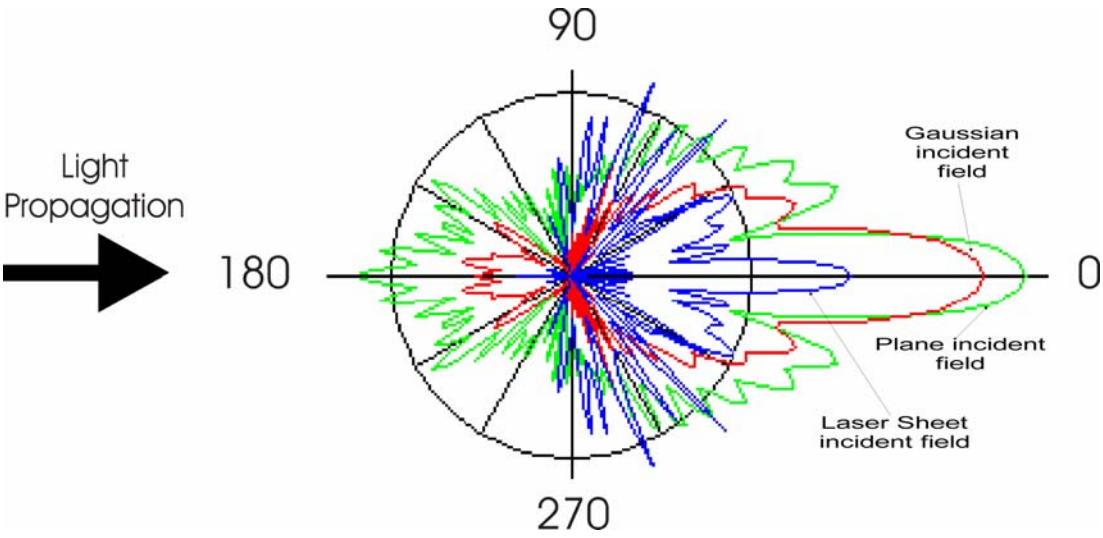

Figure 3.7. Normalised scattering pattern for a water particle 5 μm in diameter suspended in air, using different incident wavefields. (λ = 532nm, n = 1.3372 + 1.4991e-9i).

Three types of illumination were used, a plane wave-front as in classical Lorentz-Mie Theory , a Gaussian wave-front such as those used in particle-sizing, and a light sheet as in PIV. The incident beam's power is taken into account by the model used. So, although a Nd:YAG is normally used, rather than a He-Ne (at 20mW and λ = .6328 μm.) as employed for these tests, only the difference results in a change of energy delivered to the particle and a consequent change in the particle scattered field energy which is expressed in Luxes in the code, in order to allow simpler calibration of CCD camera response. It is worth mentioning that the code developed does not make any simplifying assumptions based on size. Therefore, if the code could be validated for larger particles, it can also be applied to micron-sized particles, as commonly employed in PIV. Larger particle sizes were chosen for handling convenience only.

Different kinds of particles and sizes were investigated. These ranged from water droplets [42], glass spheres to pollen. Actual particle sizes were verified by microscopic techniques. Available sizes ranged from 4 μm to 150μm.

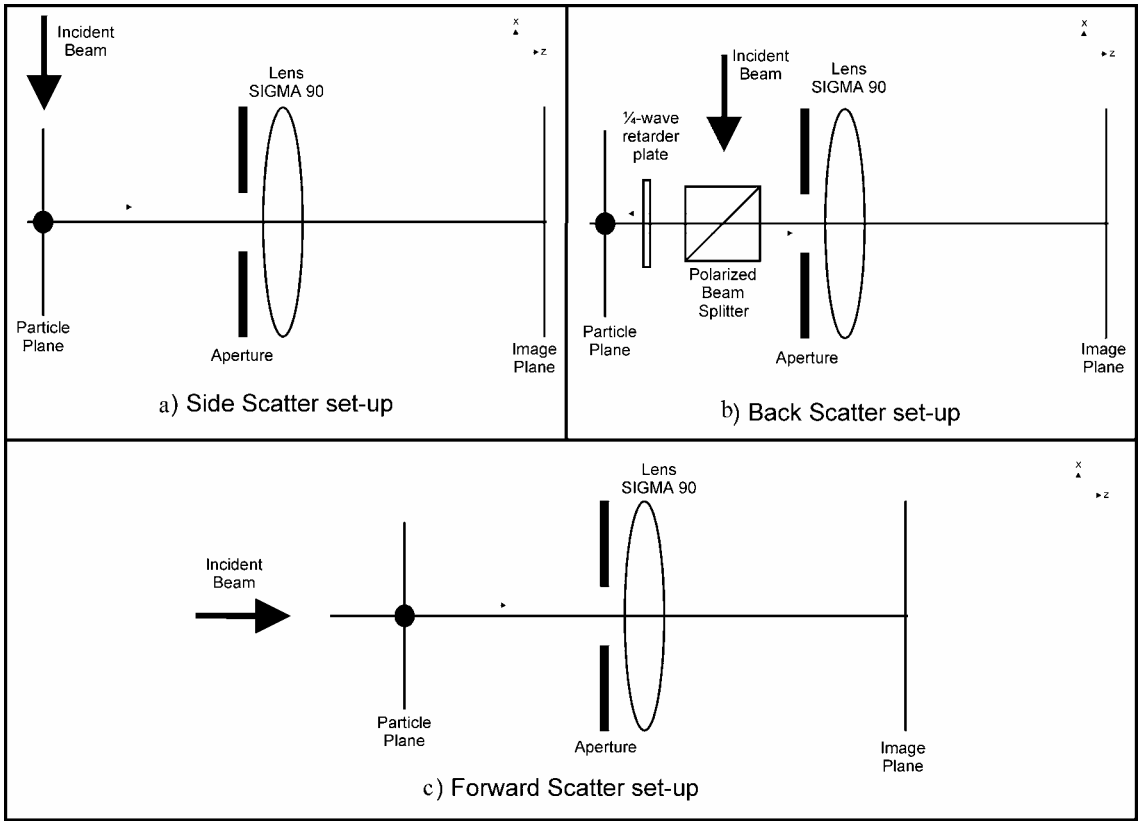

Figure 3.8. Experimental set-up. Object plane is at 102 mm and image plane is at 801 mm from the lens. In the back scatter configuration, 19 mm are added to the objet plane distance to in order to compensate prism optical path difference.

3.4 RESULTS AND DISCUSSION.

The initial part of the research work reported here consisted in carrying out a first approximation simulating particles as pin-holes and observing the variation of the diffraction pattern as defocus was applied. For these tests the arrangement used was for a forward scatter experiment as reported by other workers [19,20]. The laser beam was collimated to a diameter of approximately 2 cm. Pin-hole sizes of 5, 13, 15, 25 and 50 μm were tested. For a 5 μm pin-hole the diffraction pattern was too small to study and only the first few rings were visible, which were insufficient for code validation. As pin-hole size increased, more rings were visible. At 50 μm, corresponding to the experimental data of Schaub et al. [20], the first 4 rings had high visibility and an adequate SNR. A point of interest is that when a non-collimated beam was used defocus effects were more noticeable, with qualitative differences being visible for movements of as little as 10 μm, while for a collimated beam qualitative changes were only visible for a 20 μm movement. This is consistent with theoretical calculations, and

also with simplified calculations and experimental results dating back to 1970 using a simplified Fraunhofer treatment [32], showing that plane wave sensitivity to defocus is less than for spherical wavefronts, with Gaussian wavefronts having a sensitivity in between these two.

The next step in the research was to devise a method to work with particles. The main problem to be solved is that of working with a single particle at a given time and at a fixed position in space, with a particle size measured with microscopic techniques. To derive 3D information, data from the x-y position and the diffraction pattern is used to yield the out-of-plane component. For this, it must be assumed sphericity of particles so that seeding with pollen which is not spherical was not studied. To start with, spherical glass and polystyrene particles were used.

Several methods were tried to isolate a single particle, a layer of monodisperse polystyrene spheres was deposited on a slide, with a range of sizes tested from 3 μm to 13 μm. However, some problems were encountered as the solvent in which the polystyrene spheres were held evaporated, leaving cloudy contours on the slide surface. This noise precluded an accurate measurement of diffraction rings. Some were isolated and could be investigated but when defocus was increased near-by particles caused problems. This approach was abandoned.

Glass particles not suspended in a solvent were used in sizes from 4 μm to 150 μm. Particles, small enough to be of interest and large enough to be easy to handle, in the range 10 μm to 30 μm were selected from this distribution. These particles were deposited on a slide and stuck to the glass surface by leaving some residual humidity on the slide. This arrangement worked well for forward scatter and for large particle sizes. For smaller sizes, the system did not yield adequate ring definition due to noise. So, initially the larger 18 μm particles were selected.

Tests were carried out for three scattering configurations: back, forward and side scatter, each employing three illumination wavefronts: plane, Gaussian and a sheet of light. Under the three configurations, the distance between particle image rings appeared unaltered, qualitatively, when using different wave-fronts for particle illumination because they were all at the same out of focus distance. However, an overall difference in intensity was recorded when using the three illumination wavefronts, where this intensity variation is given by illumination wavefronts and not by incident beam intensity according to our numerical model.

In forward scatter, noise was less than expected, while both, the diffracted light from the particle and the undiffracted background light intensity, had to be adjusted to match it to the CCD camera gain to avoid saturation. In back scatter, noise increased primarily due to the fact that the scattering field goes through more optical elements. Qualitatively, the images were similar to those in forward scatter.

The interesting point to note for the side scatter case, was that the number of rings did vary significantly compared to those in back and forward scatter. This effect is due to the asymmetry of the particle field in side scattering, needing full aperture calculation rather than a simplified radial calculation. Moreover, these scattering characteristics vary over a very narrow angular movement such that the particle image varies with even a small angular displacement, leading to an almost impossible matching, with sufficient accuracy given experimental parameter uncertainty, of side scattering velocimetry images with theoretical predictions.

In order to compare the results obtained here with those obtained by other workers, particle images in forward scatter were selected for comparison to theoretical calculations using the GLMT, to other experimental data and to image predictions using other codes such as that of the University of Nebraska [28] as well as existing classical Lorenz-Mie code.

With expected CCD camera noise and experimental variations, the results presented here are encouraging, they were very close to those obtained by Schaub et al. [20], both in terms of the experimental images and numerical calculations for a comparable image size. Note, however, that the results reported in this thesis are the first where a quantitative comparison of numerical predictions to experimental images are given. Figure 3.9a, 3.9b and 3.9c shows enhanced experimental particle images for three viewing configurations: forward, side and back scatter respectively. The particle size is 18 μm and is located 2.0 mm out of focus. Figure 3.9d, 3.9e and 3.9f shows enhanced experimental particle images in side-scatter viewing for a Gaussian beam, a light sheet and plane wavefront, respectively. In this case the particle is located 1.5 mm out of focus. As previously stated, these images are similar but of varying intensity.

An important aspect of the research was a preliminary study of the most significant sources of error, both with a view to minimize them and to estimate the likely sensitivity and accuracy of the method. There are five main types of error involved in this experiment:

Mathematical modelling of a physical problem - because of the complexity of the physical problem, a variety of simplifying assumptions need to be made which have an impact on the ultimate accuracy of the technique. These involve assumptions about particle characteristics such as homogeneity and non-magnetic, symmetry assumptions, the thin-lens approximation, Seidel aberrations, and the elastic collision between the wavefront and the particle. A great deal of effort has been made in order to create a model of the scattering process so that these simplifications are not significant.

Blunders - as computer programs become complex and lengthy, the existence of a small program error may be hard to detect and correct. There are basically two methods to deal with this kind of errors. Verification against a known answer and the

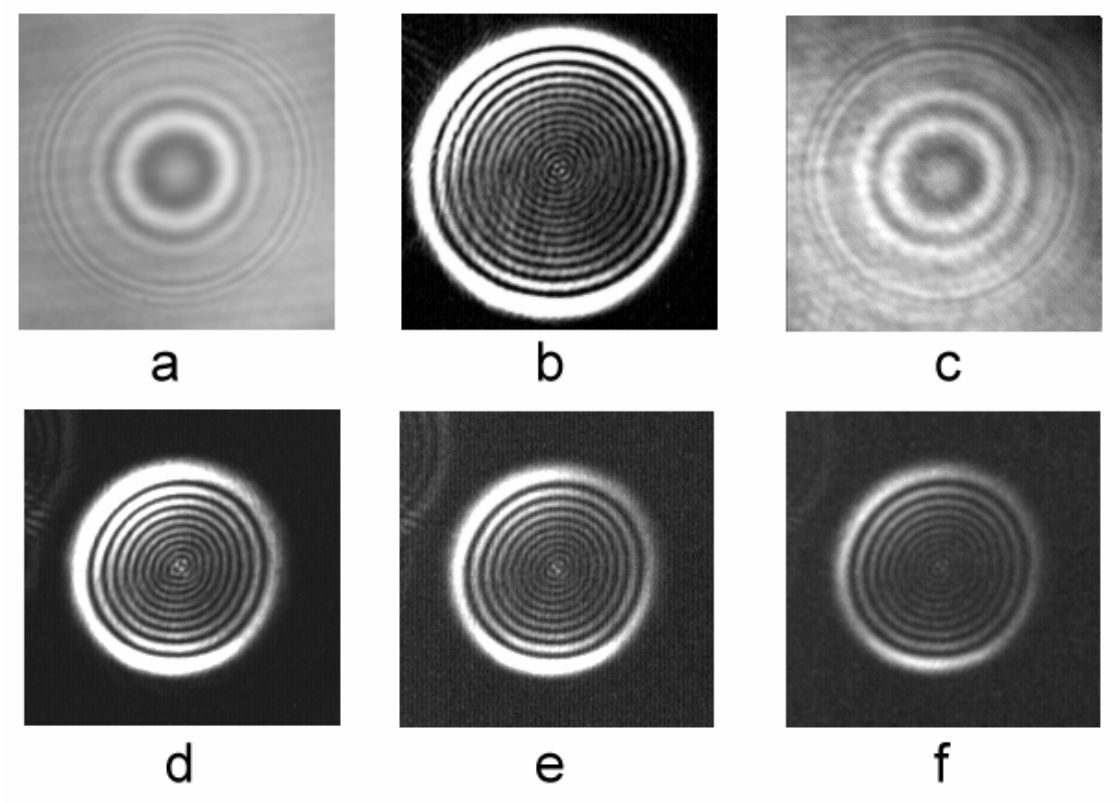

Figure 3.9. Experimental images for three viewing directions, see figure 3.7: a) forward, b) side and c) back scatter, and three illumination types for side scatter viewing: d) Gaussian beam, e) light sheet and f) plane wave.

break-up of the program into modules and the testing of these separately. The GLMT toolbox was tested by testing each of its modules separately against established algorithms and other authors calculated results and their software, where available.

Moreover, the complete software was also validated against experimental results and to predicted results produced by other authors.

Uncertainty in physical data - this is a major source of error as many physical constants of interest are not known with sufficient accuracy, such as complex index of refraction, beam parameters, camera CCD pixel size, object and image distance, particle size, etc. Here, we include camera noise as it results in an uncertainty in the measured intensity field.

Machine errors - these are errors inherent in using the floating point representation of numbers. Here we include also the imaging rounding error produced by CCD cameras as they record an image with a finite spatial and intensity scale. This imaging error is several orders of magnitude larger than machine rounding error. For these tests, CCIR CCD cameras were used, having an eight-bit intensity range and a pixel size of approximately 10 μm with a total of 768x576 pixels. This factor contributed significantly to the measured error.

Mathematical truncation error - numerically solving a mathematical problem results in this kind of error, where an infinite process is approximated by a finite one. In this instance, the use of series expansions and numerical integration contributed significantly to this type of error.

Two further sources of error were identified but not accounted for in these first results: camera calibration involving bespoke tuning, noise calibration, and pixel sensitivity correction, and the inclusion of the system Modulation Transfer Function (MTF) in producing the calculated particle image. This is a complex problem, and it will be treated in future research.

A simple study of the above-mentioned factors was carried out involving direct measurement where possible, numerical simulations to establish variances and numerical partial derivatives, analytical treatment, and the use of published data. The results were combined to yield an estimate of the expected RMS error between the predicted and experimental images. The error was estimated as at least 6 gray levels RMS.

Figure 3.10a and 3.10c shows experimental, not digitally processed, glass particle images (magnification: 7.5 in a 101x101 pixels 8-bit .tif image) of a 18 μm and 1.5 mm out of focus, and 1.5mm into focus, respectively, in forward scatter, illuminated by a 1.5 mm wide, λ = .6328 μm Gaussian beam. It may be compared to the numerical

prediction shown in figure 3.10b and 3.10d using the Generalised Lorenz-Mie Theory. Figure 3.11 shows a radial intensity comparison between experimental and the numerical prediction images given in 3.10a and 3.10b. The quantitative RMS variation between them was measured to be 9.9 grey levels, compared to a expected minimum of 6 grey levels. It is believed that the camera calibration and MTF correction will yield a further 2-3 grey levels. Pixel sensitivity was not calibrated, and camera noise can be considered to be approximately 1.0 grey levels RMS. For positional purposes, it is the relative position of diffraction rings, which predominantly determines accuracy.

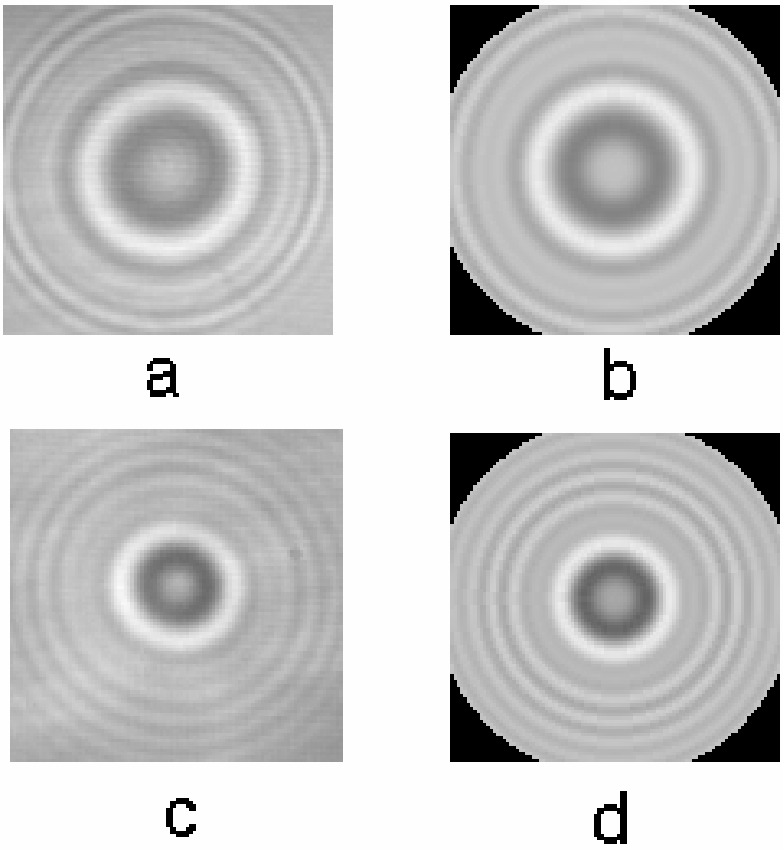

Figure 3.10. Comparison between experimental and theoretical particle images of 18 μm glass in forward scatter: a) experimental particle image 1.5 mm after the focal plane, b) numerical prediction using the GLMT for previous image, c) experimental particle image 1.5 mm before the focal plane, and d) numerical prediction using the GLMT for previous image.

Germane to this technique is primarily determining the accuracy of out-of-plane position estimation, for the image above was estimated as 5 μm out-of-plane. This accuracy can be increased at the cost of a diminished region-of-interest [23]. For many velocimetry applications, where the magnification is in the region of 1-3, the potential

accuracy of this method is estimated as 20-30 μm, using an approach of comparing predicted to experimental images and a Nelder-Mead optimisation, though this may be increased with more sophisticated approaches to optimisation.

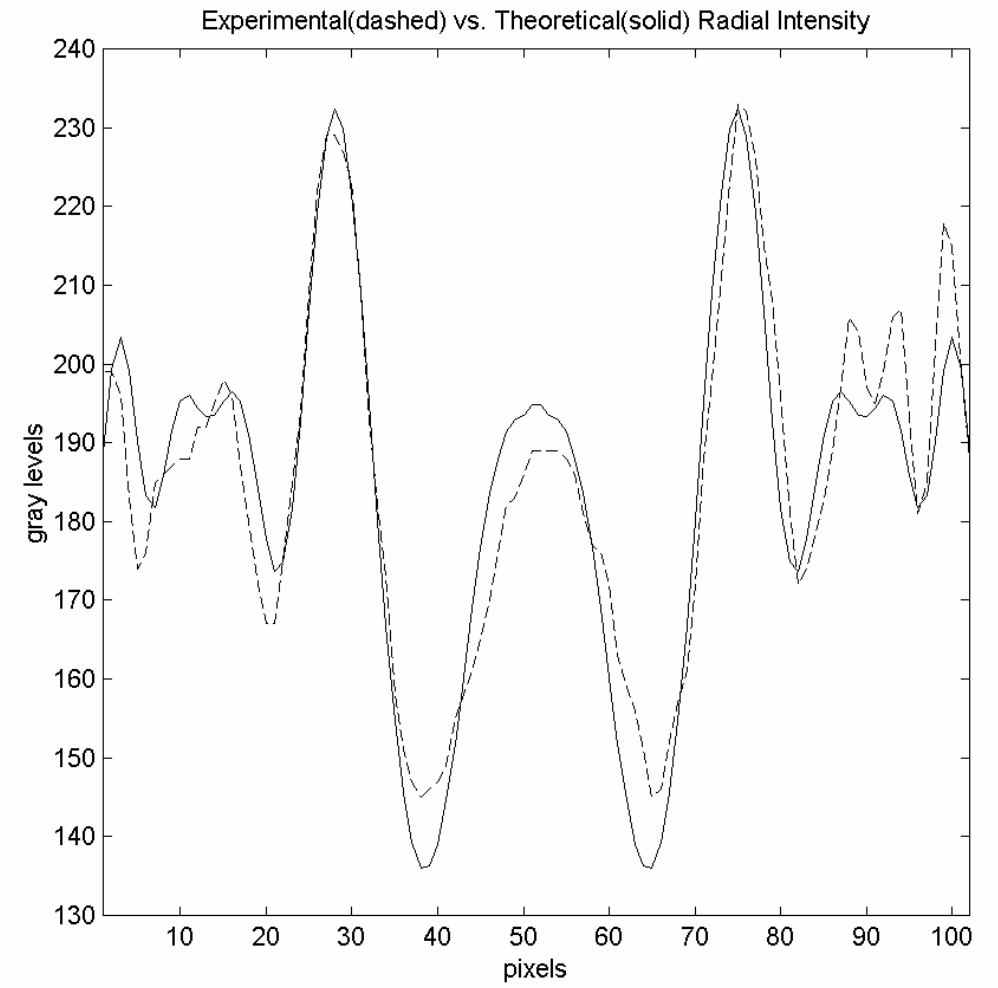

Figure 3.11. Radial intensity comparison between experimental and numerical predictions for a 18 μm glass particle image at 1.5 mm after the focal plane.

3.5 CONCLUSIONS

For the first time, the formulation of a spherical wave front in the context of the Generalized Lorenz-Mie theory is presented. This is important for velocimetry applications for two reasons: a) a larger region of interest can be illuminated, and b) the positioning of seeding particles is more accurate, as the digital representation of the

particle image now changes, not only due to particle and lens characteristics, but also due to the changing incident field for varying positions.

Moreover, the importance of considering the wavefront shape for each application has been illustrated. Much work remains to be done on refining the code, speeding it up and extending it so that all forms of aberrations may be considered. However, having a quantitatively accurate particle image model is a step forward, particularly in velocimetry applications. This step forward opens the way for routine accurate three-dimensional velocity estimation, by three-dimensional particle positioning from two-dimensional camera images.

3.6 REFERENCES

1. Gauthier V. and Riethmuller M.L, "Application of PIDV to complex flows: Measurements of third component," Von Karman Institute Lecture Series 6, Rhode Saint Genese, Belgium, (1988).
2. Westerweel J. and Nieuwstadt F.T.M., "Performance tests on 3-dimensional velocity measurements with a two-camera digital particle image velocimeter," ASME Laser Anemometry, 1, 349-355, (1991).
3. Gray C., Greated C.A., McCluskey D.R. and Easson W.J., "An analysis of the scanning beam PIV illumination system," Measurement Science Technology, 2, 717-724, (1991).
4. Meng H. and Hussain F.: Holographic particle velocimetry, "A 3D measurement technique for vortex interactions, coherent structures and turbulence," Fluid Dynamics Research, 8, 33-52, (1991).
5. Brüker, Ch. and Althaus, W., “Study of vortex breakdown by particle tracking velocimetry (PTV). Part 1: Bubble-type vortex breakdow”, Exp. in Fluids 13, pp. 339-349, 1992.
6. Bryanston-Cross P.J., Funes-Gallanzi M., Quan T.R. and Judge T.R., "Holographic particle image velocimetry (HPIV)," Optics and Laser Technology, 24, 251-256, (1992).
7. Dinkelaker F., Schaffer M., Ketterle W. and Wolfrum J., "Determination of the third velocity component with PTA using an intensity graded light sheet," Experiments in Fluids, 13, 357-359, (1992).

8. Willert C.E. and Gharib M., "Three-dimensional particle imaging with a single camera," Experiments in Fluids, 12, 353-358, (1992).
9. Ovryn B. and Hovenac E.A., "Coherent forward scattering particle image velocimetry: application of Poisson's spot for velocity measurements in fluids," SPIE, 2005, 338-348, (1993).
10. Prasad A.K. and Adrian R.J., "Stereoscopic particle image velocimetry applied to liquid flows," Experiments in Fluids, 15, 49-60, (1993).
11. Adrian R.J., Meinhart C.D., Barnhart D.H. and Papen G.C., "An HPIV system for turbulence research", ASME Holographic Particle Image Velocimetry, 148, 17-21, (1993).
12. Guezennec Y.G., Zhao Y. and Gieseke T.J., "High-speed 3D scanning particle image velocimetry (3-D PIV) technique," Proceedings of The Seventh International Symposium on Applications of Laser Techniques to Fluid Mechanics, Lisbon, 26.2.1-26.2.10, (1994).
13. Prasad A.K. and Jensen K.: Schiempflug stereocamera for particle image velocimetry in liquid flows, Applied Optics 34, 7092- 7099, 1995
14. Hinsch K.D.: Three-dimensional particle velocimetry, Measurement Science Technology 6, 742-753, 1995
15. Allano D., Lecerf A. And Trinite M. : High resolution PIV applied to 3D component velocity measurements, Report 06PT18, Contract BriteEuram BR.PR-CT95-0118, 1998.
16. Raffel, M., Westerweel, J., Willert, C., Gharib, M. and Kompenhans. "Analytical and experimental investigations of dual-plane particle image velocimetry", Optical Engineering, vol 35(7), pp 2067-2074, 1996.
17. Funes-Gallanzi, M., "High Accuracy Measurement of Unsteady flows using digital PIV", Laser & Optics Technology, Vol. 30, pp. 349-359, 1998.
18. Padilla Sosa, P. and Funes-Gallanzi, M., “"High Accuracy at Low Magnification 3D PIV Measurement Using the Concept of Locales", submitted to Laser & Optics Technology, 1999.
19. Wiles, K.J., "Development of a system for secondary liquid injection into a Mach 2 supersonic flow to study drop size and distribution by video imaging techniques", Master's thesis, Univ. of Nebraska, Lincoln, 1985.

20. Schaub, S.A., Alexander,D.R. and Barton, J.P., "Theoretical model for the image formed by a spherical particle in coherent imaging system, comparison to experiment", Opt. Eng., Vol. 23, No. 5, pp. 565-571, 1989.
21. Seeman, M.P., "Aerosol characterization using a PDPA and laser imaging/video processing system", Master's thesis, Univ. of Nebraska, Lincoln 1987.
22. Schaub, S.A., Alexander, D.R. and Barton, J.P., "Theoretical model of the laser imaging of small aerosols: applications to aerosol sizing", App. Optics Vol. 30, no. 33, pp. 4777-4784, 1991.
23. Ovryn, B., Wright, T. and Khaydarov, J.D., "Measurement of three-dimensional velocity profiles using forward scattering particle image velocimetry (FSPIV) and neural net pattern recognition", SPIE Vol. 2546, pp. 112-123, 1995.
24. Adrian, R.J. and Yao, C.S., "Development of pulsed laser velocimetry for measurement of fluid flow", in Proceedings, Eighth biennial Symposium of Turbulence, G. Patterson & J.L. Zakin, eds. (University of Missouri, Rolla, 1983).
25. Gouesbet, G. and Gréhan, G., “Sur la généralisation de la théorie de Lorenz-Mie”, J. Opt. (Paris), Vol. 13, pp. 97-103, 1982.
26. Gouesbet G., Maheu B., and Gréhan G., “Light scattering from a sphere arbitrarily located in a Gaussian beam, using a Bromwich formulation”, J. Opt. Soc. Am. A, Vol. 5, No. 9, 1998.
27. Moreno D., Mendoza Santoyo, Guerrero, J. A. F. and Funes-Gallanzi, M., , “Particle positioning from a single CCD image for Application to Velocimetry: theory and comparison to experiment”, ", Applied Optics, Vol. 39, No. 28, pp. 5117-5124, (2000)
28. The software was kindly made available by Prof. Alexander from the Center for Electro-Optics in the Mechanical Engineering Department at the University of Nebraska-Lincoln.
29. Debye, P., "Der Lichtdruck auf Kugeln von beliebigem Material", Ann. Phys. 30, 57-136, 1909.
30. Mie, G., "Beiträge zur Optik trüber Medien, speziell kolloidaler Metallösungen", Ann. Phys. 25, 377-445, 1908.
31. Goodman, J.W., "Introduction to Fourier Optics", McGraw-Hill, New York, 1968.
32. Menzel, R. and Shofner, F.M., “An investigation of Fraunhofer Holography for Velocimetry Applications”, App. Opt., Vol. 9, pp. 2073-2079, 1970.

33. Jackson J. D., “Classical Electrodynamical”, John Wiley & Sons, New York, (1975) 183.
34. Gouesbet G., Letellier C., Ren K. F., and Gre´han G., “Discussion of two quadrature methods of evaluating beam shape coefficients in generalized Lorenz–Mie theory,” Appl. Opt. **35,** 1537–1542 ~1996.
35. Gouesbet G., Gre´han G., and Maheu B., “Expressions to compute the coefficients *gn m* in the generalized Lorenz–Mie theory, using finite series,” J. Opt. ~Paris! **19,** 35–48 ~1998!.
36. Gre´han G., Maheu B., and Gouesbet G., “Scattering of laser beams by Mie scatters centers: numerical results using a localized approximation,” Appl. Opt. **25,** 3539–3548, ~1986!.
37. Ren K. F., Gouesbet G., and Gre´han G., “The integral localized approximation in generalized Lorenz–Mie theory,” Appl. Opt., Vol. **37,** 4218–4225 ~1998!.
38. Dave J. V., “Scattering Of The Electromagnetic Radiation By Large Absorbing Sphere”, IBM Journal of Research & Development, 13(3), pp. 302-313, 1969.
39. Abramowitz M. and Stegun I. A., “Handbook of Mathematical Functions”, pp 332-334, Dover, New York, 1972.
40. Ren, K.F., Gréhan, G. and Gouesbet, G., “Electromagnetic field expression of a laser sheet and the order of approximation”, J. Optics (Paris), Vol. 25, no. 4, pp. 165-176, 1994.
41. Gréhan, G., Gouesbet, G.,Guilloteau, F., Chevaillier, J.P., "Comparison of the diffraction theory and the generalised Lorentz-Mie theory for sphere arbitrarily located into a laser beam", Optics Communications, Vol. 90, pp. 1-6, 1992.
42. Hale, G.M. and Querry, M.R., "Optical constants of water in the 200nm to 200 microns wavelength region", Appl. Opt. 12 (3), 555-563, 1973.

CHAPTER IV

TUNNELING VELOCIMETRY

4.0 INTRODUCTION

One of the problems to be solved when performing volumetric measurement is the illumination system. In-line holographic velocimetry schemes, which use particle back/forward scattering, have been widely used in holographic approaches because of their simple optical configuration and low laser power and coherence requirements. However, in some cases the inherent speckle noise proves to be a major obstacle. A way around this problem is to use off-axis holography, which uses particle side scattering, at the cost of increased laser power because of the low scattering efficiency obtained in side scattering. Variations using a Fourier-transform lens have been proposed in an in-line holographic arrangement. Holographic approaches are generally not robust enough for industrial applications and are not real-time, a most desirable feature.

Adrian [1] describes the PIV technique as a method of measuring fluid velocity almost instantaneously, over extended regions of a flow domain. This approach combines the accuracy of single-point methods such as Laser Doppler Velocimetry with the multi-point nature of flow visualization techniques. As a measuring technique and illumination technique, PIV suffers several major disadvantages, namely: the need for orthogonal viewing of the light-sheet places severe restrictions on its applicability, as many flow fields of interest do not allow the required optical access; since a thin light-sheet is normally used, it is intrinsically a 2D technique; the separation between the optics that produce the light-sheet and the imaging optics means that the latter need to focus and align on to the light-sheet plane, making of this process a source of experimental constraints and errors, as well as unsuitable where any component is likely to suffer vibrations; side-scattering efficiency is very low compared to back-scatter and forward-scatter, so high illuminating powers are required for small particles. Finally it cannot cope with arbitrary magnitudes for the velocity components in all three dimensions. For a given viewing position, the largest velocity component needs to lie

in-plane as otherwise the particle transit time through the light sheet severely limits the technique's accuracy.

4.1 REQUIRED CAPABILITIES AND TOOLS

The required capabilities for 3D real-time measurement include the following three aspects: illumination of a volume rather than a plane, particle positioning in 3D from 2D camera information, and positioning calculation at low-magnification. Tunneling Velocimetry [2] is able to provide the means to obtain particle images in a volume of interest rather than on a light sheet.

The second requirement of obtaining 3D particle position information from 2D CCD/film camera information is quite challenging. An accurate analysis of the wave field, applicable for arbitrarily shaped incident beams, relies on the Generalized Lorenz-Mie theory (GLMT) [3]. A computer program has been developed, capable of calculating the image, including aberrations at the image plane of an imaging system, of a spherical particle due to a plane/Gaussian/spherical wavefront in any illuminated 3D position [4], with experimental results obtained in full agreement [5].

For practical whole-field applications a magnification close to unity is required. This objective has been achieved by considering in detail the effect of image digitization based on the concept of “locales” [6] as applied to PIV [7], and recently extended to 3D [8]. At low magnifications, the particle image is scrambled and the problem of inferring co-ordinates is more akin to cryptology. The GLMT acts as the encryption algorithm, co-ordinate information is the key, and the low-magnification image is the enciphered message. Since the GLMT is a smooth-varying function, it is possible to iterate to a solution by pattern matching, subject to digitization constraints. To solve the problem by applying inverse-value techniques is theoretically possible, though there are very complex stability issues. A function-fitting approach comparing the radial intensity field of an experimental particle to a calculation is impractical. In order to obtain say a 25-point vector, an image of 50x50 pixels needs to be obtained, which amounts to 2500 pixels from which only 25 would actually be used. Therefore, a pattern-matching approach was chosen. In this way, if a 25x25 pixel image is generated, all 625 pixels will be used, thus allowing a higher accuracy at a lower magnification than otherwise available. This approach depends crucially on two factors:

an accurate digital representation of the scattered field and a robust image-matching algorithm.

Pressure and temperature sensitive paints offer a unique and inexpensive means of determining body surface pressure and temperature distributions [9], not easy to obtain using conventional measurement techniques. These distributions are critical for understanding complex flow mechanisms, and allow direct comparisons with results from computational fluid dynamic (CFD) calculations. The cost of the PSP/TSP technique is competitive in comparison to the cost of pressure/temperature transducers. Not only is the cost and size of installing these conventional probes an issue, but the aerodynamics and structural dynamics of the component can be seriously altered by modifications when accommodating such transducers. Data rates for PSP/TSP are also faster than those for conventional techniques.

4.2 TUNNELING VELOCIMETRY.

This is a new technique which aims at improving over previous methods of the kind described by Adrian [1]. It proposes for the first time a 3D, real-time, non-intrusive, instantaneous and simultaneous measurement of all physical variables of a fluid, as well as near-surface pressure/temperature. A tunneling velocimeter is shown schematically in Figure 4.1. A flow streams along a profile. The flow is seeded with particles, such as polystyrene spheres. A collimated laser beam - typically vertically polarized - introduced into the optical axis of a video detector, by a polarization-sensitive beam splitter arrangement, illuminates the flow field. A quarter-wave retarding plate is placed between the polarizing beam splitter and the volume of interest. It is used to circularize the polarization of the illuminating beam on its way to the measurement volume, and to make the particle-scattered light horizontally-polarized on the return path, and so the polarizing beam splitter arrangement transmits the light onto the imaging lens and CCD camera. Hence the name of the technique, tunneling velocimetry: it is as if the camera was viewing the particles, from whose motion velocity is derived, inside a lit tunnel. With the pulsed laser the CCD camera records multiple images of the light scattered back by the seeding particles. The light power density falling on the particles is lower than for PIV for instance, since power is being distributed over a volume rather than a light sheet. However, the resulting light intensity scattered by the particles in this arrangement is actually higher than for a

comparable light sheet because the efficiency of back/forward scattering is much higher for micrometer sized particles. A further advantage of this arrangement is that the drop in power density allows the use of conventional optical components, many of which have a power threshold of 0.1 J/cm^2. A ½-wave retarding plate is placed in the beam path before the beam splitter. This allows the adjustment of the power to be transmitted to the measurement volume, providing power level measurement through a photodiode. The flow field images, captured after passing through a filter which excludes all frequencies other than that desired, are then processed in a computer to extract the motion information from which, knowing the time separation between pulses of light, the velocity field can be derived in 3D. If fluorescent or phosphorescent particles are used, the filter acceptance frequency can be altered to be that of the fluorescence frequency rather than that of the laser.

The imaging lens and CCD sensor setting characteristics give the effective depth of field over which the camera will be able to record particle images. Thus the camera can view a "tunnel" of varying length. With reference to figure 4.2, a mesh plot of image intensity as a function of position for a 10 mm particle movement is shown, where the particle is only 21 μm in diameter. Note that the intensity field is not symmetric about the focal plane and that the particle image is not identical either side of the focal plane. Therefore, there can be no ambiguity of particle position based on particle image analysis.

Figure 4.3 is a plot of a side-view of the scattering field in figure 4.2, which shows a particle illuminated by a Gaussian wavefront and viewed at a distance of 12 cm with a 90 mm SIGMA macro lens. Several points can be illustrated using this figure. The plot shows the on-axis intensity (Poisson Spot) with a solid line, the maximum intensity of the scattering field with a dotted line, and the minimum intensity is shown with a dashed line. It is clear that it is important for ease of camera calibration to carry out this type of calculation in Luxes. Thus, knowing the minimum sensitivity of the camera and the largest intensity to be measured, the gain can be calculated with the gain set to "manual", as the automatic gain control makes the whole approach impractical. In this forward scatter arrangement it is comparatively easy to adjust the camera, as the mean background level to which the field tends, i.e. 250 Luxes, can be set equal to mid-range gray levels (for instance 128 gray levels in an 8-bit system) by the right amount of defocusing. The peak intensity is then clipped at peak levels where position is estimated taking this clipping into consideration. Now, if the black-clip is set at a suitably large

level such as 350 Luxes in this case, the particle will only be visible in a depth of field of less than 0.5mm and so the measurement will be essentially a 2D measurement, though the whole volume might be illuminated. Furthemore, it can be seen from the dashed line that information is contained not only by

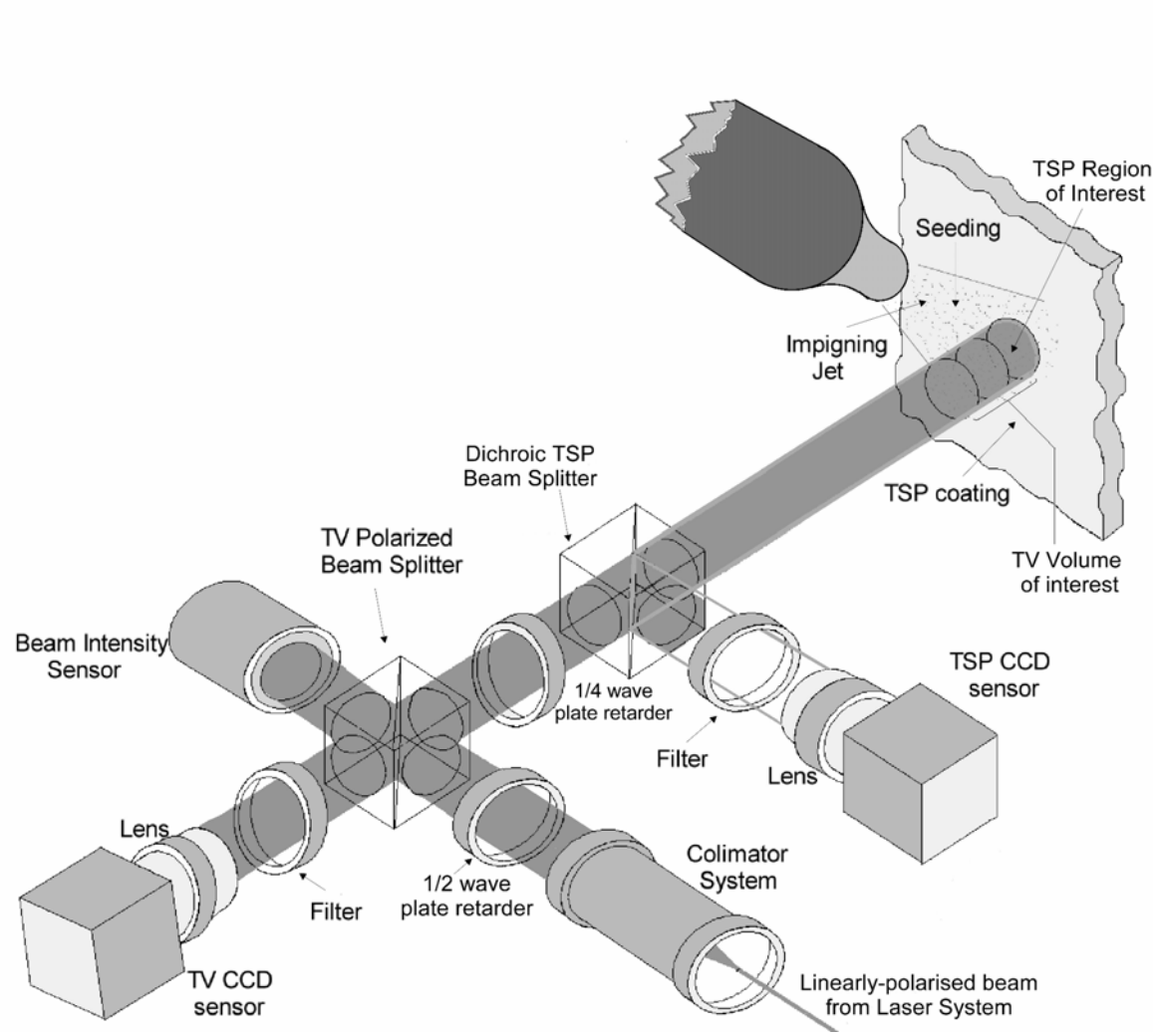

Figure 4.1 - Experimental system for Tunneling Velocimetry (TV).

the peaks but also by the minima of the scattering field. Finally, the dotted line shows clearly how the maxima provides information about particle position over a range of almost 25 mm, while if one considers simultaneously the maxima and minima we can see that information extends beyond 30 mm.

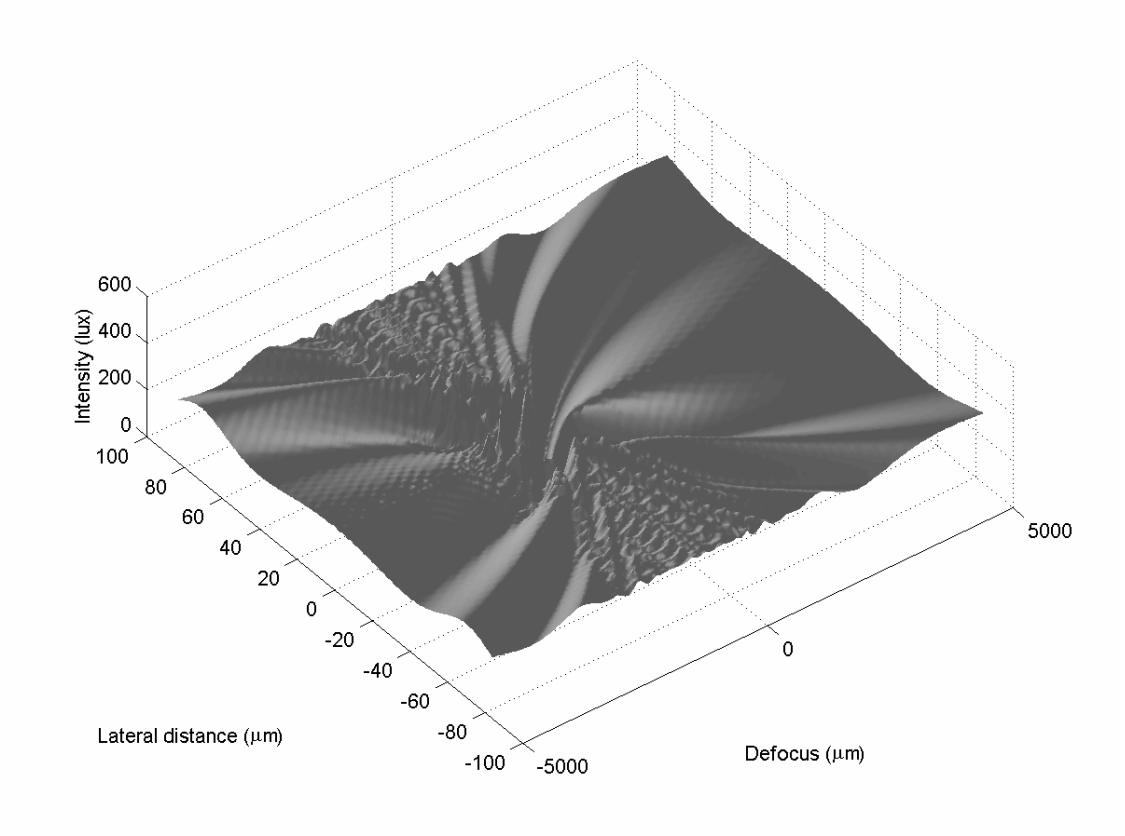

Figure 4.2 - 21μm glass particle intensity as a function of depth over the measurement volume.

The dichroic beam splitter in front of the ¼-wave retarder plate is used to separate the fluorescent signal coming from the object surface, redirecting it to the near-surface parameter-sensing camera. These paints can be excited either by the tunneling velocimeter laser, for instance when using an Argon Ion or Nd/YAG laser, or an external source such as an ultraviolet lamp.

To evaluate TV in comparison to the more conventional use of holography, the relative measurement density capability of both techniques needs to be considered. Holography, albeit the wet-process, has the advantages of a larger sensing area and higher resolution. The former advantage however, is only valid for laboratory conditions, large particles and low speeds. As flow speeds increase, light power density considerations to obtain enough particle scattering energy to expose the plate, limit the usable plate area since typical Nd:YAG pulsed lasers have energy deliveries of the order of 200 mJ/pulse. Attempts at using forward scattering where particle scattering

efficiency is larger has proven to be much more complicated than conventional in-line methods and often also require multiple optical access, thus unsuitable for industrial applications.

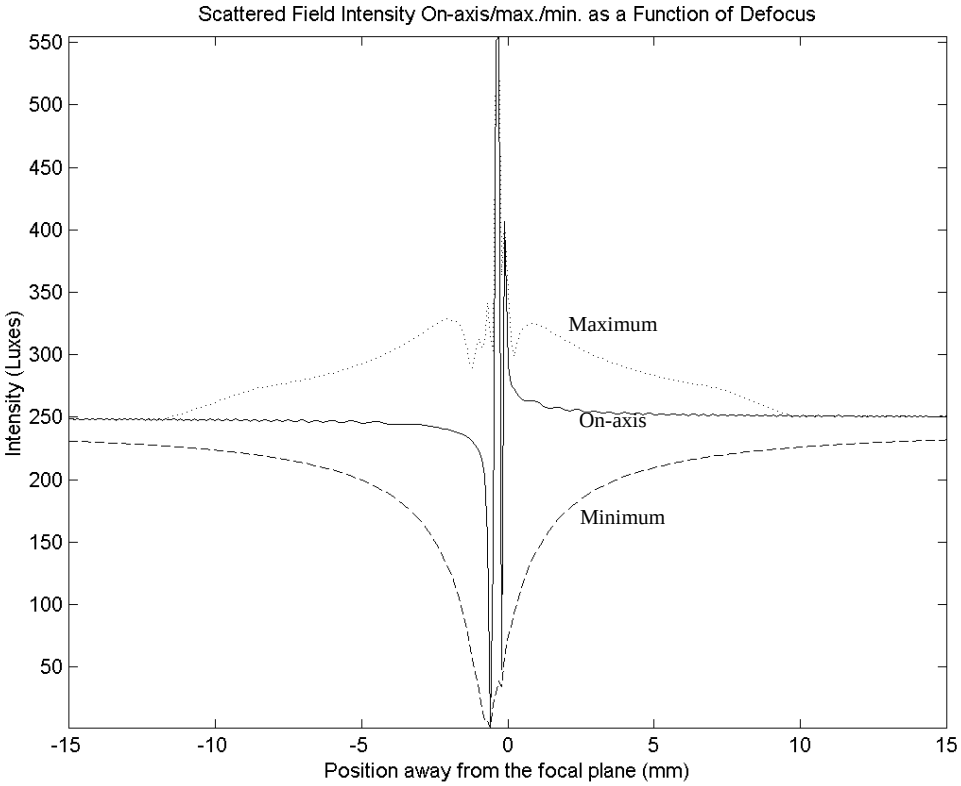

Figure 4.3 – Side view of particle scattering as a function of defocus.

The latter advantage is applicable for the case where noise is low compared to high noise levels found in industrial applications. The geometric precision of a noise-free digital image can be improved by increasing either the spatial or intensity resolution. If **a** is the width of the sampling interval and **b** is the number of bits per pixel, based on theory [7], precision varies as $2^{\mathbf{b}}/\mathbf{a}$. Setting quantization steps to be larger than the noise level can minimize noise in digital images. Thus, this is the limitation for increasing the number of intensity levels to achieve increased accuracy. The noise level also depends to a large degree on the system aperture. In high speed PIV the aperture is limited to a narrow range, in order to match the system aperture to the sampling interval **a**. Assuming this condition is achieved, for spatially uncorrelated noise, the noise power will vary as 1/**a**. The noise level determines the number of useful quantization levels so that the number of levels will also vary linearly with pixel

size. Since precision varies linearly with quantization levels and inversely with the sampling interval, there will be no change in precision as pixel size changes, in the presence of noise. This result has been supported by experimental evidence [10]. Once the pixel size is small enough to ensure a noise power of 1 quantization level, allowing for particle recognition, theory predicts that precision will not be improved by reducing pixel size. So, for the case of holographic PIV, accuracy is not improved by the large resolution of holographic emulsions in the presence of noise.

It is generally assumed that to extract velocity data conventional 2D correlation methods can be extended to 3D, and used for Holographic PIV (HPIV) [11]. It is well known that the success of correlation methods requires high-density particle recording. However, the high densities required are difficult to achieve at an acceptable signal-to-noise ratio. Typically, at a density of 10 particles/mm^3 HPIV encounters speckle noise [12]. Although speckle noise can be controlled to various extents at the cost of increased complexity, densities are still rather low, leading to measurement rates of the order of 0.5 measurements/mm^3 or less using correlation approaches. In order to overcome this problem, research work has been reported on more advanced 3D velocity extraction algorithms which can cope with the low seeding densities of HPIV using, for instance, artificial intelligence [13]. This particular method, however, still uses a low accuracy convoluted method to obtain the particle vectors in the first place. The particle tracking method however, has been shown to work successfully in HPIV also achieving a considerable reduction in data processing compared to frequency methods [14]. So, speckle noise limits the potential measurement density of HPIV, pointing to tracking methods as the most appropriate for 3D velocity estimation, due to the low particle seeding density required by these methods compared to frequency approaches.

The potential measurement density of Tunneling Velocimetry can be calculated for a typical macro lens, starting from a comparison with the planar PIV case, which is reasonable since the technique typically uses a CCD camera to view the volume of interest in real-time. A standard CCD sensor of 768x576 pixels, where each pixel is roughly 8.5 μm in size, can be assumed to contain 500-700 particle pairs for a typical PIV arrangement. This is equivalent to (at a magnification of 1) 20 measurements/mm^3. If an ideal sensor of 10x10 mm is considered, and an equal-sided volume symmetrically about the focal plane, the volume becomes 10x10x20 mm^3 and the measurement density will then drop close to that obtained for holography, of the order of 0.5

measurements/mm^3. Naturally, the more advanced cameras now available would improve this number, particularly by using double-frame correlation cameras at higher sensor sizes and higher Analogue-to-Digital Conversion resolution.

An important point to be investigated is how much detail can be glanced at by sparse random 3D point measurements of a velocity field. In the 2D case where data refers to a light-sheet, two or three components of velocity can be readily related to a position. However, in three dimensions the minimum grid size must be derived based on the data field. To this end some work has previously been performed with the aim of producing a method which determines the optimum grid size for interpolated velocimetry data, without making any a-priori assumptions about the velocity fields, the system or analysis method used [15]. The method employs condition number as the main criterion for deciding the adequate grid size for a given data set and was developed for the case of PIV, but it is equally valid for 3D Tunneling Velocimetry. Data sets are directly comparable, independently of differing experimental parameters or data processing methods. This method illustrates the advantage of using velocimetry for unsteady flow research, i.e., using a comparatively small number of measurement points a detailed mesh of the underlying flow field can be derived. Thus, although velocimetry delivers a limited number of measurement points compared to Doppler Global velocimetry, for instance, which essentially yields a measurement per pixel, in general a high measurement data rate is not required to adequately reconstruct a flow field.

Conceptually, the grid separation determined by this method can be considered to yield an estimate of the number of mesh points required to compute an equivalent CFD field, which is much larger than the number of velocimetry measurement points. There are three sets of independent constraints in velocimetry measurements, which must be related. Firstly, the physical characteristics of the sensor with which the velocimetry image is to be recorded. Secondly, the range of scales in the velocity field under investigation (ranging from those of the same order as the characteristic length down to the Kolmogorov scale). Thirdly, once the data has been analyzed and the velocity vectors calculated, the grid size for an interpolated representation of the continuos field must be defined. The unifying concept for these three constraints is the condition number. The latter can be regarded as the ratio of the resolution to the largest sensor axis in the first case, the ratio of the characteristic length to the Kolmogorov scale in the second, and the sensitivity of the approximating matrix to perturbations in the third. By setting the resolution to be equal to the Kolmogorov scale, the required

sensor size and magnification are fixed, and setting the resolution to be equal to the Kolmogorov scale makes the first and second constraints consistent. The third constraint requires the determination of a grid size, which exhibits minimum error, without detailed knowledge of the velocity field under investigation. This is achieved by setting the condition number of the interpolation to twice the condition number of the flow field. Finally, the calculated grid size requires the number of mesh points, which need to be used to compare numerical calculations to experimental data. Much work remains to be done. An analytical description of all the parameters involved has started to be developed to enable the implementation of high-accuracy measurements in all conditions. This approach opens the way for the investigation of complex flows with high accuracy and detail at the cost of extra processing, though this is increasingly economically feasible and widely available.

It is also an important advantage for practical applications that the Tunneling Velocimetry method uses virtually the same equipment as conventional PIV, except for the polarized beam-splitter arrangement and retarder plates.

It is worth mentioning that it is well known that non-spherical particles exhibit a scattering field, which is very close to that of the equivalent spherical particle on-axis, but differ significantly for larger angles [16]. Therefore, this method can be used for high temperature seeding, such as stabilized alumina seeding, since high temperatures are not uncommon in subsonic and transonic flows, which are of particular interest in turbomachinery component testing.

The technique can be extended to measure simultaneously velocity, density, viscosity (from which temperature can be deduced for both air and water), and pressure. A mixture of three mono-disperse seeding particles is used to derive an estimate of density and viscosity as well as velocity. A marker seeding is chosen to follow the flow as closely as possible, while intermediate and large seeding populations provide two supplementary velocity fields, which are also dependent on fluid density and viscosity. A particle motion equation is then solved over the whole field to provide both density and viscosity data. The three velocity fields can be separated in a number of ways. One way is to color the different populations with fluorescent dyes. Since CCDs have a wavelength and frequency dependent sensitivity, each population will appear to have different size and peak intensity on the image plane. The combination of the three measured variables and the perfect-gas law then leads to an estimate of the flow field

thermodynamic pressure. Thus, the instantaneous state of a flow field can be completely described.

In summary, the major characteristics of TV can be considered to include an intrinsically volumetric method, low to moderate power requirements, single optical access position required, camera focal position defining the volume of interest, high seeding scattering efficiency as back or forward scattering is used, and the ability to cope with arbitrary 3D flow velocity fields. The technique allows the simultaneous measurement of near-surface temperature/pressure using TSP/PSP, and finally it is versatile as it includes variations such as off-axis and in-line holography, stereo-viewing, and image-shifting.

Surfaces behind the measurement volume can cause the particle scattered light to be overwhelmed by the light reflected back from those surfaces. To avoid this effect, a number of solutions can be employed, such as: to cover the surface with a fluorescent paint which will emit light of a lower frequency and thus will be blocked by the viewing filter, if the latter only passes the laser frequency; use fluorescent particles and set the filter to pass only at the fluorescence frequency, thereby also blocking harmful background glare; direct the light beam towards a light dump; if the surface is specular then, since this apparatus has no preferred orientation of the measurement volume relative to the flow direction, the apparatus can be aimed at a slight angle relative to the surface so the reflecting light does not enter the primary optical axis but is reflected away from it, for instance towards the plenum of a wind tunnel; and if the back-surface can be made specular, the beam can be aimed so that it reflects back along the optical axis, hitting the particles on their return path as well, thereby generating a forward scattering field. Since this is larger than the back scattered field, the CCD camera can be tuned to record forward particle scattering, for cases where the particles are too small and require the higher scattering efficiency of forward scattering to be recorded.

The first option mentioned for suppressing light reflected by a surface behind the flow measurement volume, i.e., using a fluorescent coating, provides two benefits: it allows particle-scattered light discrimination and achieves a means by which TSP/PSP measurements can be accomplished. If the fluorescent/phosphorescent coating used is parameter-sensitive, then the surface's temperature/pressure, for instance, can be calculated. Therefore, the remaining portion of the light beam not striking any seeding can be used, in conjunction with parameter-sensing paints (parameters such as temperature, pressure, or shear-stress), to derive back-surface temperature/pressure.

Thus, this apparatus is capable of providing simultaneously, through a single integrated measurement means, aerodynamic together with back-surface heat transfer and/or pressure information.

TSP/PSP are sometimes employed using a number of cameras to gather whole-body forces and in conjunction with flash lamps for instance, rather than the very local nature of the TV area sensing. However, the use of TV is very useful for registration purposes so that it can be used to calculate the exact volume where aerodynamic information was obtained when combined with the whole-body TSP/PSP data. Often this is of crucial importance as certain small areas create a large proportion of losses such as wakes, secondary flow, surface/vortex and shock/boundary layer interactions.

4.3 EXPERIMENTAL TESTING.

For the initial tests a plate was coated with an in-house TSP, and excited with a Nd:YAG. This forms part of current research to further develop this technique. The ultimate aim is to produce a good PSP/TSP bi-luminophore paint in the near future.

An inclined hot jet at a temperature of 50º Celsius and a peak velocity of 10 m/s was employed as the sample flow. Modeling and calibration have established accuracies for this method, in laboratory conditions, as 0.5 kPa for pressure and 0.2 ^{o}C for temperature, with a spatial resolution, for a 20 μm layer, of 0.1 mm. The temperature accuracy is comparable to that of thermal imaging cameras, though they are nowhere near their dynamic range which can measure object temperatures from 200 to 2,000 ^{o}C. These results being consistent with those obtained by other authors. However, it is worthy to note that errors in industrial applications have been reported to be of the order of one order of magnitude larger.

The system uses three 8-bit 768x576 pixel genlocked CCD cameras together with all the concomitant standard color image capture and triggering electronics. A PENTAX 35mm SLR camera using TMAX 3200 ASA film is also currently being tested, in order to yield 3200x2000 pixels and 12-bit resolution by digitizing film, as a scientific grade camera is not available. A Nd:YAG 100mJ/pulse twin cavity frequency-doubled laser was employed for the velocimetry and the TSP illumination. The lens was a standard 90mm SIGMA macro for the velocimetry data and a 70mm SIGMA zoom for the TSP measurements. The complete instrument is contained in a single assembly with adjustments for light intensity to be projected to the measured volume, TSP lens

focus and velocimetry lens focus. A high-speed photodiode was also employed for power level measurement.

Figures 4.4 and 4.5 show the initial system results of the TSP and double-pulse velocimeter tests respectively. The TSP data extended from 20 to 50 degrees Celsius. In the velocimetry data the seeding material was flowing in a free jet at a speed of 9.5 m/s and an angle of 32^{o} degrees to the image plane. A frequency-doubled Nd/YAG laser with energy of 100 mJ per pulse and a pulse separation of 100 μs illuminated the seeding. The resulting image was recorded at a magnification of 1.7x, and viewed through a 90mm SIGMA lens. A conventional analysis of the data is shown in Figure 4.6, where the average velocity of the field was measured to be 8.05 m/s, which was consistent with the incidence angle and the speed of the free jet.

Figure 4.7 shows the resulting full 3D-velocity field. There are only a few particle pairs in this image but it does serve to illustrate the feasibility of the method. The mean measured velocity was 9.77 m/s, some 3% higher than the actual velocity. This discrepancy led to a further review of the velocity vectors and the corresponding experimental image. Four of the velocity vectors were found to have a large error in terms of peak signal-to-noise ratio, compared to the corresponding experimental image. After further investigation it was concluded that the jet contained some water particles that had not yet evaporated, as well as the intended polystyrene seeding. Since the GLMT code requires knowledge of the complex refractive index and seeding particle size, it generated erroneous positions for those seeding particles that were not made from the same material as the seeding. Therefore, this is an effective means to isolate contaminant particles in velocimetry images. However, there are some cases, such as two-phase flow studies, where a number of seeding populations might be used and need to be identified separately. For this type of application, which is actively being developed in the laboratory where the research was done, the method herein described needs to be extended to both position a given particle and also identify to which population it belongs. This is currently the subject of much research and beyond the scope of this thesis, so it will be reported in the near future.

The theoretical calculation used for positioning purposes does not make any simplifications related to size and so is equally applicable to micrometer-sized particles. Larger particles were used for handling convenience only.

Where the magnification is in the region of 1 to 3, using an approach of comparing calculated to experimental images and a Nelder-Mead optimisation, the accuracy of this

method is estimated as 20-30 μm, though this may be increased with more sophisticated positioning algorithms. Pixel sensitivity was not calibrated, and camera noise was considered to be approximately 1.0 grey levels RMS. For positional purposes, it is the relative position of the diffraction rings, which predominantly determines accuracy. Naturally, at these low magnifications the positional accuracy is nevertheless diminished [8]. However, since TV analyses particle images belonging to a volume, rather than a light sheet as in conventional PIV, the probability of pair ambiguity is much reduced and so larger pulse separations can be used. This fact results in two advantages: increasing the distance traveled between pulses increases velocity accuracy, and the dynamic range of the method is also larger than for PIV. In initial tests, pulse separations about 5 times larger have been employed.

Figure 4.8 shows a simplified prototype, currently under final development, for use on a two-stage air turbine at a free-stream velocity of 0.5 Mach, aimed at secondary flow research in power generation. The tube and adapter at the front of the instrument allows the velocimeter to go into the passage in place of conventional hot-wire probes between the stator and rotor rows. The investigation region is a cylinder of 10 mm diameter and 20 mm depth. The pulsed laser used is a two-cavity frequency-doubled 200 mJ Nd:YAG, with λ = 532 nm. The results of this research are currently being produced and will be reported elsewhere.

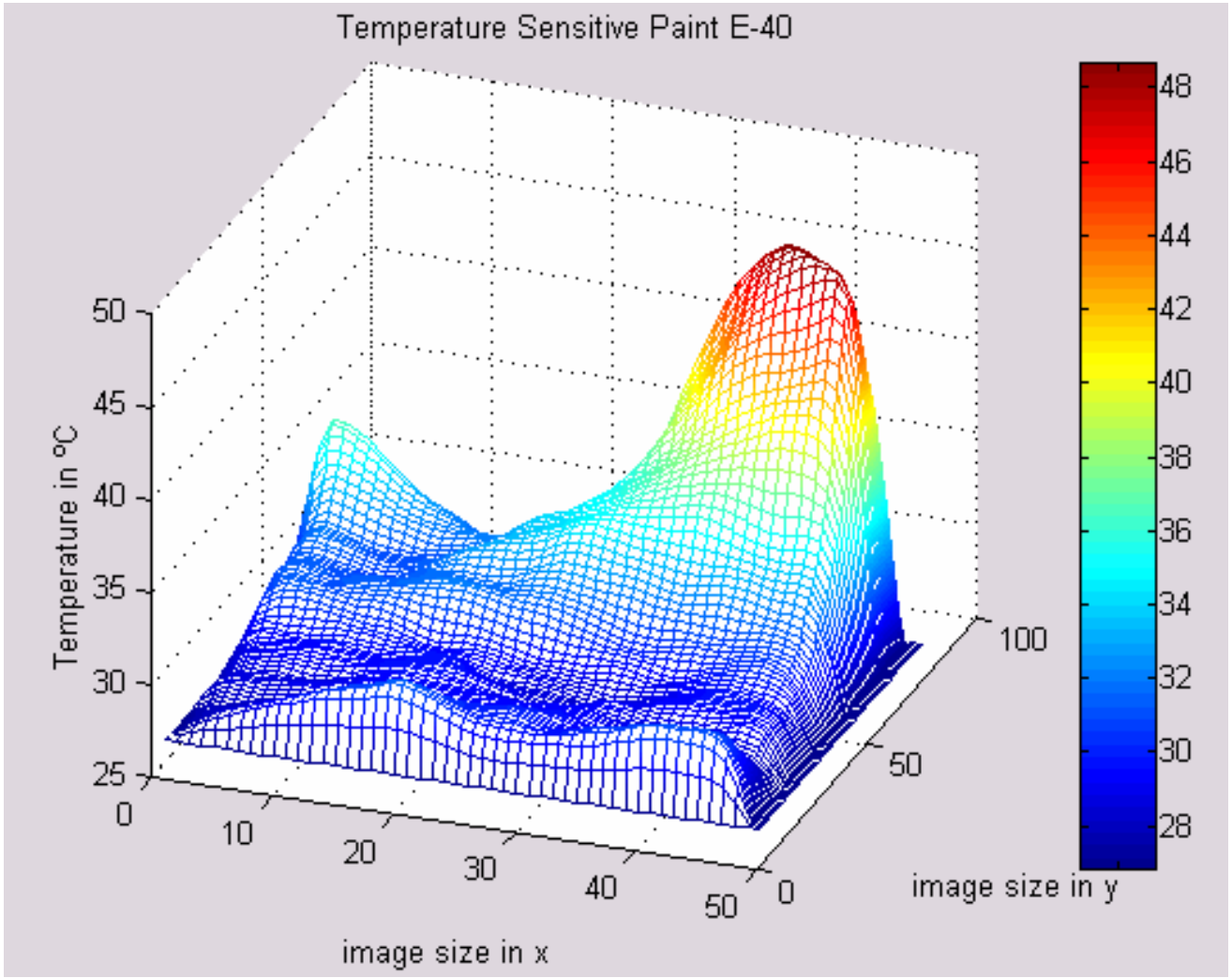

Figure 4.4 - TSP Measurement using TV technique.

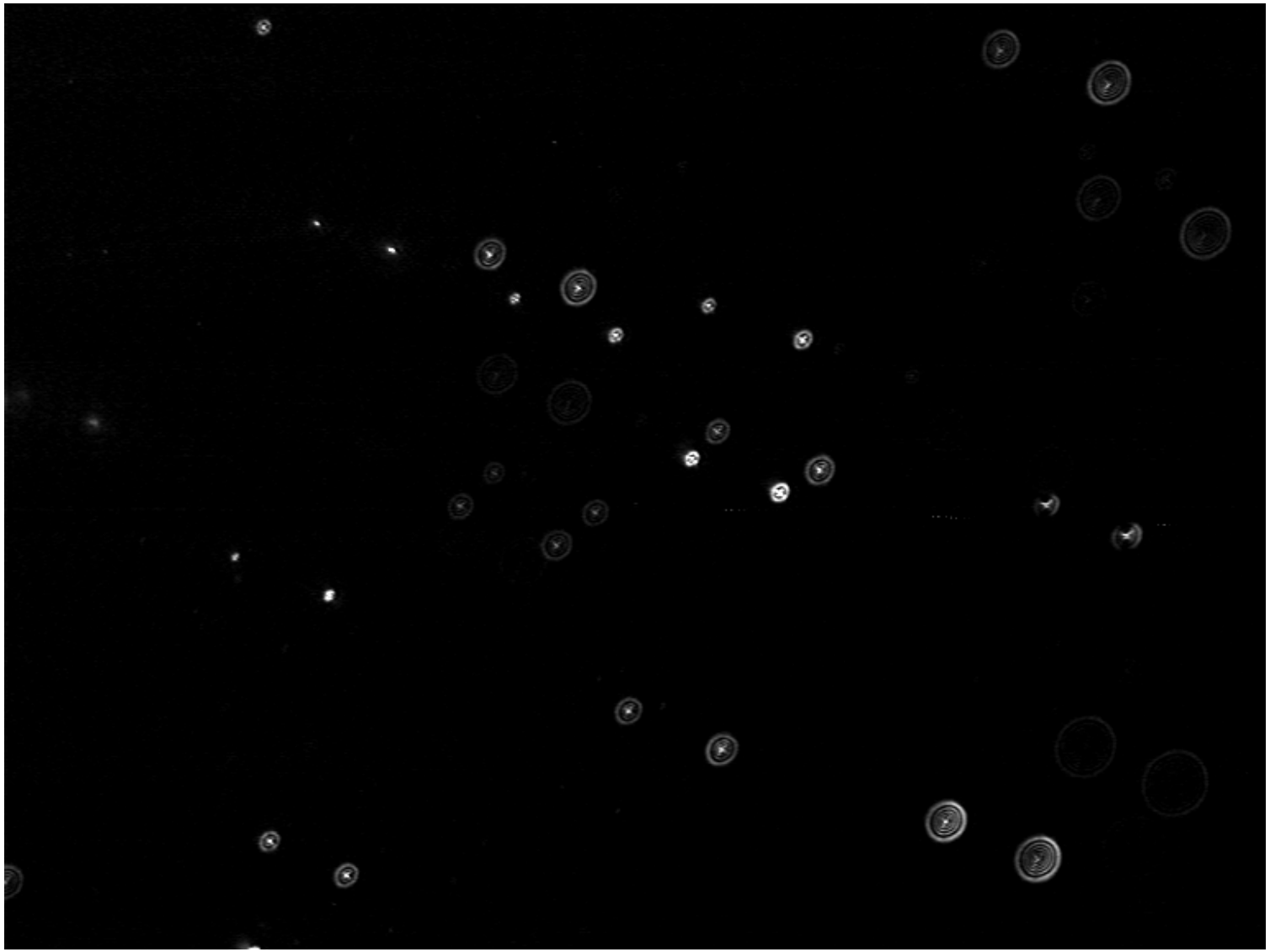

Figure 4.5 - Velocimetry data using TV technique.

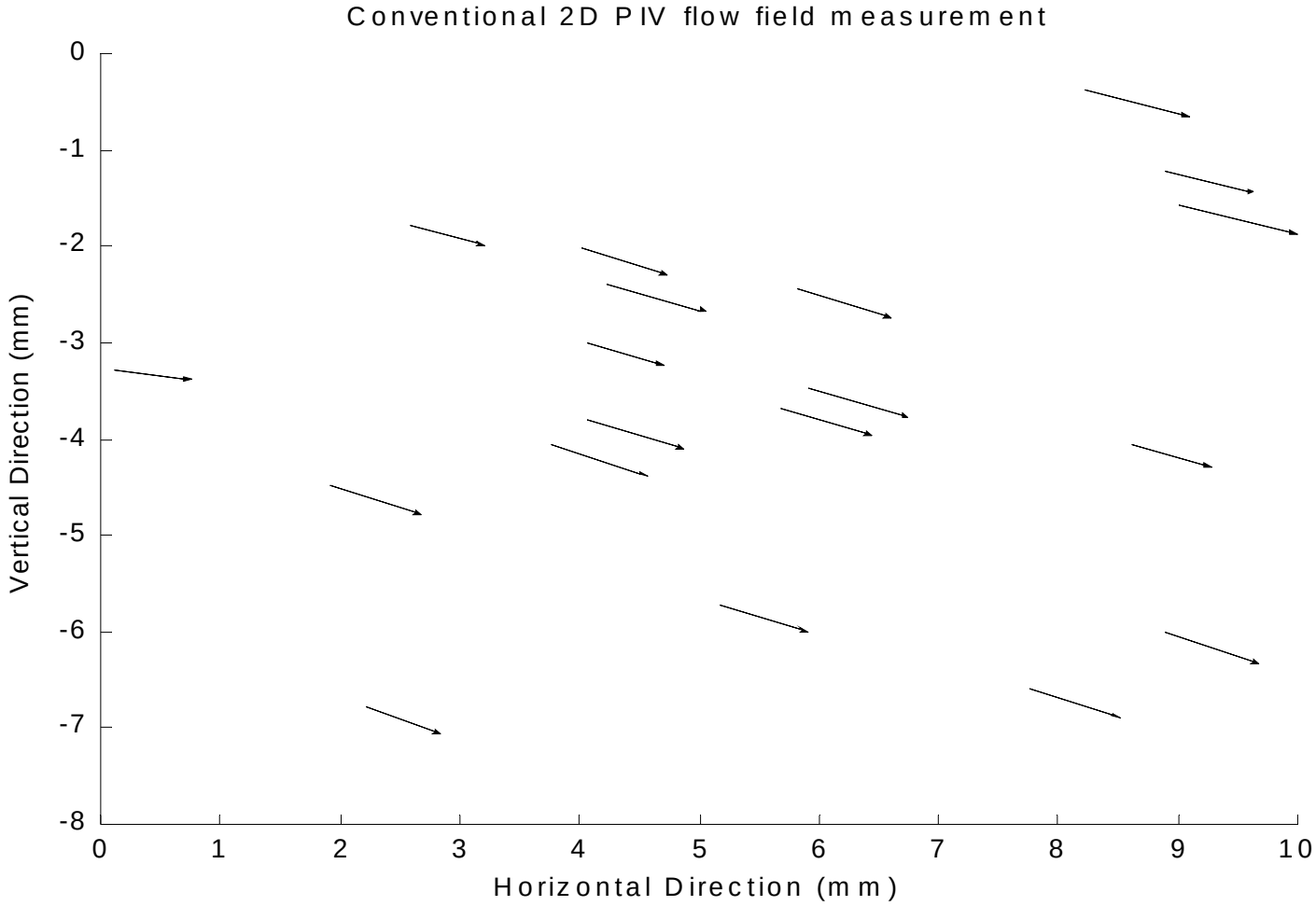

Figure 4.6. Conventional 2D PIV analysis of data shown in Figure 4.5.

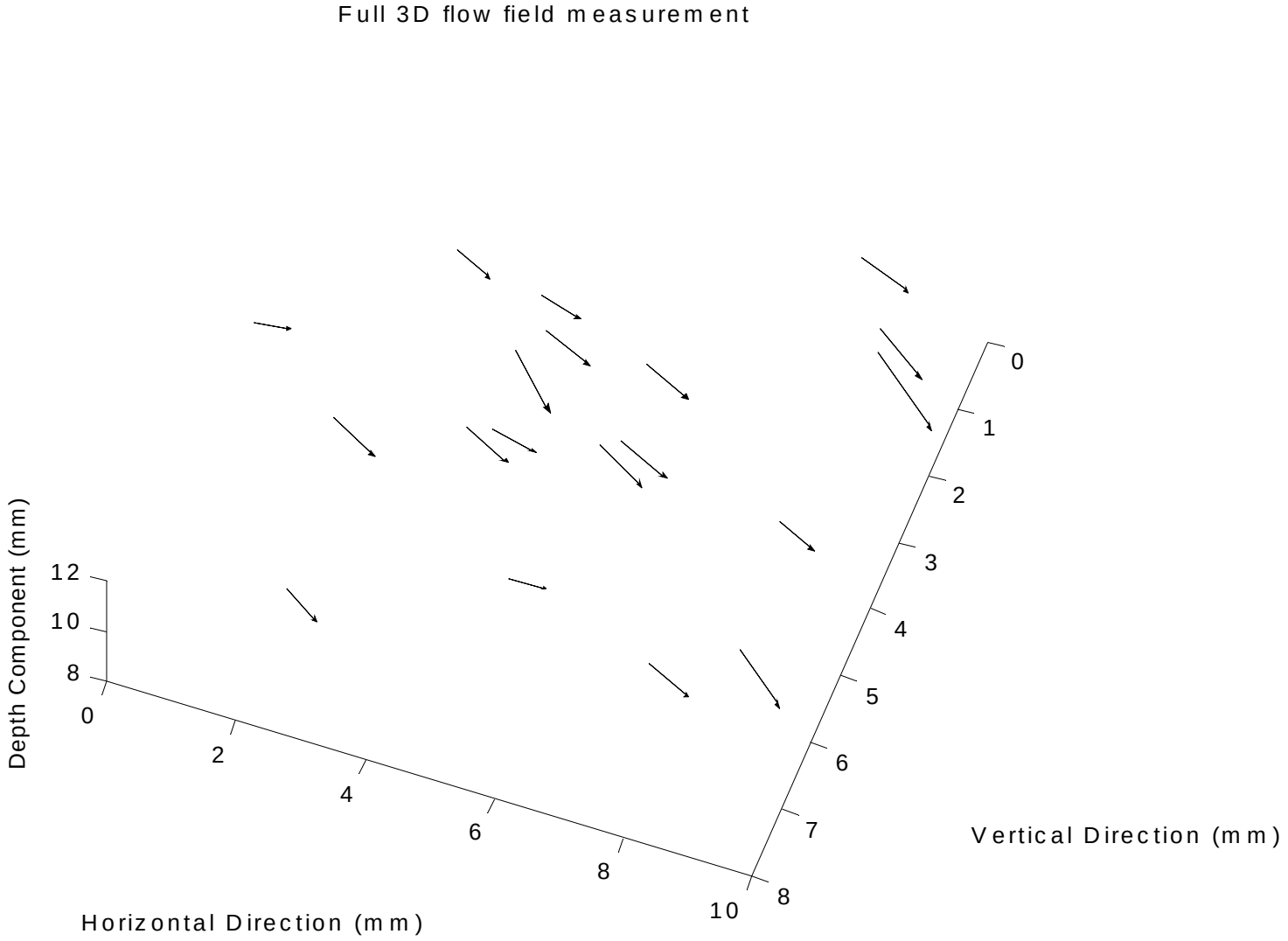

Figure 4.7. Full 3D flow field velocity data shown in figure 4.5

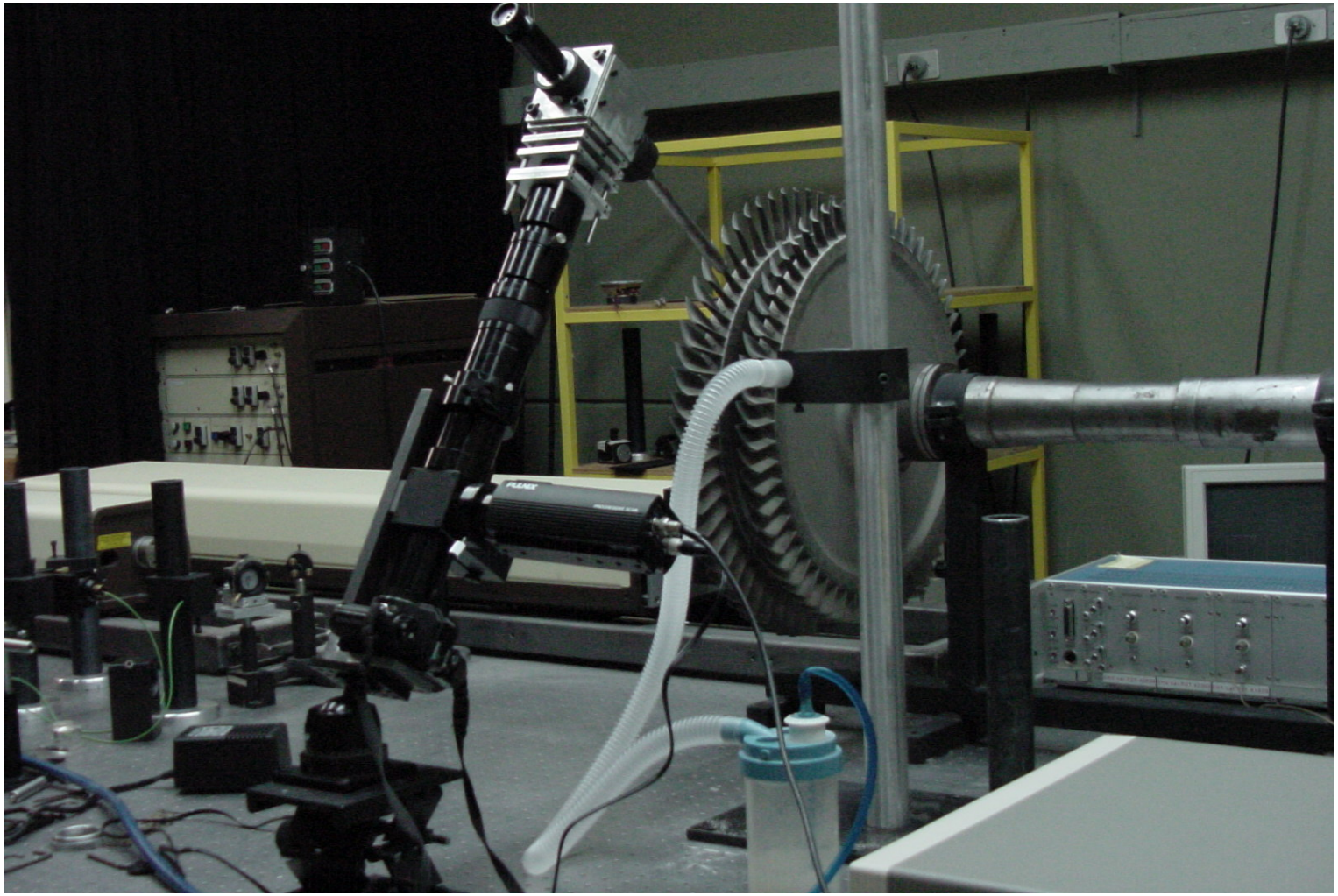

Figure 4.8 - Prototype for secondary flow research on two-stage air turbine

4.4. CONCLUSIONS

Tunneling Velocimetry has the following characteristics, which make it ideal for unsteady fluid flow studies:

- It is a volumetric method.
- It requires low to moderate illuminating powers, and so can potentially be used with high-pulse-rate lasers.
- It requires a single optical access point.
- It can cope with arbitrary 3D velocity fields.
- It can be combined with PSP/TSP near-surface measurement.
- It is a robust method as it is contained within a single instrument.

These concepts are at an early state of application and much work remains to be done but there are many areas of application, ranging from turbomachinery to fluid mixing in chemical engineering, as well as fundamental questions in the field of turbulence. These results support the feasibility of the technique to make combined surface and fluid velocity measurements.

So far, the system has been used to obtain 3D velocimetry data in conjunction with TSP data, in a uniquely integrated robust instrument. The TSP data had an accuracy of 0.5% while the velocimetry data had an estimated accuracy of 1.0%.

4.5 REFERENCES

1. Adrian R. J., "Particle-Tracking Techniques for Experimental Fluid Mechanics", Annu. Rev. Fluid Mech., 23, 261-304, 1991.
2. Funes-Gallanzi M., “Tunnelling Velocimetry: conciliation comes to the study of fluid dynamics”, Tenth International Symposium on Applications of Laser Techniques to Fluid Mechanics, Instituto Superior Tecnico, LADOAN, Lisbon, July 10-13, 2000. U.K., U.S. and P.C.T. patents pending.
3. Gouesbet G. and Gréhan G., “Sur la généralisation de la théorie de Lorentz-Mie”, J. Opt. (Paris), Vol. 13, pp. 97-103, 1982.
4. Moreno D., Mendoza Santoyo F., Guerrero, J. A. and Funes-Gallanzi, M., “Particle positioning from a single CCD image for Application to Velocimetry: theory and comparison to experiment”, ", Applied Optics, Vol. 39, No. 28, pp. 5117-5124, (2000)

5. Guerrero J. A., Mendoza Santoyo F., Moreno D., Funes-Gallanzi M. and Fernandez-Orozco S., "Particle positioning from CCD images: experiments and comparison to the Generalized Lorenz-Mie Theory", Meas. Sci. Technol., Vol. 11, No. 5, pp. 568-575, 2000.
6. Havelock D. I., "High precision position estimation in digital image metrology", Ph.D. Thesis, Carleton University, Dept. Syst. Eng. Comput. Sci., Ottawa, Canada, July 1989.
7. Funes-Gallanzi M., "High Accuracy Measurement of Unsteady flows using digital PIV", Optics and Laser Technology, 30, pp. 349-359, 1998.
8. Padilla Sosa P., Moreno D., Guerrero J. A. and Funes-Gallanzi M., "Low-Magnification Particle Positioning for 3D Velocimetry Applications", Accepted to Optics & Laser Technology, 2001
9. Mosharov V., Orlov A., Petunin A., Radchenko V., Rozanov N., Talykov V., Fonov S. and Chikin I., "Luminescent Coating for Pressure Distribution Investigation on the Models Surface in Wind Tunnels", CIAM Proceedings, N1232, (in Russian), 1988.
10. Unruh J. E. and Mikhail E. M., "Mensuration tests using digital images", Photogramm. Eng. Remote Sensing, Vol. 48, no. 8, pp. 1343-1349, 1982.
11. Bryanston-Cross P. J., Funes-Gallanzi M., Quan C. and Judge T. R., "Holographic particle Image Velocimetry(HPIV)", Optics & Laser Technology, Vol. 24, No. 5, pp. 251-256, 1992.
12. Gray C. and Greated C. A., "Processing system for the analysis of particle displacement hologram", SPIE, Vol. 2005, pp. 636-647, 1993.
13. Meng H., "Development of holographic particle image velocimetry", Ph.D. Dissertation, University of Houston, 1994.
14. Sheng J. and Meng H., "A genetic algorithm particle pairing technique for 3D velocity field extraction in holographic particle image velocimetry", Exp. In Fluids, Vol. 25, pp. 461-473, 1998.
15. Moreno D., Mendoza Santoyo F., Funes-Gallanzi M. and Fernandez Orozco S., "An Optimum Velocimetry Data Display Method", Optics & Laser Technology, No. 2, Vol. 32, pp. 121-128, 2000.
16. Bohren C. F. and Huffman D. R., "Absorption and Scattering of Light by Small Particles", John Wiley & Sons, 1983

GENERAL CONCLUSIONS AND FUTURE WORK

The first part of this thesis shows that there was a need to provide a system for measuring and visualizing an arbitrary velocity field. A system that: minimized alignment/experimental errors, for instance by integration of all components into a single instrument; required low power so high repetition lasers can be used; could be operated in real-time; was intrinsically volumetric in order to measure flows more reliably; and had single optical-access requirements.

It was also desirable to have a system capable of measuring temperature/pressure of near-surfaces, using a single apparatus able to derive fluid flow and surface data. The aim of such a system was to provide a technique to solve the disadvantages of holography, conventional PIV, and 3SA, complementing it with parameter-sensitive coating information.

Tunneling Velocimetry was developed to enable the four-variable investigation of fluids (velocity, viscosity, density and pressure) and their interactions with surfaces. This technique opens the way for the investigation of complex flow phenomena with high accuracy, using a robust and cost-effective means of measurement.

Future work will include:

- Post-processing refinements, full fluid flow variable measurements and further particle scattering code development.
- Characterization of the velocimeter for all of its different applications such as: holography, stereo configuration and Three State Anemometry. The latter consists of seeding the flow with a mixture of three different size monodisperse particles to get three different velocity fields and hence derive an estimate of density and viscosity as well as velocity.
- The use of two or more laser beams to eliminate the ambiguity direction of the tracer particles.
- Characterization of the velocimeter to perform velocity measurements of the complete fluid flow. Also, temperature and pressure measurement

characterization in the background surface, and volume, of a structure using Temperature and Pressure Sensitive Paints at the same wavelength.

- Design and test different systems to be coupled to the velocimeter such as endoscopes, periscopes and optical fibers, with the purpose of achieving remote viewing in constrained geometries such as in turbomachinery, turbines, aircrafts and chemical industry, among others.